86

SATELLITE & MESOMETEOROLOGY RESEARCH PROJECT

Department of the Geophysical Sciences
The University of Chicago

Reprint of

PALM SUNDAY TORNADOES OF APRIL 11, 1965

by

Tetsuya T. Fujita and Dorothy L. Bradbury
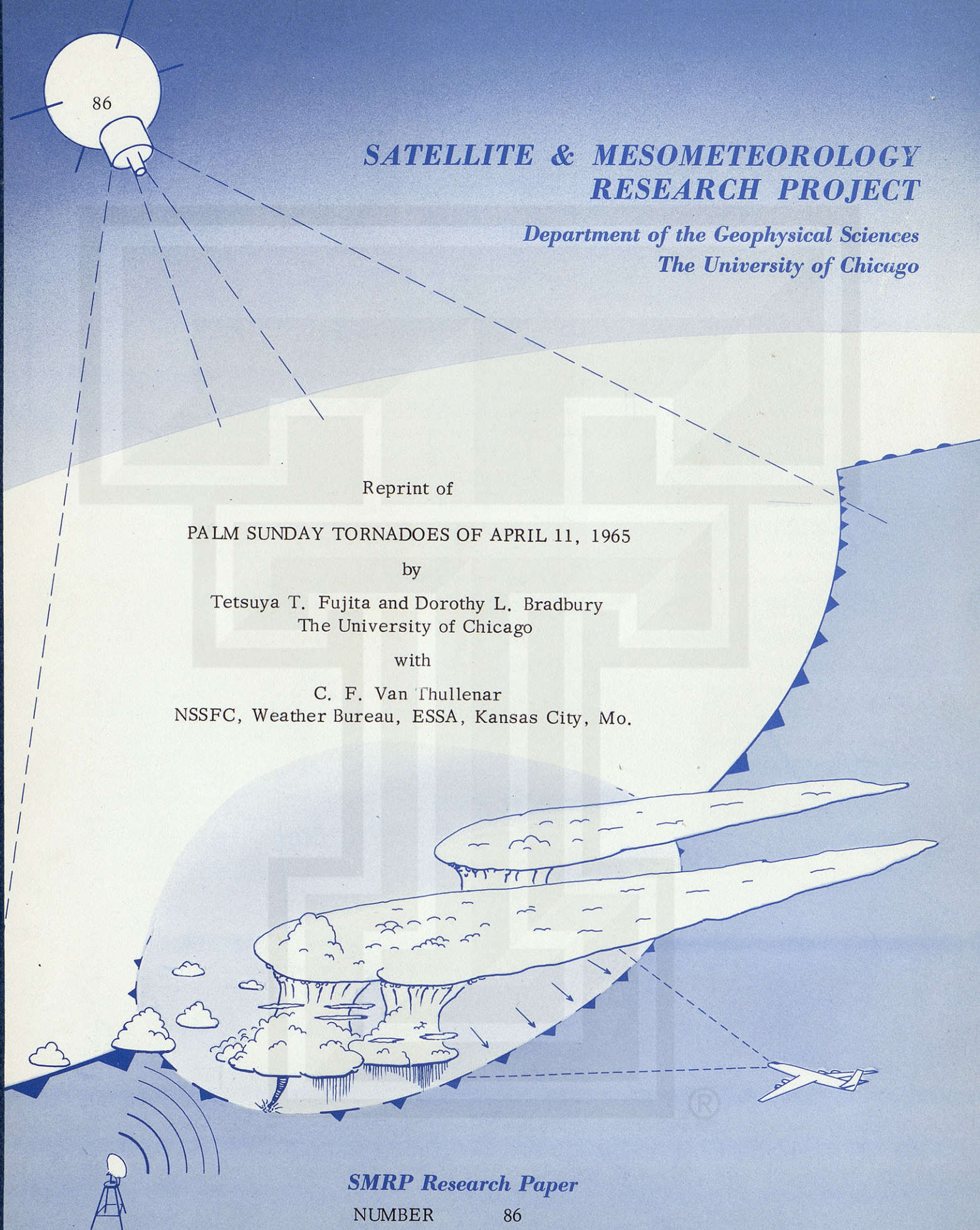The University of Chicago

with

C. F. Van Thullenar
NSSFC, Weather Bureau, ESSA, Kansas City, Mo.

MESOMETEOROLOGY PROJECT --- RESEARCH PAPERS

1.*   Report on the Chicago Tornado of March 4, 1961 - Rodger A. Brown and Tetsuya Fujita

2.*   Index to the NSSP Surface Network - Tetsuya Fujita

3.*   Outline of a Technique for Precise Rectification of Satellite Cloud Photographs - Tetsuya Fujita

4.*   Horizontal Structure of Mountain Winds - Henry A. Brown

5.*   An Investigation of Developmental Processes of the Wake Depression Through Excess Pressure Analysis of Nocturnal Showers - Joseph L. Goldman

6.*   Precipitation in the 1960 Flagstaff Mesometeorological Network - Kenneth A. Styber

7.**   On a Method of Single- and Dual-Image Photogrammetry of Panoramic Aerial Photographs - Tetsuya Fujita

8.   A Review of Researches on Analytical Mesometeorology - Tetsuya Fujita

9.*   Meteorological Interpretations of Convective Nephsystems Appearing in TIROS Cloud Photographs - Tetsuya Fujita, Toshimitsu Ushijima, William A. Hass, and George T. Dellert, Jr.

10.*   Study of the Development of Prefrontal Squall-Systems Using NSSP Network Data - Joseph L. Goldman

11.   Analysis of Selected Aircraft Data from NSSP Operation, 1962 - Tetsuya Fujita

12.   Study of a Long Condensation Trail Photographed by TIROS I - Toshimitsu Ushijima

13.   A Technique for Precise Analysis of Satellite Data; Volume I - Photogrammetry (Published as MSL Report No. 14) - Tetsuya Fujita

14.   Investigation of a Summer Jet Stream Using TIROS and Aerological Data - Kozo Ninomiya

15.   Outline of a Theory and Examples for Precise Analysis of Satellite Radiation Data - Tetsuya Fujita

16.   Preliminary Result of Analysis of the Cumulonimbus Cloud of April 21, 1961 - Tetsuya Fujita and James Arnold

17.   A Technique for Precise Analysis of Satellite Photographs - Tetsuya Fujita

18.*   Evaluation of Limb Darkening from TIROS III Radiation Data - S.H.H. Larsen, Tetsuya Fujita, and W.L. Fletcher

19.   Synoptic Interpretation of TIROS III Measurements of Infrared Radiation - Finn Pedersen and Tetsuya Fujita

20.*   TIROS III Measurements of Terrestrial Radiation and Reflected and Scattered Solar Radiation - S.H.H. Larsen, Tetsuya Fujita, and W.L. Fletcher

21.   On the Low-level Structure of a Squall Line - Henry A. Brown

22.*   Thunderstorms and the Low-level Jet - William D. Bonner

23.*   The Mesoanalysis of an Organized Convective System - Henry A. Brown

24.   Preliminary Radar and Photogrammetric Study of the Illinois Tornadoes of April 17 and 22, 1963 - Joseph L. Goldman and Tetsuya Fujita

25.   Use of TIROS Pictures for Studies of the Internal Structure of Tropical Storms - Tetsuya Fujita with Rectified Pictures from TIROS I Orbit 125, R/O 128 - Toshimitsu Ushijima

26.   An Experiment in the Determination of Geostrophic and Isallobaric Winds from NSSP Pressure Data - William Bonner

27.   Proposed Mechanism of Hook Echo Formation - Tetsuya Fujita with a Preliminary Mesosynoptic Analysis of Tornado Cyclone Case of May 26, 1963 - Tetsuya Fujita and Robbi Stuhmer

28.   The Decaying Stage of Hurricane Anna of July 1961 as Portrayed by TIROS Cloud Photographs and Infrared Radiation from the Top of the Storm - Tetsuya Fujita and James Arnold

29.   A Technique for Precise Analysis of Satellite Data, Volume II - Radiation Analysis, Section 6. Fixed-Position Scanning - Tetsuya Fujita

30.   Evaluation of Errors in the Graphical Rectification of Satellite Photographs - Tetsuya Fujita

31.   Tables of Scan Nadir and Horizontal Angles - William D. Bonner

32.   A Simplified Grid Technique for Determining Scan Lines Generated by the TIROS Scanning Radiometer - James E. Arnold

33.   A Study of Cumulus Clouds over the Flagstaff Research Network with the Use of U-2 Photographs - Dorothy L. Bradbury and Tetsuya Fujita

34.   The Scanning Printer and Its Application to Detailed Analysis of Satellite Radiation Data - Tetsuya Fujita

35.   Synoptic Study of Cold Air Outbreak over the Mediterranean using Satellite Photographs and Radiation Data - Aasmund Rabbe and Tetsuya Fujita

36.   Accurate Calibration of Doppler Winds for their use in the Computation of Mesoscale Wind Fields - Tetsuya Fujita

37.   Proposed Operation of Intrumented Aircraft for Research on Moisture Fronts and Wake Depressions - Tetsuya Fujita and Dorothy L. Bradbury

38.   Statistical and Kinematical Properties of the Low-level Jet Stream - William D. Bonner

39.   The Illinois Tornadoes of 17 and 22 April 1963 - Joseph L. Goldman

40.   Resolution of the Nimbus High Resolution Infrared Radiometer - Tetsuya Fujita and William R. Bandeen

41.   On the Determination of the Exchange Coefficients in Convective Clouds - Rodger A. Brown

     *   Out of Print
     **   To be published

PALM SUNDAY TORNADOES OF APRIL 11, 1965

TETSUYA T. FUJITA and DOROTHY L. BRADBURY

Department of the Geophysical Sciences, The University of Chicago, Illinois

C. F. VAN THULLENAR

National Severe Storms Forecast Center, Weather Bureau, ESSA, Kansas City, Mo.

ABSTRACT

An extensive aerial survey was made over a large portion of the area affected by the outbreak of tornadoes on Palm Sunday on Apr. 11, 1965. The destruction from the tornadoes extended over parts of six Midwestern States. Aerial and ground damage surveys were combined with eyewitness reports to determine the exact location and time of each tornado occurrence and its path. Radar pictures of the squall line clouds were used to verify the direction and speed of the tornado-producing clouds. Almost simultaneously with the first tornado touchdown in eastern Iowa, TIROS IX took pictures of the Midwest United States that showed a large tongue of cloud-free dry air behind the cold front. The vertical structure of the cold dome is discussed in connection with its role in the development of the tornadoes.

Two predictive parameters, namely, the best lifted index (BLI) and material differential advection (MDA) were developed and evaluated with data gathered on this outbreak of tornadoes.

The wind speed of a tornado in relation to its parent tornado cyclone is discussed in terms of an anemometer trace showing a peak gust speed of 151 mi hr^{-1}. An indirect wind-speed estimate was also attempted by examining characteristic cycloidal marks left on the fields along the tornado paths. The ground speeds computed ranged from 166 to 180 mi hr^{-1} for one tornado.

CONTENTS

1. INTRODUCTION

The Palm Sunday tornado outbreak of Apr. 11, 1965, affected six Midwestern States and was considered to be one of the largest single-day tornado disasters in the history of recorded data. At least 37 separate tornadoes were identified over an area encompassing Iowa, Wisconsin, Illinois, Indiana, Michigan, and Ohio. The toll of 258 dead and 3,148 injured (reported by the American Red Cross) is exceeded only by the Mar. 18, 1925, tornado outbreak in Missouri, Illinois, and Indiana, which caused the death of 689 persons and injuries to 1,980. The greatest property damage occurred over Indiana, with an estimated value of $145 million, followed by Michigan with $51 million and Ohio with $42½ million. A Weather Bureau Survey team toured the stricken areas and prepared a comprehensive report (1965) with recommendations for improvement in methods of alerting the public to hazardous weather conditions.

The number of tornadoes, the tracks of individual tornado families, and the areal distribution of the entire outbreak are of greatest meteorological significance. A very detailed study required that all available information relating to individual tornado occurrences be collected. This included eyewitness reports, aerial and ground damage surveys over the area, and radar films of squall line clouds. TIROS IX took pictures over the Midwest United States almost simultaneously with the occurrence over eastern Iowa of the first tornado touchdown of the outbreak. It showed a large tongue of cloud-free dry air behind the cold front; the role of this cold dome of dry air in the development of the tornadoes will be discussed. On the basis of these data, it was possible to construct the mosaic of the tornado outbreak from its inception in northeast Iowa around 1230 CST until its weakening activity over eastern Ohio around 2300 CST.

Two predictive parameters, the best lifted index (BLI) and material differential advection (MDA) were devel-

oped and evaluated to study these tornadoes. The BLI is fairly conservative with respect to time of day and thus can be advected, knowing the movements of the other meteorological systems. The MDA gives the rate of change in the lapse rate above horizontally advected air that rises sharply upon reaching the region of steep temperature lapse rate.

The wind speed of a tornado in relation to its parent tornado cyclone is discussed, using an anemometer trace showing a peak gust speed of 151 mi hr^{-1} at a point very near the center of the tornado. An indirect wind-speed estimate was determined by examining characteristic cycloidal marks left on the fields along the tornado paths. These computed speeds ranged from 166 to 180 mi hr^{-1} for one of the tornadoes.

2. SYNOPTIC SITUATION

The major portion of this study is concerned with the mesoscale features of the tornado outbreak, but in order to relate this to the synoptic scale, a brief summary of the large-scale features is included.

At 0600 CST on April 11, a weak low-pressure center was located over western Iowa and the northwestern part of Missouri. From this center, a weak warm front extended eastward over central Iowa, northern Illinois, and Indiana, and a dry cold front stretched southward over eastern Kansas. Thunderstorm activity was occurring along a line across northern Missouri and central Illinois. This appeared to be associated with a short-wave upper trough moving through the area.

By 1200 CST the low center had moved to central Iowa, and the central pressure had fallen to 985 mb (fig. 1). South of the warm front, southerly winds of 15 to 25 kt were transporting moist warm air with dew points above 60°F toward the front. The area of this moist warm air is designated "A." Behind it, a rather cold but extremely dry air mass B was pushing eastward, forming a sharp dry cold front extending from the cyclone center to Arkansas. Air mass B was followed by the relatively moist cold air D that was pushing southeast from Wyoming. As air mass B moved over the Rocky Mountains in Colorado, it became much drier than air mass D. Air mass C was of maritime polar origin, with easterly winds up to about 20 kt.

An isotherm chart for 1200 CST covering the area of the surface isobar chart is shown in figure 2. The warmest spot in warm sector A with a temperature of over 85°F, was located south of St. Louis, Mo. A cold spot near Louisville, Ky., and another near Dubuque, Iowa, were associated with local thunderstorm activities within the warm sector.

Within air mass B, the air temperature gradually decreased westward from 80°F near the dry cold front to about 45°F along the foothills of the Rockies. Air mass D was colder than B, because it slipped out from the northwest without moving over the high mountains.

The horizontal temperature gradient within the air mass C was the greatest of all the air masses surrounding
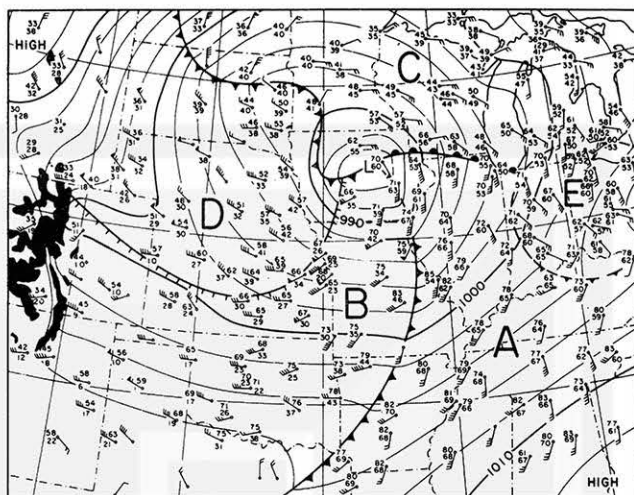

FIGURE 1.—Surface winds and isobars at 1200 CST on Apr. 11, 1965. A long wind barb and a flag drawn to represent 5 kt and 25 kt, respectively, emphasize the intensity of surface winds. A, moist warm air; B, dry cold air; C, moist colder air; D, moist cold air; and E, outflow from a dissipating High.

the continental cyclone centered over Iowa. The surface temperature of Lake Michigan created a marked cold temperature ridge over the lake, resulting in 10° to 20°F temperature drops between weather stations located on the east and west sides of the lake.

The most significant contrasts between air masses A, B, and D were reflected in the dew-point temperatures, which are plotted in figure 1. The dew-point temperature within the warm sector was fairly uniform, varying only between 60° and 70°F. A significant drop in the rear of the cold front resulted in 20°F near Kansas City, Mo., and there was a further drop to only 6°F in the northwest corner of New Mexico. Since the dew-point temperatures from the mountain stations were as high as 20° to 22°F, we may suspect that the extreme dryness east of the Rockies was caused by their mesoscale blocking action. The dew-point temperature inside air mass D was at least 10°F higher than that of B. A line with short spikes dividing these two air masses designates a front, the passage of which produced a drop in temperature and a simultaneous increase in dew-point temperature. Such a front may be called the "moist cold front." A line dividing air masses A and B, on the other hand, is a cold front, but it is accompanied by a marked drop in dew-point temperature and is referred to as the "dry cold front."

Charts for the 850-, 500-, and 200-mb surfaces for 0600 and 1800 CST are shown in figure 3. There was little indication of deepening at the upper levels of the cyclone during the 12-hr interval. The most outstanding feature in these charts is the stronger than normal jet stream at 0600 CST on the 500- and 200-mb charts. Wind speeds aloft were generally of the order of 122 kt, with an absolute maximum over Dodge City, Kans., of 159 kt. Several weather stations were not reporting winds at
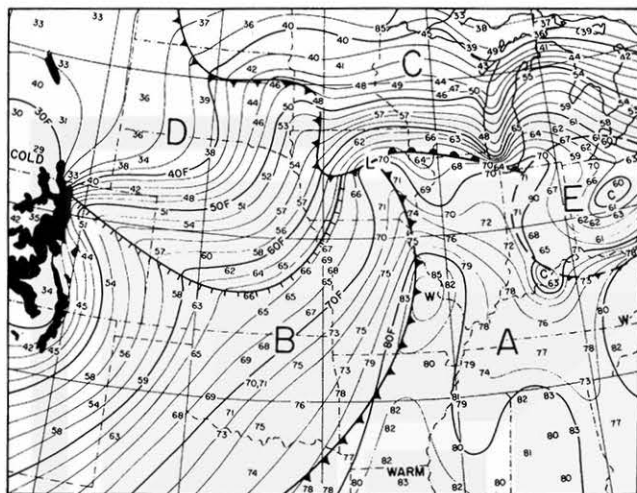
FIGURE 2.—Isotherms at 1200 CST on Apr. 11, 1965, contoured for every 2°F. A through E, same as in figure 1.

the 200-mb level because the rawinsonde was lost in low elevation angles. At 1200 CST, just before the first tornado report, Topeka, Kans., reported winds of 123 kt at 14,000 ft, and Columbia, Mo., showed winds of 87 kt at 10,000 ft, 99 kt at 14,000 ft, and 102 kt at 16,000 ft. Peoria, Ill., reported winds of 97 kt at 14,000 ft and strong shear between 12,000 and 14,000 ft. Winds of such high speeds at relatively low levels are indicative of very strong convergence below these levels.

3. DATA SOURCES FOR TIMES AND LOCATIONS OF TORNADOES

Immediately after the Palm Sunday tornado outbreak, we realized that the occurrence of so many storms over such a large area made the event worthy of a special effort to collect and record data. With the cooperation of the Weather Bureau in Chicago, the press wire services were solicited for assistance. They transmitted a request to all their member newspapers and radio and television outlets in the affected areas to publicize our interest in obtaining all the information possible from those who had witnessed the occurrence of severe weather on this date. Letters were addressed to many newspapers, including weeklies, asking them to carry news items of the storm.

The response was excellent. Many letters were received from eyewitnesses, giving precise locations and times of the storms. The number of newspapers received was somewhat overwhelming and their pictures of damage were valuable aids in locating storm occurrences. Meteorologists in charge of local Weather Bureau offices were solicited for additional information.

When all reports were combined, checked and rechecked, a consistent pattern of tornado paths was constructed. The paths were verified by an aerial survey over a large part of the affected area. The flight tracks with the dates on which the surveys were made are shown

in figure 4. With such surveys the damage path can be precisely plotted, giving evidence that the funnel was touching the ground along the path.

A combination of the unsurveyed and the aerially surveyed paths was used in preparing an index map of the entire area as shown in figure 5, identifying the individual paths as tornado families A through R. There were probably more funnels than those charted in this map, but if they had not been substantiated by damage marks or photographs, they were not indicated on the chart. Several reports of two or more tornado funnels being observed simultaneously were received, but only one case was verified by a photograph. The few tornado paths that were not surveyed were judged from available reports to be less destructive or were too far from the base of operations of the aircraft to be included in the survey on that specific day. Any aerial survey after April 19 would show little destruction as most of the debris would have been cleaned up by then.

4. AERIAL SURVEY

On the morning of April 12, arrangements were made to charter a Cessna–310 aircraft to fly over the affected area and to take pictures of the damage from an altitude of 1,500 to 2,000 ft. Four separate survey flights were made, as follows: 3.5 hr on April 12 over Illinois; 5.3 hr on April 13 over Indiana and Michigan; 8.6 hr on April 16 over Indiana, Ohio, and Michigan; and 6.5 hr on April 19 over Wisconsin and Michigan. These tracks are shown in figure 4. A total of about 7,500 mi was flown by Professor Fujita, accompanied by either Mr. Bernhard Ginsburg, a photographer, or Mr. Ronald Reap, a research meteorologist. As soon as tornado damage was spotted, it was plotted in the air on a 1:250,000 U.S. Geological Survey map. Significant damage patterns were then photographed with hand-held 35-mm cameras equipped with 25-mm, 50-mm, and 135-mm lenses so that wide- and narrow-angle views could be used later for general mapping and detailed examination of significant damage.

During the picture taking, it was found that some types of damage are visible only when viewed from particular directions with respect to the sun. The faint marks left on a newly plowed field, especially, appear to be bright when viewed from the direction of large or small backscattering angles. Otherwise, they cannot be distinguished from the undisturbed surface or may sometimes appear to be dark. When interesting damage patterns were seen from one direction, a series of high-bank circular flights was made to obtain the best possible pictures for further research.

The areas of aerial survey were divided into sectional maps, including either 45-min longitude by 15-min latitude or 45-min longitude by 20-min latitude as shown in figure 5. Twenty aerial survey maps of damage paths were finally completed. Each map shows major highways, railroads, cities, lakes, photographic locations, and spotted tornado damage.
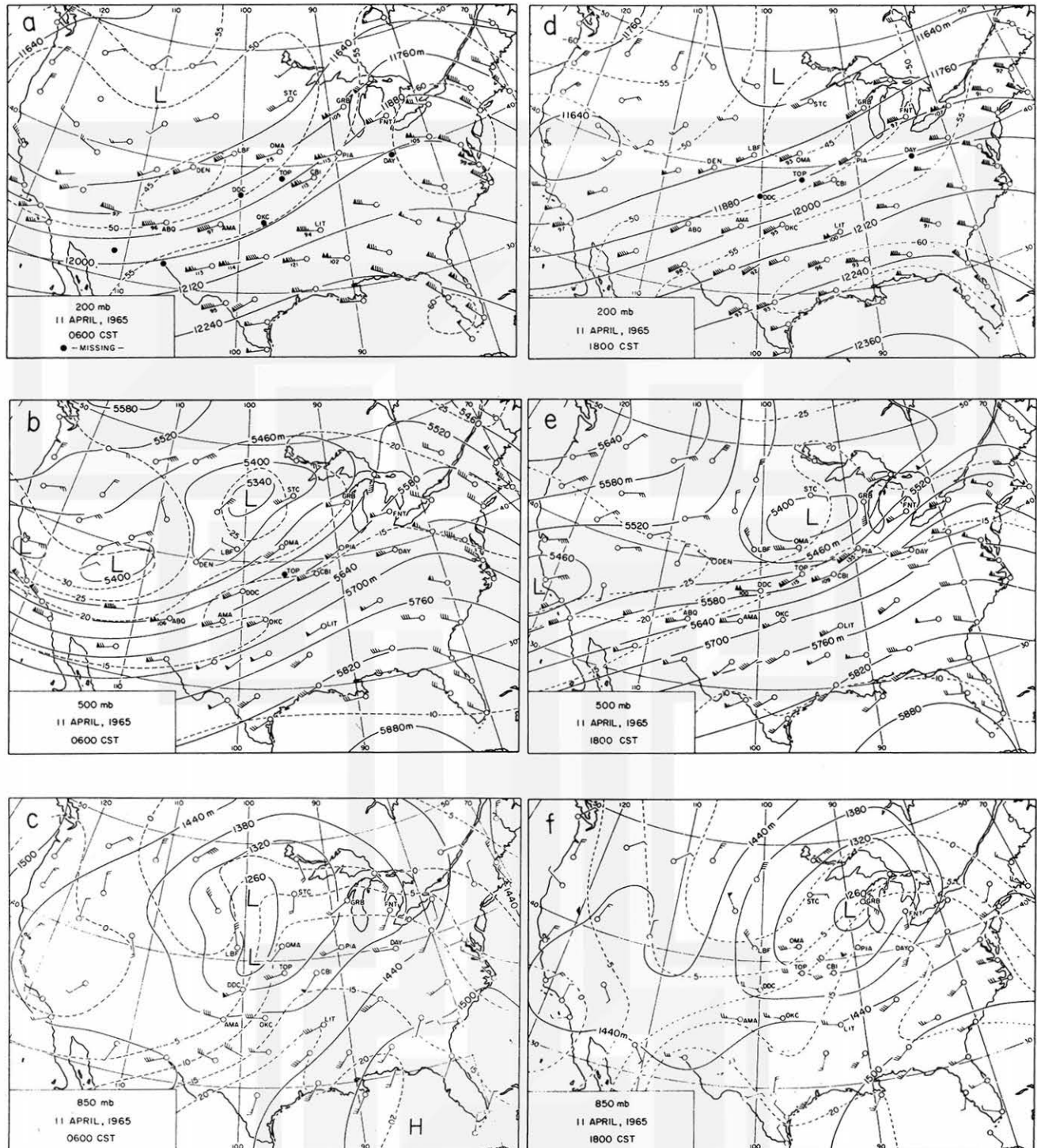
FIGURE 3.—Contours in meters (solid lines) and isotherms in °C (dashed lines) at the 200-, 500-, and 850-mb levels for Apr. 11, 1965, at 0600 and 1800 CST.

CHARACTERISTICS OF DAMAGE BY EACH TORNADO SURVEYED

A detailed examination of 24 damage paths covered by this aerial survey revealed that some significant features can be used for estimating a storm's characteristics, that is, the horizontal dimensions and the wind speed required to produce particular damage. Common damage, such as exploded houses and scattered debris, was used only for
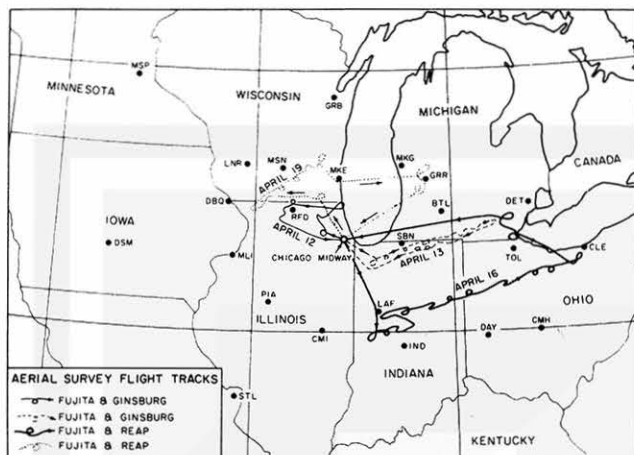
FIGURE 4.—Flight tracks of a Cessna-310 aircraft chartered for damage survey of the Palm Sunday tornadoes of Apr. 11, 1965. About 7,500 mi were flown over the five-State areas of tornado damage.
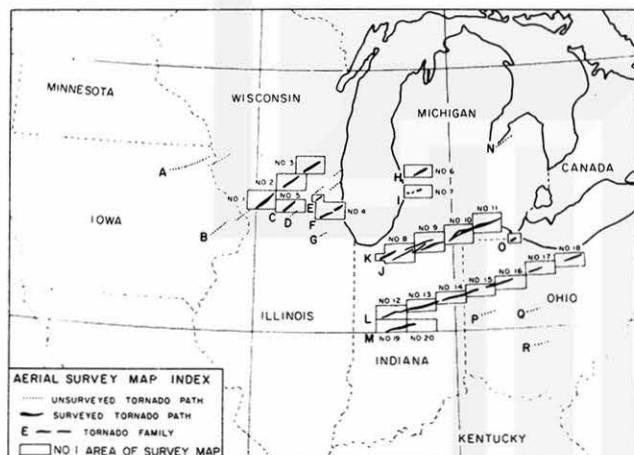
FIGURE 5.—Index map showing 20 aerial survey maps that include damage paths and positions according to aerial photographs. Tornadoes formed out of each parent echo were grouped together in families identified by letters A, B, . . ., R.

FIGURE 6.—Aerial survey map covering an area of Wisconsin and Illinois.

confirmation, since it can be seen after practically all tornadoes.

Included in this section are 20 aerial survey maps showing damage paths and photographs of significant damage patterns, as well as tornado pictures taken from the ground. Circled in the survey chart is the photograph identification number in the series of pictures taken. The small black dots in the damage path represent observed damage to buildings, trees, etc.

The aerial survey map in figure 6 includes the 29-mi damage path of tornado B–3, the third tornado of family B. The first tornadolike damage from B–3 was spotted about 1½ mi north of the intersection of Ill–78 and US–20. Some 15 trees in a small patch of forest were uprooted. Northeast of these trees, no damage was confirmed until scattered debris was found on the southwest side of the
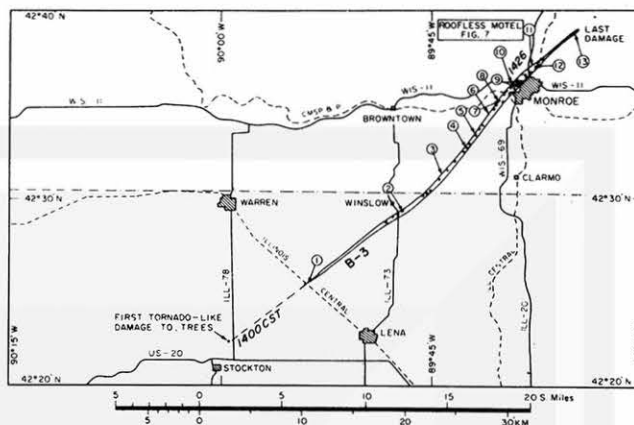
Illinois Central Railroad. Damage then gradually became more severe as the path widened to the northwest suburb of Monroe, Wis., where extensive damage to buildings and trees was photographed.

An aerial view of a damaged motel on Wis–69, 1 mi North of Monroe, is shown in figure 7. The entire roof of the motel was gone, but the walls remained standing, practically undamaged. Destruction occurred around 1430 CST. The picture was taken on April 19 toward the south, the tornado center having passed about half a block south of the motel, from southwest to northeast.

The first damage from tornado B–4 (fig. 8) was spotted on Wis–15 about ½ mi south of Evansville, Wis. There was no appreciable damage to houses, but debris was scattered over the plowed fields. This tornado left a rather narrow path of moderate destruction before disappearing near US–12 northwest of Ft. Atkinson. The damage path was 23 mi long with a maximum width of 0.2 mi. No particular damage features were spotted from the air.

Figure 9 shows that after the first damage of tornado B–5 had been spotted on US–18, 5 mi west of Jefferson, the width of the damage increased rapidly to about ¾ mi as the tornado moved northeastward. Considerable damage to trees was sighted in forests east of Lake Mills. A forest 1-mi square south of Wis–30 was practically leveled: 60 percent uprooted, 30 percent torn apart, and the rest badly damaged. Past the Chicago and Northwestern Railroad tracks, damage became less severe. The path remained about ¾ mi wide until the whole storm weakened after having crossed US–16. A search for a possible sixth tornado over the Hartford area turned out to be negative. The length of the B–5 damage path was 24 mi, and the maximum width, ¾ mi.

The path of a weak and short-lived tornado that caused some damage in the Lake Geneva, Wis., area is shown at the upper left of figure 10. This tornado, identified as E–1, formed near the western edge of Williams Bay, where several damaged houses were spotted, but the storm weakened considerably as it moved through Como. Very
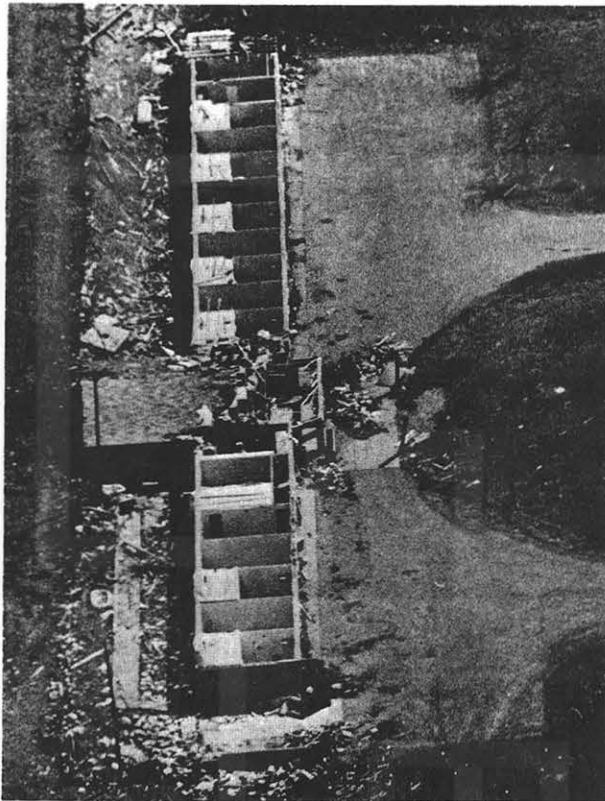
FIGURE 7.—Aerial view on April 19 of a roofless motel on Wis-69, north of Monroe, Wis. Time of destruction estimated at 1430 CST on April 11. For exact location refer to figure 6.
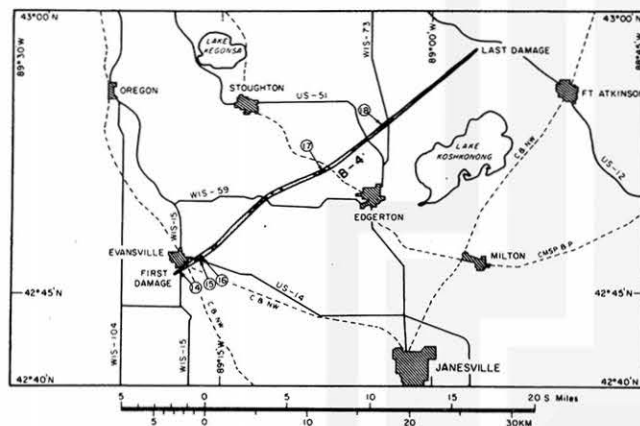
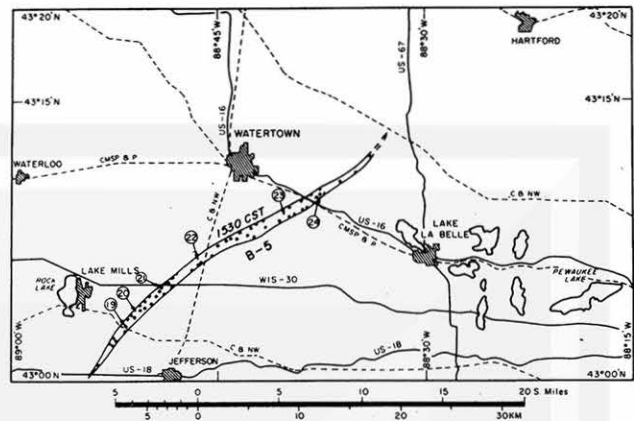

FIGURE 9.—Aerial survey map covering an area of Wisconsin.
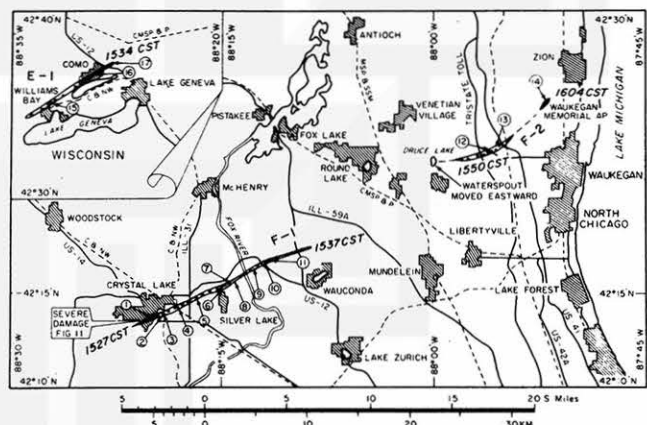
FIGURE 10.—Aerial survey map covering an area of Wisconsin and Illinois.

FIGURE 8.—Aerial survey map covering an area of Wisconsin.

little tree damage was spotted from the air. Tornado E–1 left a 5-mi path less than one block wide.

The Crystal Lake tornado, F–1, left devastating damage to a residential district and a shopping center in this northern Illinois community. Figure 11 shows an aerial view of severe damage to frame houses. The tornado's

path runs from right to upper left in the picture. A detailed survey from the ground was reported by Feris et al. (1965). The tornado lasted only about 10 min before disappearing over the forest north of Wauconda. It may be classified as intense; the damage it left was less than ½ mi wide. There was some local indication of a double damage path which might have been caused by more than one funnel.

The second tornado, F–2, moved over Druce Lake, according to the report cited above. It left moderate damage to suburban houses, resulting in about a 4-mi path. The last damage was confirmed at the Waukegan Memorial Airport where airplanes were turned over and hangars suffered wind damage. It is debatable whether F–2 was one or two tornadoes. In view of our limited ability to spot all tornado damage from the air, each tornado path was considered as single even though there were small discontinuities such as the ones observed in this case. It is well known that a tornado that can be followed visually for some distance does not always pro-

FIGURE 11.—Picture taken on April 12 of severe damage in the residential section of Crystal Lake, Ill. The damage occurred at 1527 CST on April 11. For exact location refer to figure 10.
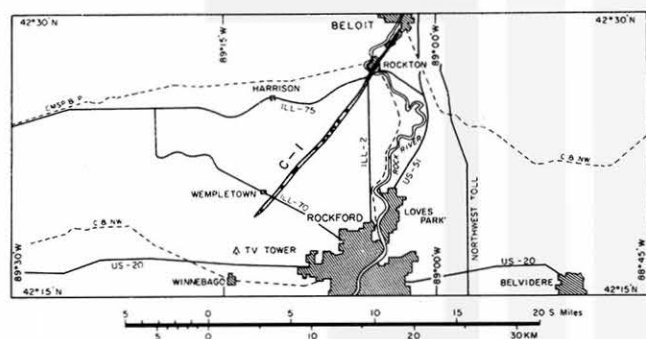

FIGURE 12.—Aerial survey map covering an area of Illinois.

FIGURE 13.—Aerial survey map covering an area of Michigan.

duce a long continuous path because of the storm's short-period pulsation, asymmetric structure, slight lifting, etc., combined with the conditions of the buildings and vegetation.

The damage path of tornado D–1 is shown in figure 12. The first damage was sighted from the air at the midpoint between the Rockford TV tower and Wempletown. After the tornado had crossed Ill–70, it left a continuous but very narrow damage path extending to Rockton where several airplanes were blown over and a restaurant was damaged. The storm weakened considerably after moving over Rockton, then probably disappeared over downtown Beloit, Wis. The total path length was 14 mi, with a maximum width of no more than ⅛ mi.
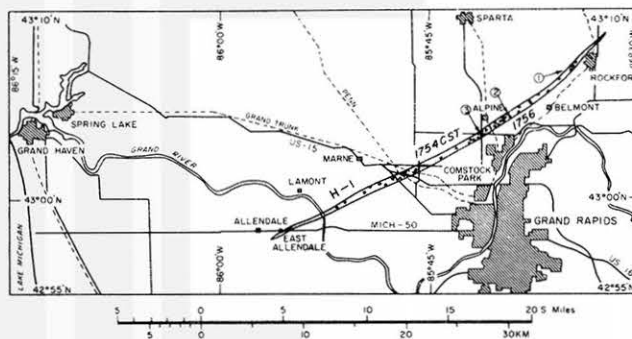
As seen in figure 13, the first damage by tornado H–1 was spotted on Mich–50 near East Allendale. The width of the storm's path and intensity gradually increased until the tornado reached the northern suburb of Comstock Park where its intensity was estimated to be moderate. The maximum width was not more than ½ mi. The last damage was spotted in the area north of Rockford. The path length was 24 mi.

Figure 14 shows that only a short damage path, 2 mi long and ⅛ mi wide, of tornado I–1 was surveyed in the vicinity of Burnips, Mich. Ground reports of debris from Saugatuck and damage from Hamilton might have indicated a continuous path if the entire area had been surveyed more completely.
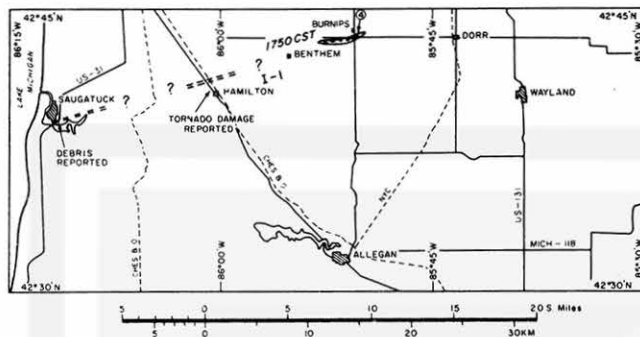
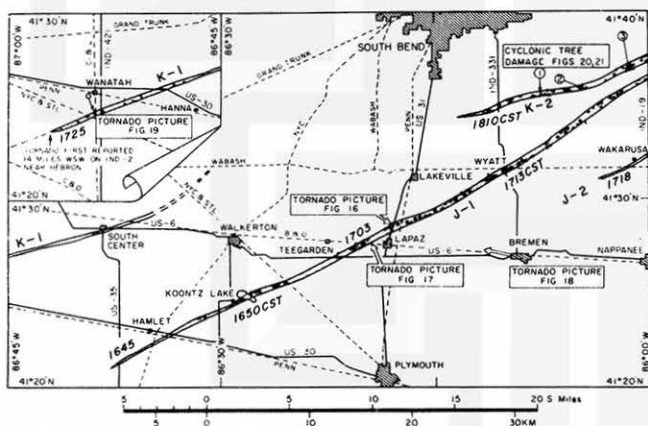FIGURE 14.—Aerial survey map covering an area of Michigan.

FIGURE 15.—Aerial survey map covering an area of Indiana.

FIGURE 16.—"White tornado" identified as J–1, photographed by Indiana State Trooper Robert Candler on US–31 north of Lapaz, Ind. Because of the sky light from the west, it appears white against the extremely dark eastern background. The tornado funnel consisted mainly of water vapor that condensed into droplets due to the low pressure inside the tornado vortex. For exact location refer to figure 15. (Courtesy of Mr. Robert Candler.)

FIGURE 17.—Photograph of tornado J–1 taken at 1701 CST, 2 min before that of the white tornado in figure 16. From this direction the tornado appeared against a brighter background. For exact location refer to figure 15. (Courtesy of Mrs. Helen Elliott.)

The survey map in figure 15 includes damage paths of four tornadoes belonging to families J and K. Tornado J–1, first reported by the Indiana State Police at 1645 CST, left a rather narrow path across Koontz Lake where severe damage was seen from the air. The path widened gradually and after the storm had crossed US–31 a remarkable picture of a "white tornado" (fig. 16) was taken by Indiana State Trooper Robert Candler near Lapaz. The picture was taken at 1703 CST facing eastward, less than 1 min after the storm had crossed the highway about two blocks south of where he was standing beside his car. The tornado appeared white because it was illuminated by sky light from the west, while the background to the east was very dark. Figure 17, a picture of the same tornado, was taken by Mrs. Helen Elliott of South Bend at 1701 CST, facing northwest. This picture shows a dark funnel against a rather bright northwest background. Note that the funnel shows a more or less cylindrical shape almost all the way to the ground, with debris and dust clouds circling around the bottom of the funnel. Another picture (fig. 18) was taken by Mr. Willis Haenes at Bremen at 1703 CST, almost at the same time that the white tornado was photographed. The direction

of view is toward the west-northwest. The tornado was located at the south end of the low cloud base. A similar relative position of tornado and low cloud base has been studied by Fujita (1960), using pictures of the Fargo tornadoes. After crossing US–31 north of Lapaz, the storm left a narrow but heavy damage path to Wyatt where it started weakening.

Tornado K–1 (upper left corner of fig. 15) was first reported on Ind–2 near Hebron, but damage was not observed from the air until south of Wanatah where several farms were damaged along a very narrow path. A picture taken by Mr. Nicolas J. Polite, looking south from Wanatah at 1726 CST, is shown in figure 19. After

FIGURE 18.—Tornado J-1, photographed by Mr. Willis Haenes at Bremen, showing a simultaneous view of the white tornado taken from the direction opposite to that in figure 16. Note the bright background to the west. For exact location refer to figure 15. (Courtesy of Mr. Willis Haenes.)
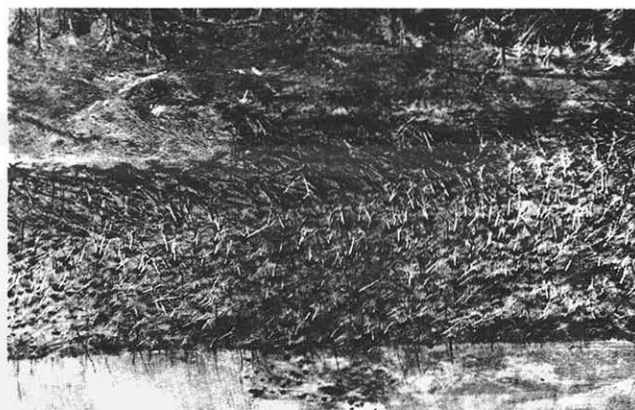

FIGURE 20.—Aerial view, taken April 13, of uprooted trees oriented along the streamlines of cyclonic winds. The damage occurred at about 1815 CST on April 11. Although the view was south, the picture is oriented with north at the top. For exact location refer to figure 15.

FIGURE 19.—Tornado K-1 seen from Wanatah, Ind. (view south-southeast at 1726 CST). The damage path left by this tornado was only about half a block wide. For exact location refer to figure 15. (Courtesy of Mr. Nicolas J. Polite.)
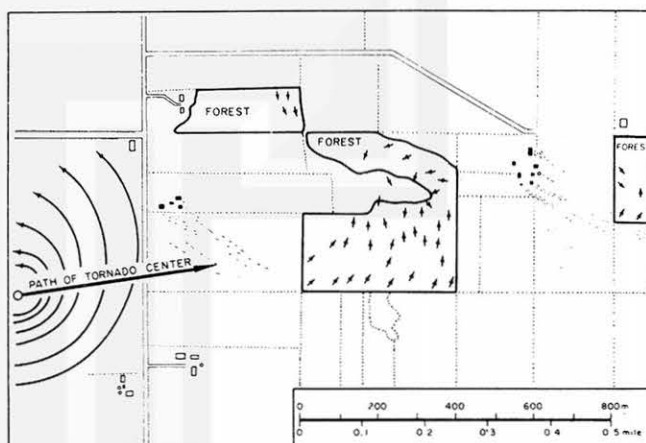

FIGURE 21.—Rectified patterns showing the orientation of uprooted trees and debris marks in the vicinity of the area seen in figure 20. About 10 aerial photographs were used for this mapping. For the exact location refer to figure 15.

crossing Ind-421, the storm left a very narrow damage path, about half a block wide, then continued to South Center where the last damage to buildings could be spotted from the air.

The first damage by tornado K-2 (upper right of fig. 15) was spotted 1 mi west of Ind-331. After the tornado had crossed the highway, the damage path widened to ½ mi. Figure 20 shows cyclonic tree damage. This picture, taken toward the south, is printed upside down to fit the rectified map shown in figure 21. The radius of curvature of the streamlines of the tornado winds when these trees were uprooted was measured to be 300 m or 0.2 mi, while the width of the damage path was 800 m or 0.5 mi. These figures indicate that the trees were uprooted along

the fringe of the damaging tornado winds rather than along the circle of maximum winds surrounding the central core of the tornado. Close examination of the picture reveals that only a few trees were torn up and that most of them were uprooted before their branches and trunks were finally broken by high winds. Such tree damage may be related to the type of trees, not identifiable from the air, but the condition of the ground, either dry or soaking wet, could also be the cause. In the latter case, a tree could easily be uprooted by winds with a mean speed of 50 mi hr^{-1}.

The damage path of tornado K-2 shown in figure 22 is an extension of the first part shown in figure 15. The damage along this ½-mi-wide path was extremely severe
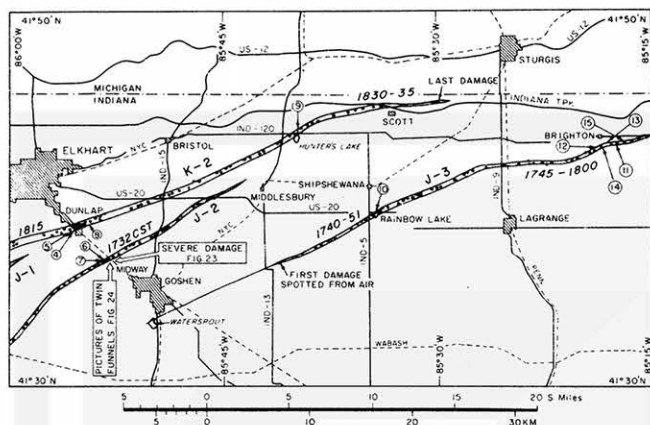
FIGURE 22.—Aerial survey map covering an area of Michigan and Indiana.

FIGURE 24.—Spectacular photograph of the twin-funnel tornado taken by Mr. Paul Huffman, Staff Photographer of the *Elkhart Truth*, at 1732 CST on April 11, one of a series of six pictures appearing in figure 46. For exact location refer to figure 22. (Courtesy of Mr. Paul Huffman.)

FIGURE 23.—Aerial photograph of severe damage to the Midway Trailer Court northwest of Goshen, Ind. The devastation near the center of the picture was caused by the left funnel of the tornado shown in figure 31. The right funnel moved over the plowed field from right to left, cutting across the upper corner of the court. For more detail see figure 52. Damage occurred at 1732 CST on April 11; the picture was taken on April 13. For exact location refer to figure 22.

especially in the residential area of Dunlap, where many houses were exploded and completely leveled. The tornado then weakened slightly, leaving a severe to moderate damage path extending to Hunter's Lake where debris from nearby homes was seen along the east shore of the lake. A continuous path was traced from the air across the Indiana Turnpike north of Scott. Newspaper reports show that several cars were blown off the turnpike between 1830 and 1835 CST. The last damage to trees was spotted north of the turnpike about 3 mi east of the point where the tornado had crossed the turnpike.

Tornado J-2, reported near Wakarusa at 1718 CST, moved into the area shown on the survey map in figure 22, leaving a rather narrow path. Approaching Midway,

northwest of Goshen, the storm became considerably more intense and destroyed a large number of trailers, as shown in figure 23. Its movement runs from right to upper left in the picture, which was taken toward the southeast. The photo of the twin tunnel shown in figure 24 was taken by Mr. Paul Huffman of the *Elkhart Truth*, looking northwest from the shoulder of US-33, 0.7 mi southeast of this trailer court, while devastation by the left funnel was taking place. He took a total of six pictures in succession to show how a single funnel split into two and then reorganized into one after about a minute. A photogrammetric analysis of these pictures will be presented later. A continuous narrow but severe damage path was spotted from Midway to the west of Middlesbury where it was lost completely. A local witness reported that a car traveling west on the rural highway north of Goshen was pushed backward toward the east, then was blown off the highway into a field.

Tornado J-3 was first reported as a waterspout crossing a small lake south of Goshen. Damage was not clearly visible until about 1 mi east of Ind-13 where demolished farms were spotted. Near the Rainbow Lake area, damage appeared to be devastating. The storm then gradually weakened until its path was lost at a spot about 3 mi east of Brighton.

Figure 25 shows that the damage caused by tornado J-4 was first spotted about 2 mi west-southwest of Lake Pleasant. Destruction along the eastern shore of this lake (fig. 26) was almost complete, probably because of the additional effect of water sucked up and carried by the tornado. Most of the trees along the shore were stripped and torn, as though water spray and droplets caught in the tornado wind had acted like flying bullets. As the storm approached Coldwater Lake, the damage path widened to about 1 mi, covering almost half of the western shore. As shown in figure 27, there were exploded houses
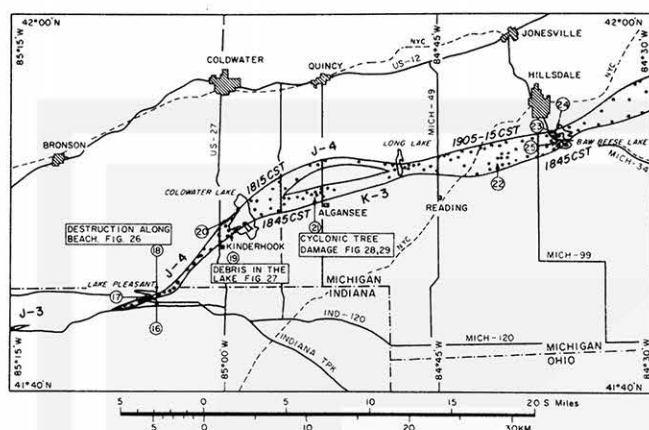
FIGURE 25.—Aerial survey map covering an area of Michigan, Indiana, and Ohio.
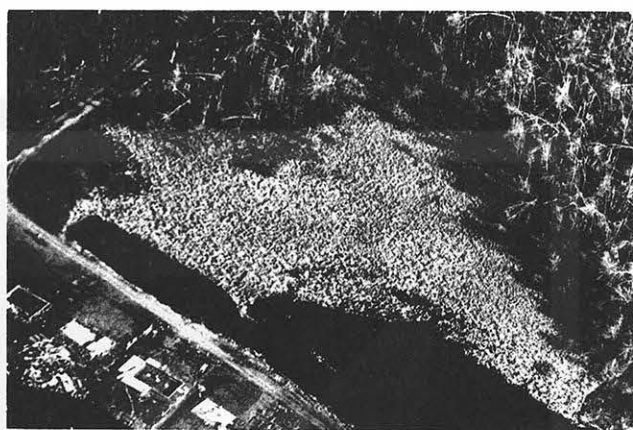

FIGURE 27.—Concentration of debris in a small cove of Coldwater Lake, Mich. Two tornadoes, J–4 and K–3, moved over the lake at about 1815 and 1845 CST on April 11; the picture was taken on April 13. For exact location refer to figure 25.
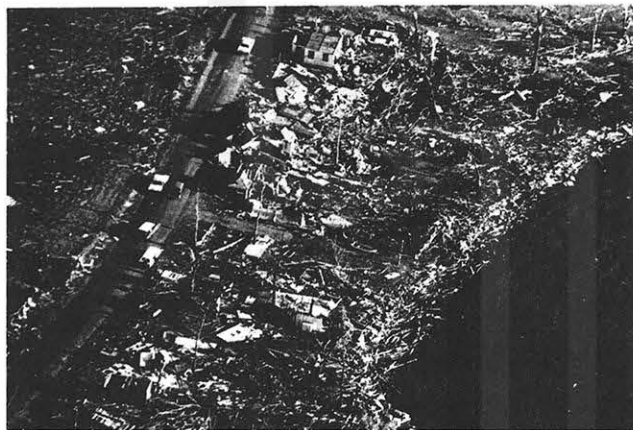

FIGURE 26.—Destruction along the eastern shore of Lake Pleasant, Ind. Tornado J–4 moved from right to left, sucking up water from the lake. The time of the tornado was about 1800 CST on April 11; the picture was taken on April 13. For exact location refer to figure 25.
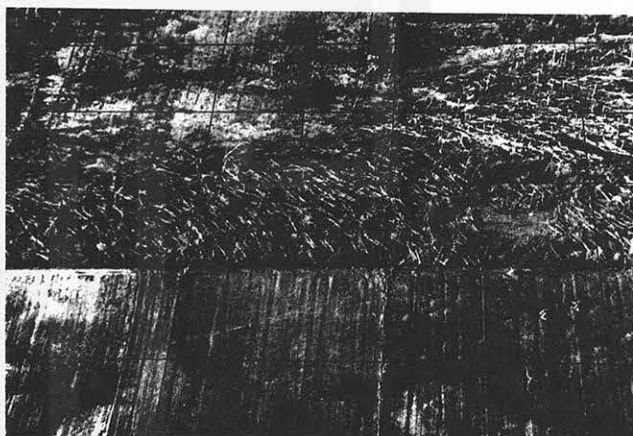

FIGURE 28.—Picture, taken April 13, of cyclonic tree damage spotted near Algansee, Mich. Damage was caused by tornado K–3 as it moved over this area about 1845 CST on April 11. For exact location refer to figure 25.

along the lake front and floating debris in many parts of the lake. The damage path east of the lake was extremely wide, reaching over 2 mi in the area north of Algansee. Detailed examination of the damage, which was relatively heavy and scattered in nature, revealed that it was caused by two tornadoes, J–4 and K–3. A photograph and map of cyclonic tree damage left by K–3 is shown in figures 28 and 29. The large radius of curvature of the streamlines (600 m) determined from the directions of uprooted trees suggested a diameter of about 0.7 mi. Some areas of little or no damage north of this area of uprooted trees seemed to indicate the presence of two separate damage paths caused by J–4 and K–3, and witnesses from the Coldwater Lake area stated that two tornadoes moved over the area about 30 min apart.

The path width, which was about 1 mi near Long Lake, widened to 2 mi, then narrowed to 1 mi over Baw Beese Lake. The damage was moderate, except in local areas near the lake, where many houses were completely demolished. Two separate tornadoes, 30 to 45 min apart, were also reported from this area.

The combined tornado damage path of J–4 and K–3, as shown in figure 30, was between 2 and 3 mi wide, characterized by scattered light-to-moderate damage to buildings and trees. Some houses between Devils Lake and Round Lake were badly damaged. A wind tower operated by the Tecumseh Health Study Project north of Tecumseh survived recording a 150-mi hr^{-1} wind from the west at 1907 CST and a 74-mi hr^{-1} wind from the south at 2004 CST. These two maxima were evidently caused by two separate tornadoes, J–4 and K–3, moving east-north-
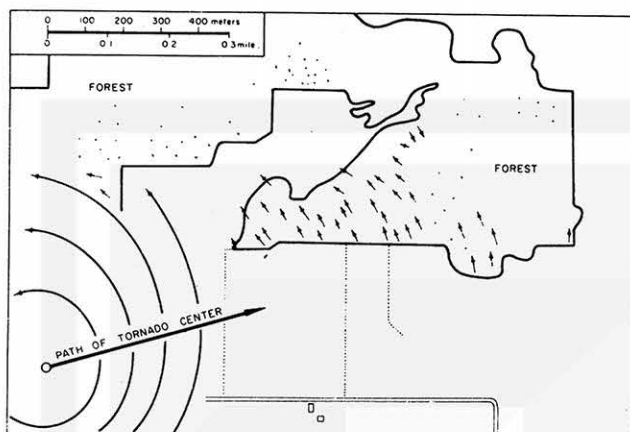
FIGURE 29.—Rectified pattern of uprooted trees seen in figure 28. Note that the radius of curvature of streamlines is much larger than that in figure 21. For exact location refer to figure 25.
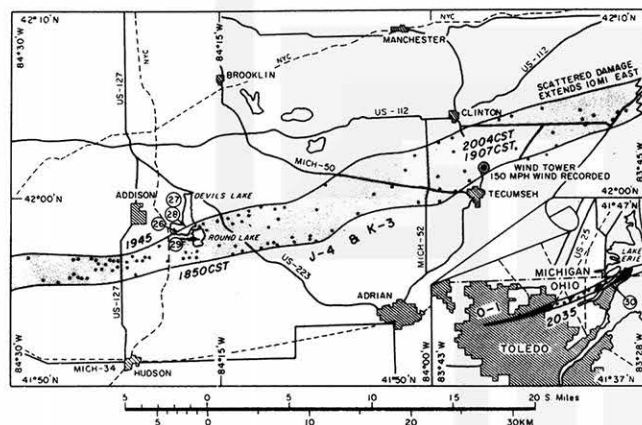

FIGURE 30.—Aerial survey map covering an area of Michigan and Ohio.

FIGURE 31.—Aerial survey map covering an area of Indiana.
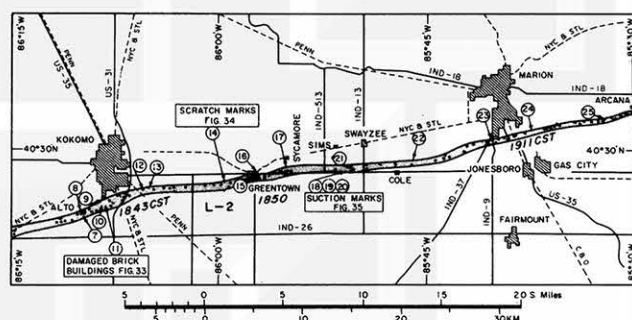
FIGURE 32.—Aerial survey map covering an area of Indiana.

eastward along almost identical paths. Since records of such tornado winds are very rare, meteorological analyses dealing with the computation of tornado winds are presented in section 8.

Another tornado left a damage path that started in northwestern Toledo. The width and destruction increased as the storm moved toward the Fuller's Creekside Addition about 2035 CST. It then moved out over the lake. Because of darkness, no reports on tornadic storms over Lake Erie were received.

The first damage of tornado L–1, shown in figure 31, was spotted southeast of Lafayette, Ind. This tornado was the first of six that covered a total distance of 274 mi in 4 hr 23 min, maintaining an amazingly constant speed of 62.5 mi hr^{-1}. Because of definite indications of weakening and redevelopment of the storm, the damage path east of US–29 was identified as that of L–2, a tornado that
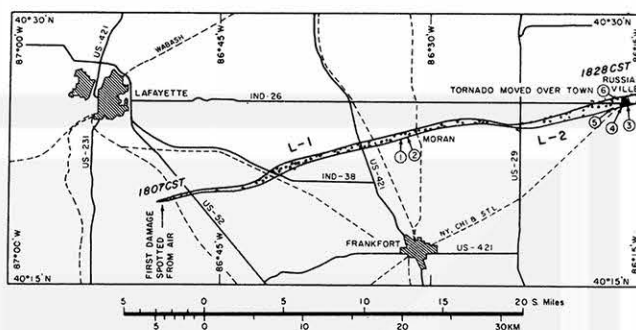
developed very rapidly and, moving directly over Russiaville, badly damaged the whole town and left a path ¾ mi wide.

The aerial photograph of the damage path of tornado L–2 (fig. 32) indicated that the entire community of Alto was demolished before the tornado moved to the south of Kokomo, Ind. Figure 33 shows eight brick apartments that suffered various degrees of destruction. The picture was taken facing south, with the tornado center moving from right to left near the top of the photograph. The southwest corner apartment was completely destroyed, probably down to the basement of this two-story building. The roofs of the northern buildings were lifted and probably smashed when they were blown against the others to the left. After completing destruction in southern Kokomo, the storm moved eastward, leaving a ½-mi path as far as the southern suburb of Marion, Ind. In Greentown, this tornado was reported to have dug the lawn out from many backyards. A scratch mark, probably made by a heavy object, was photographed in a field 2 mi west of Greentown (fig. 34). This picture was taken toward the south, with the tornado center moving from right to left through the center of the photograph. Note the difference between the trajectories of relatively light debris and of the heavy object that left a curved scratch mark extending from lower right to upper left.
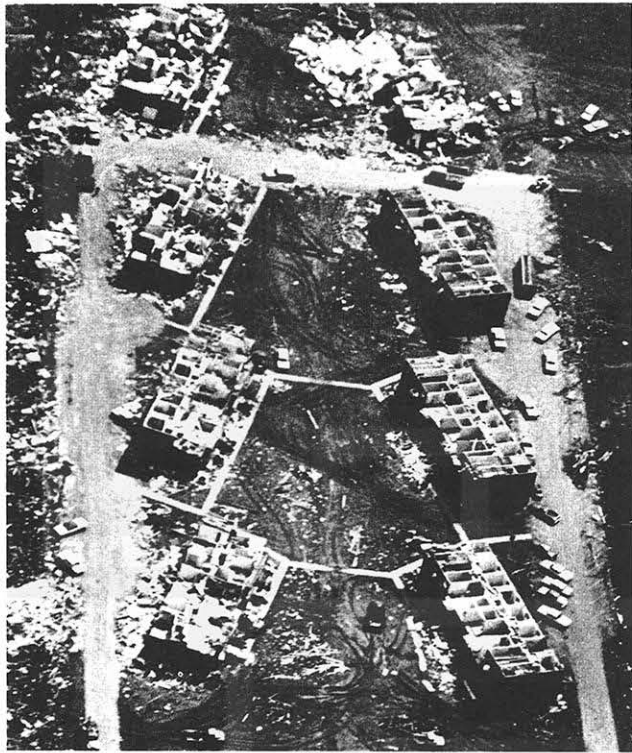
FIGURE 33.—Eight brick apartment buildings south of Kokomo, Ind., in various stages of destruction, ranging from loss of roofs to collapse of walls. Destruction occurred at 1843 CST on April 11; the picture was taken on April 16. For exact location refer to figure 32.

FIGURE 34.—Dark curved scratch mark of a heavy object extending from lower right to upper center, photographed over a field west of Greentown, Ind. Tornado L-2 moved over the field shortly before 1850 CST on April 11; the picture was taken on April 16. Note the difference in the direction of the scratch mark that forms an angle of about 20° from that of the debris. For exact location refer to figure 32.

FIGURE 35.—Aerial view, taken April 16, of suction marks at several points around the periphery of the funnel of tornado L-2 where localized suction was especially intense. The marks represent sandy soil loosened by the suction. The tornado moved over this area at about 1900 CST on April 11. For exact location refer to figure 32.

Standing in contrast to the black scratch mark in figure 34 is a group of white cycloidal marks photographed east of Greentown and shown in figure 35. In this picture, tornado L-2 is seen moving from lower left to upper right. Similar marks have been reported only twice in the past. The first ones near Scottsbluff, Nebr., were reported by Van Tassel (1955), who assumed that they were produced by an object trapped inside a tornado vortex scratching the newly plowed surface as it circled around the vortex center. The second ones were reported by Prosser (1964), who gave no explanation regarding the cause of the marks. For the aerial photographs of the L-2 marks, a 135-mm telephoto lens was used and the Cessna-310 was brought down to about 1,000 ft above the ground. Detailed examination indicated that the marks represented a high reflectivity of sandy soil loosened probably by the pressure effect of the tornado funnel that had dug out the lawns in Greentown a few minutes earlier. The fact that there were four to five cycloidal marks during one rotation of the funnel suggests the probable existence of the same number of suction heads attached to the periphery of the funnel. In section 8, the marks and their use in computing a 200-mi hr^{-1} wind are discussed in detail. In order to distinguish these marks from the scratch marks presented earlier, they will be referred to here as suction marks.

Figure 36 shows that the path of tornado L-3 was no more than ½ mi wide and was characterized by moderate damage to farms and trees in rural areas. A number of exploded farm houses were spotted from the air, though no unusual damage was found or photographed.
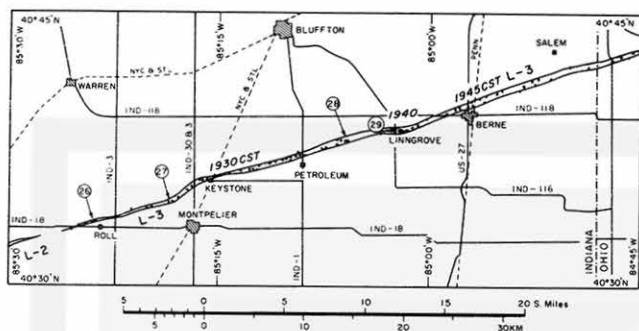
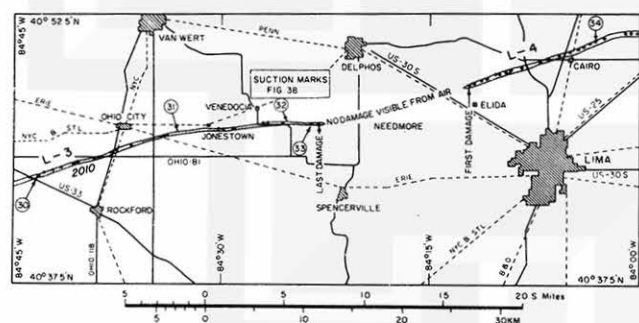FIGURE 36.—Aerial survey map covering an area of Indiana and Ohio.

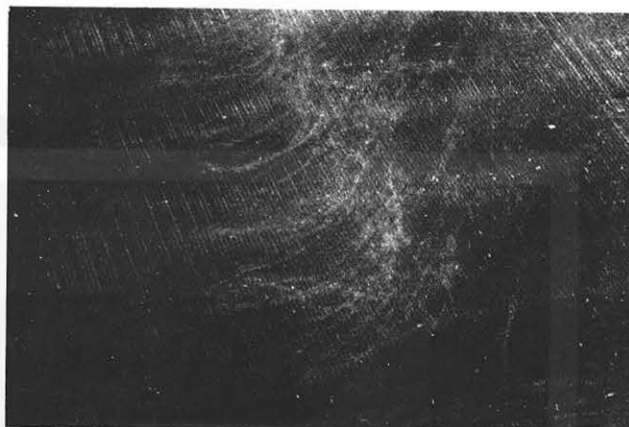FIGURE 37.—Aerial survey map covering an area of Ohio.

FIGURE 38.—Suction marks appearing 2 mi to the west of the last damage visible from the air. The tornado wind speed computed from these marks was 100 mi hr⁻¹. Time was about 2020 CST on April 11; picture was taken on April 16. For exact location refer to figure 37.
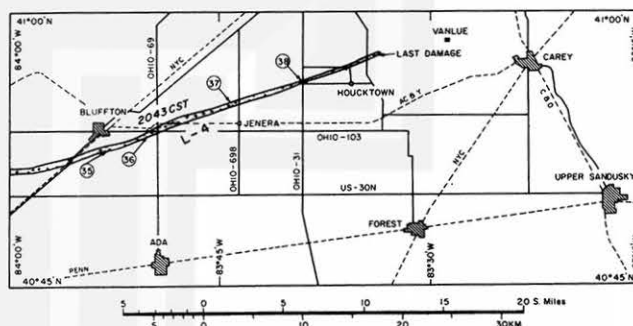

FIGURE 39.—Aerial survey map covering an area of Ohio.

Figure 37 shows the narrow damage path of tornado L-3 before its dissipation southwest of Delphos, where the well-defined suction marks shown in figure 38 were photographed. The wind speed of the tornado computed from these marks was about 100 mi hr⁻¹, indicating that it was still very high even at a spot only 2 mi from the last damage visible from the air. These particular marks and the wind-speed computation will be discussed separately.

The damage by tornado L-4 was first spotted east of US-30S, northwest of Lima, Ohio. The storm then continued beyond Cairo, Ohio. The damage was moderate to light.

Shown in figure 39 is the remainder of the damage path of tornado L-4. With a path width varying between ¼ and ½ mi, the tornado left typical explosive damage to structures and wind-blown debris. No funnel was sighted by local residents because of darkness. The last damage was spotted northeast of Houcktown, Ohio.

The 17-mi-long and ½-mi-wide damage path of L-5 is shown in figure 40. The first damage was spotted along Ohio-100 where considerable damage to barns was visible, but no farm residences next to the barns were destroyed. The heaviest damage to buildings was at Rockaway near

the intersection of Ohio-18, US-224, and the Pennsylvania Railroad tracks. Damage east of Rockaway gradually became spotty, disappearing near Ohio-162, 2 mi east of Omar, Ohio.

Figure 41 shows that the damage by the last tornado belonging to the L-family, L-6, was observed west-southwest of Pittsfield. A continuous damage path ½ mi wide ran through Grafton and the northern part of Strongsville. The damage to buildings in these two towns was moderate to severe. The path was visible almost to the Ohio Turnpike. The aircraft circled the area beyond the turnpike for almost 10 mi, but no damage was seen.

The damage path of M-1, shown in figure 42, started near Crawfordsville, Ind., gradually widening to 1 mi near US-52. East of this highway, northwest of Lebanon, Ind., a group of seven distinct marks was photographed. Figure 43 shows an overall view of these marks, with the
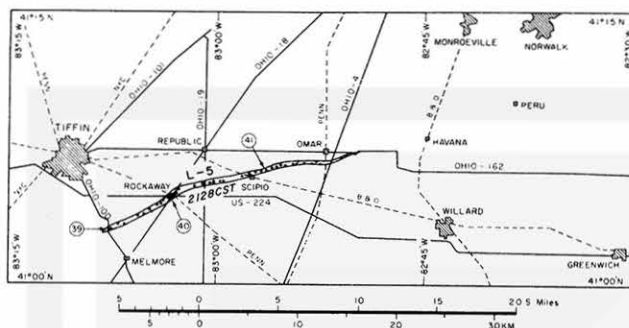
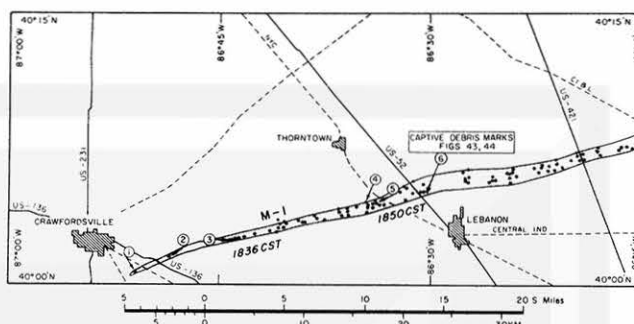FIGURE 40.—Aerial survey map covering an area of Ohio.

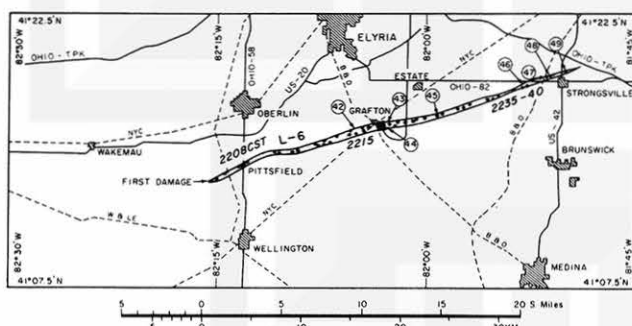FIGURE 42.—Aerial survey map covering an area of Indiana.

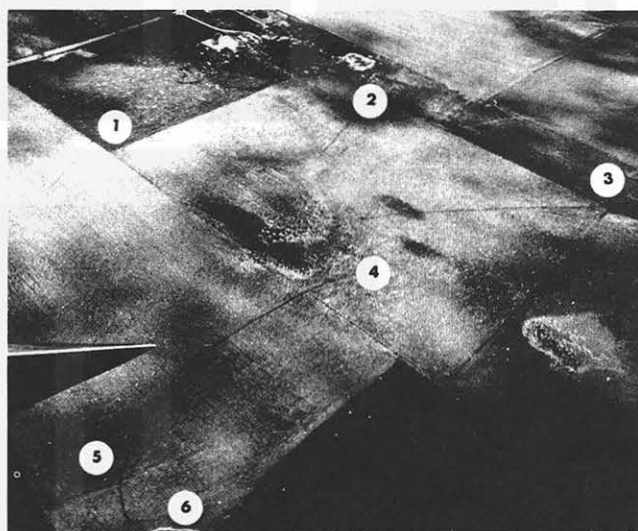FIGURE 41.—Aerial survey map covering an area of Ohio.

FIGURE 43.—Six scratch marks left on a plowed field after tornado M-1 had moved over the area northwest of Lebanon, Ind. The time of the tornado was about 1850 CST on April 11; picture was taken on April 16. For exact location refer to figure 42.

exception of the seventh one, and figure 44 shows enlarged views of marks 2, 4, 5, and 6. They appear to be what might be classified as captive debris marks, which are produced when flying debris, such as dried weeds, straw, corn stalks, etc., are caught by barbed and woven fence wire. The impact of the tornado winds upon this debris is sufficient to unfasten the wire from the fence posts or even pull up the post with the wire still attached.

Figure 45, the final survey map, includes the last 12-mi section of tornado M-1. The path became narrower after the tornado had crossed the CI&L Railroad tracks and was finally lost near Ind-19.

DAMAGE PATHS ASSOCIATED WITH TWIN FUNNELS

When an aerial photogrammetric survey of the damage by tornado J-2, which devastated the Midway Trailer Court (figs. 22 and 23) was taken, extremely severe damage could be traced along two paths that seemed to represent those of the twin funnels photographed by Huffman (fig. 24). Standing at the same spot between US-33 and the New York Central Railroad tracks about 0.7 mi from the Midway Trailer Court, Huffman took a series of six pictures, which, gridded with azimuths and elevation angles for every 10°, are shown in figure 46. The grid lines were computed after a visit to the photographed site by Fujita.

Huffman's site and the damage path are shown in the topographic map at the top of figure 47. His first photograph (fig. 46A) was taken looking almost due west. His second reveals a single funnel which in the third picture, when examined carefully, shows some evidence of splitting. The fourth one (fig. 46D) shows twin funnels on both sides of the highway, giving an impression that US-33 runs through a tunnel between the funnels. The fifth photograph very clearly indicates the patterns of stratified low clouds wrapping around the twin funnels, permitting us to determine the direction of both funnels to be identical and cyclonic. The patterns also give dimensions of circulation that are closely related to the tilt of the tornado axis. The best estimate of the tilt is 29° north-northeast.

In figure 47, the middle chart represents photogrammetric positions of the funnels appearing in Huffman's six
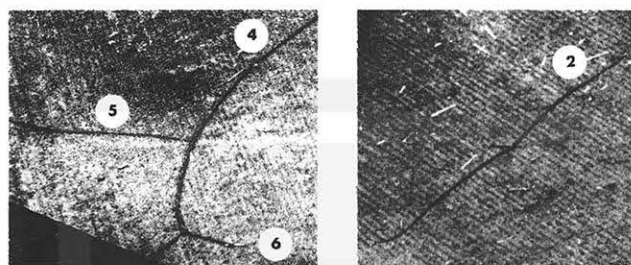
FIGURE 44.—Enlarged views of captive debris marks 2, 4, 5, and 6 as shown in figure 43. The dark triangular section in the lower left corner represents an area outside the film. Note a lumberlike object, probably a fence post, at the end of mark 6.

FIGURE 45.—Aerial survey map covering an area of Indiana.

pictures (fig. 46). Black circles designate the initial funnel touching the ground; the small circles, the complemental funnel that appears in the third picture. The sequence reveals that the funnel near the ground increased rapidly in diameter between the first and second pictures, then began splitting in two. After the split, the two funnels rotated about each other around their common center. The bottom drawing in figure 47 illustrates the rotation and the photographic directions.

The above offers a speculative explanation that the split in the funnel was caused by the rapid increase in the funnel diameter, while the tilt of the funnel axis was in excess of 30°. From the translational speed of the tornado, about 50 mi hr^{-1}, the estimated time intervals between successive pictures in seconds are: numbers 1–2, 17 sec; numbers 2–3, 27 sec; numbers 3–4, 13 sec; numbers 4–5, 8 sec; and numbers 5–6, 31 sec. Thus the increase in funnel diameter between the first and second pictures took place within no more than 17 sec. When a tilted column of rotating air increases its diameter very rapidly, the air parcels near the ground cannot move around the center. The motion beneath the tilted axis, especially, is restricted because of limited flow space and surface friction. As a result, the funnel may quickly take the shape of a shortcut circulation while the rest of the vortex starts forming another funnel. This began to occur at position 3, and when position 4 was reached, the initial vortex was dying out rapidly while the complemental vortex intensified. About 50 sec after the funnel had started to split, the twin funnels changed again into an almost single one at position 6, the entire process having taken less than 1 min.

Eyewitness accounts of double, or even multiple, funnels near Kokomo, Ind., were gathered through local newspapers. The *Kokomo Morning Times* of Apr. 13, 1965, indicated that at least three swiftly moving funnel-shaped tornadoes swept down across Alto (fig. 32). Some said they saw even more than three funnels touch the ground in a bounding motion and according to one witness the tornado had an unusually broad base, which appeared as if it had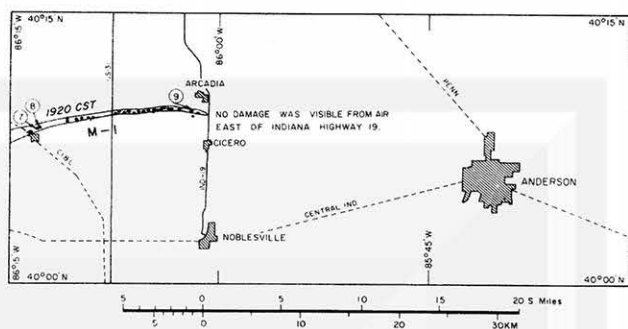 three or four spouts. When the storm was moving over southern Kokomo, a local resident spotted four funnels moving in approximately the same plane and in the direction of Greentown. He saw two directly over his house, with several hundred yards between them, and two others perhaps ¼ mi from the twin funnels. Twin funnels were seen also by several other witnesses, one of whom stated that the funnels came together and hovered over Greentown. A photograph of the suction marks (fig. 35), taken over a plowed field 10 mi east of Greentown, shows only one funnel.

Although it is extremely difficult to draw reasonable scientific conclusions from eyewitness accounts, unless they are supported by some photographic evidence such as that presented by Huffman, the structure of each tornado is so complicated and different that evidence of any kind should be gathered to permit construction of reasonable tornado models.

5. FEATURES AND MOTIONS OF THE RADAR ECHOES

For several years radar has been a basic tool in the study of the structure and motion of severe storms, including squall lines and tornadoes. It has been especially useful in research on tornadoes since the tornado can be readily identified by matching the location of the echoes it produces with damage paths, visual reports, and photographs. One of the earlier works on tornado motion in terms of echoes produced was Fujita's case study (1958) of the Illinois tornadoes of Apr. 9, 1953. A very detailed study of tornadoes with the use of radar was also made of the May 26, 1963, tornadoes near Oklahoma City by Browning and Fujita (1965).

Because the 1965 Palm Sunday tornadoes were so numerous and widespread and occurred over such a long period of time (approximately 11 hr), they provided the opportunity for making a detailed synoptic study based on radar data to determine the rate and direction of motion of the individual storms as well as the change in the features of individual echoes. For best available radar coverage before and during the outbreak of the numerous tornadoes on Apr. 11, 1965, radar film was obtained from the WSR–57 radars operated by the Weather Bureau
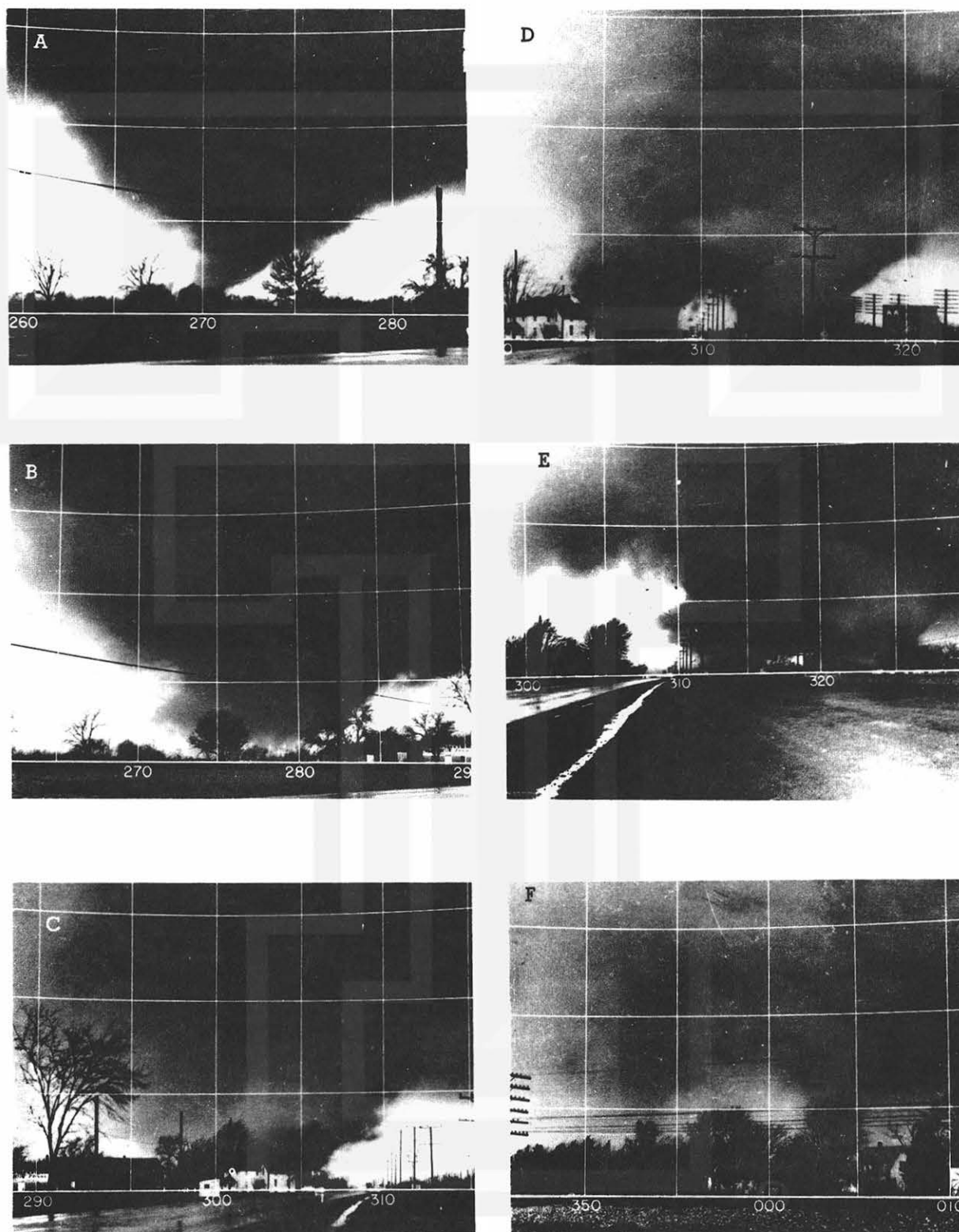
FIGURE 46—Series of six pictures taken by Mr. Paul Huffman, Staff Photographer of the *Elkhart Truth*, at about 1732 CST on April 11. For exact location refer to figure 22. (Courtesy of Mr. Huffman.)
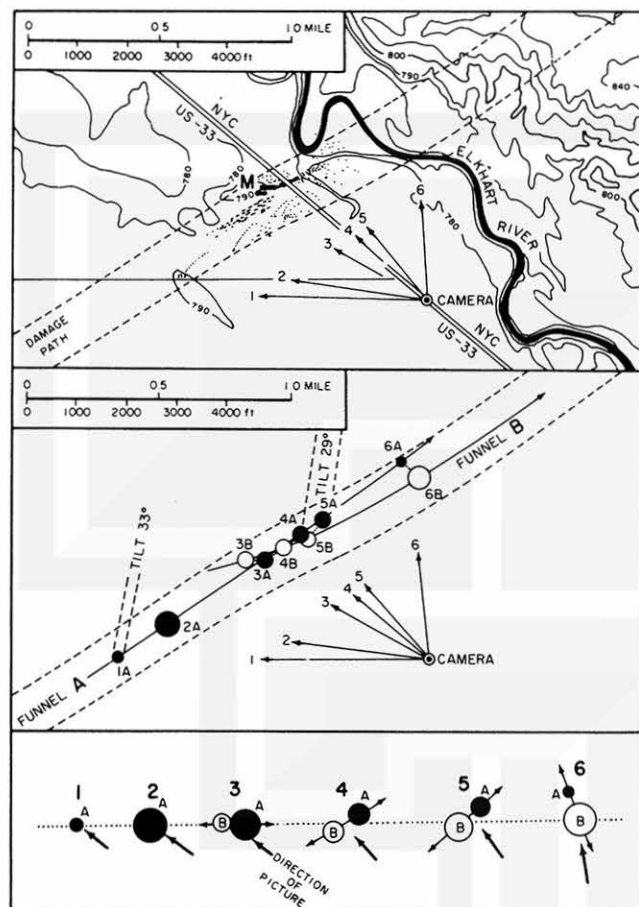
FIGURE 47.—Damage path and debris marks near the Midway Trailer Court indicated by letter M (top). Mr. Paul Huffman took six pictures (fig. 46) in the directions indicated by the arrows. The initial funnel shown by black circle A was overtaken by the complementary funnel B. Each photograph was from a direction perpendicular to the line connecting A with B as the twin funnels were moving over the trailer court.
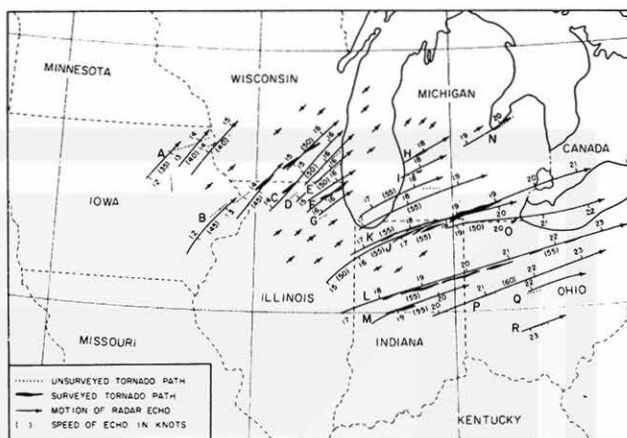

FIGURE 48.—Chart showing aerially surveyed and unsurveyed tornado damage paths. Long lines with arrowheads represent direction of motion of cyclone echoes, and short arrowheads are direction of motion of other echoes. The approximate time of occurrence (CST) is indicated at tick marks; numbers in parentheses are the average speed of the tornado cyclone echoes. Letters A, B, C, etc. designate the individual tornado families.

within range of the storm area, and from the radar at Selfridge AF Base, Mich., and the Illinois State Water Survey's CPS–9. The Weather Bureau stations included Minneapolis, Des Moines, Chicago, Detroit, Evansville, Cincinnati, and Akron. To follow the cloud echoes, traces were made from the film onto grids for each station at approximately 10-min intervals between the hours of 1100 and 2300 CST. Some of the radars were in operation during only part of this period, and as the storm approached the station the radar was changed over to short range. This made it somewhat difficult to obtain complete coverage of the entire area; however, in many cases the radar ranges overlapped and the area eliminated by one station was picked up by another.

TORNADO FAMILIES AND THEIR PARENT ECHOES

When all the radar data were combined with information gathered from eyewitness and newspaper reports

(section 3) and aerial surveys (section 4), the time and location of the various tornadoes and their damage paths were reconstructed as accurately as possible. In order to study echo motions, the locations of individual echoes were plotted on a base chart that included range markers for each radar station drawn as polar coordinates. In this manner the echo could be tracked from its inception to dissipation. Echo positions were matched with damage paths, thus separating the tornado-producing echoes from the nonproducing echoes. The tornado-producing echo paths were assigned an identifying family letter as shown in figure 48, which shows the damage paths of the individual tornado families, the paths of tornado cyclone echoes, and the approximate time of tornado occurrence.

The complicated pattern of echo paths, damage paths, and reported time of tornado occurrences over northern Indiana and southern Michigan made it somewhat difficult to match the echoes with times of tornado occurrence and the damage paths, partly because of the different elevation angles and gain settings of the various radars and the distance of the echoes from the stations. In several cases, two or more echoes followed each other on almost the same path 30 to 50 min apart. One such case is shown in figure 53a, which is a composite of radar pictures taken by the Illinois State Water Survey's CPS–9 at 2-min intervals between 1624 and 1714 CST. The first echo of family J was picked up by the Illinois State Water Survey radar (CMI) and Chicago Weather Bureau's WSR–57 (CHI–F) at approximately 1500 CST. By 1636 CST a new echo, family K, had formed in almost the same location where the echo of family J had been at 1550 CST. This second echo followed nearly the same path as the first but slightly to the left. This is verified by the fact that some areas experienced two tornadoes within less than 1 hr, and it also accounts for the especially
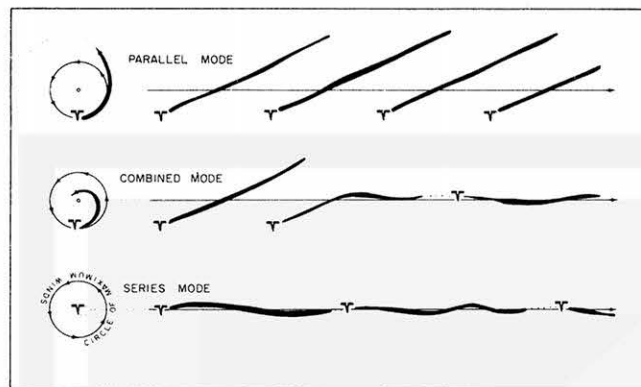
FIGURE 49.—Three modes of damage paths produced by a family of tornadoes.

FIGURE 50.—Chart showing 500-mb contours in meters and direction of motion of damage-producing (solid line arrow) and nonproducing (broken line arrow) echoes at 1800 CST on April 11. Solid circles represent position of tornadoes at the time.

wide damage path over southern Michigan where the two paths converged.

Comparing the paths of the cloud echoes with the damage paths (fig. 48), one can see that they do not exactly coincide. Surveys indicate that a family of tornadoes forming inside a tornado cyclone may do so in one of three modes: the parallel mode, the combined mode, and the series mode. Based on the damage surveys of the Scottsbluff tornadoes by Van Tassel (1955), the Fargo tornadoes by Fujita (1960), the Dallas tornadoes by Hoecker (1960), the Worcester tornadoes by Penn et al. (1955), the Blackwell tornadoes by Staats and Turrentine (1956), the Illinois tornadoes by Fujita (1958), and section 4 of this report, the positions of the tornadoes relative to the tornado-cyclone center are shown in figure 49. In this model of tornado paths, the parallel-mode tornadoes form mostly on the right side of the eye of a tornado cyclone and the series mode near the center of the eye. Of interest is the frequently observed change from the parallel mode to the series mode. No case in which a series-mode family changed into a parallel-mode family has been found, however, which would imply that the structure of a tornado cyclone—favorable for the production of a parallel-mode family—somehow changes into one likely to produce a series mode. Further study has indicated that the parallel-mode family forms out of storms in the development stage while the series-mode family forms out of storms in the mature stage. The reason is not yet known, but we may suspect that a concentration of vorticity around the center of a tornado cyclone takes place as the storm progresses from the initial through the mature stage.

RATE AND DIRECTION OF MOTION ECHOES ASSOCIATED WITH TORNADOES AND OTHER ECHOES

Fujita (1958) and Browning and Fujita (1965) have shown that as soon as a severe thunderstorm or tornado-cyclone cloud begins rotation, the echo tends to veer at an angle of about 25° from its original direction of movement or from that of other cloud echoes in the
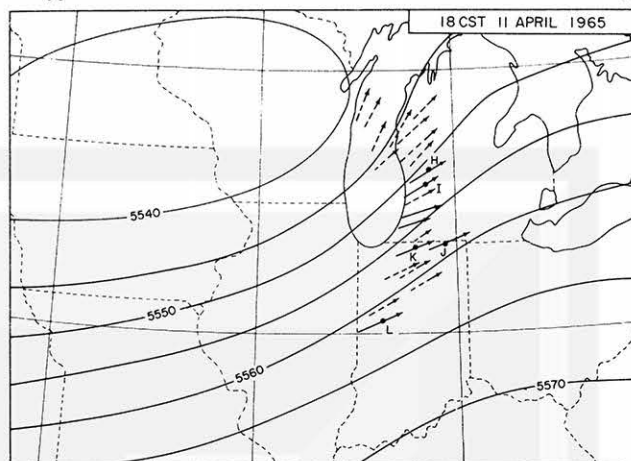
vicinity. Newton and Katz (1958) found that convective rain storms generally moved with an appreciable component to the right of the 700-mb wind direction. Newton and Fankhauser (1964) also found that severe weather phenomena tend to follow a path to the right of the direction of the middle tropospheric winds.

The only upper wind data available during the entire period of the tornadic activity on Palm Sunday 1965 were obtained at 1800 CST. At or near this hour, at least five tornadoes were in existence. Figure 50 is a chart showing the contours at the 500-mb level and the direction of movement of all trackable radar echoes during a 40-min period centered at 1800 CST. The tornadoes occurring at this time are indicated by the solid circles. In all echoes their motion was to the right of the direction of the 500-mb winds, but the degree of veering was not the same in all cases. The maximum angle of veer was approximately 22°. Echoes that did not produce tornadoes or intense damage-producing thunderstorms moved generally in the direction of the streamlines of the 500-mb winds.

Between 1200 and 1500 CST, the average movement of the dry cold front in the area of the tornado outbreaks was between 35 and 40 kt (fig. 51), while that of the echoes was between 40 and 45 kt. The echoes and the resulting tornadoes and severe thunderstorms appear to be closely associated with the advancing dry cold front. However, the individual echoes could not be tracked for more than approximately 1½ hr and on the average for slightly less than 1 hr. The tornado damage paths were relatively short and interrupted.

Between 1500 and 1800 CST, the average rate of movement of the dry cold front in the area with tornado outbreaks was around 40 kt, while that of the echoes was between 55 and 60 kt. Hence the echoes moved much ahead of the cold front which, as it advanced, would
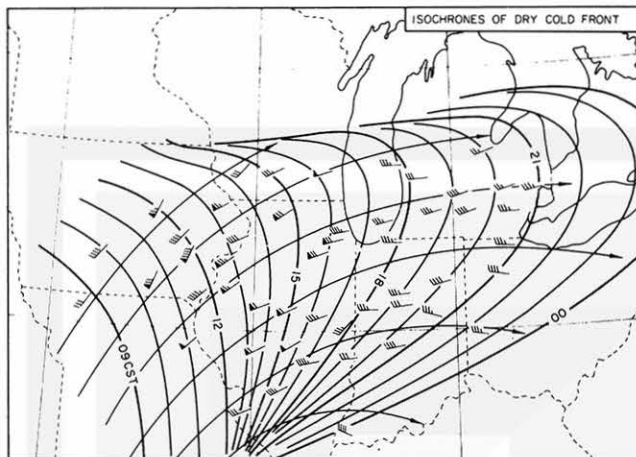
FIGURE 51.—Isochrones of the dry cold front are represented by heavy solid lines. Plotted surface winds (1 full barb=5 kt) are those reported after the wind shift that accompanied the frontal passage. Fine lines with arrowheads represent the streamlines of the winds.
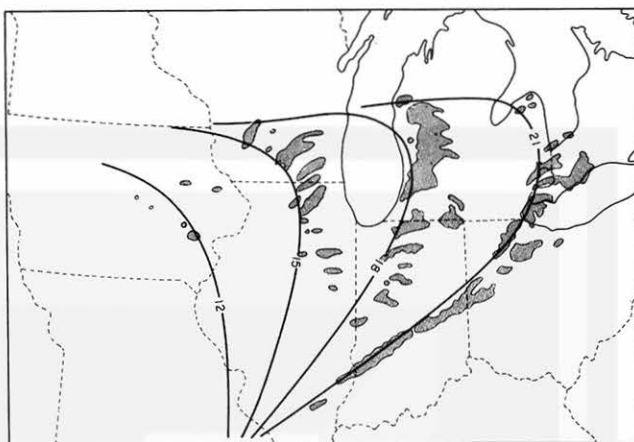

FIGURE 52.—Three-hour positions of the dry cold front are indicated by heavy solid lines. Stippled areas are radar echoes associated with the advancing front.

initiate another series of echoes that would follow almost the same path as the first echoes.

Between 1800 and 2100 CST, the maximum forward motion of the dry cold front had increased to approximately 50 kt, while the echo speed remained between 50 and 60 kt. Thus by 2100 CST, the line of echoes and the front were nearly coincident as the severity of the storm began to decrease. Figure 52 shows the position of the dry cold front and the radar echoes in the vicinity of the front at 3-hr intervals between 1200 and 2100 CST.

CHANGES IN FEATURES OF RADAR ECHOES

As stated previously, isolated radar echoes of the intense storms could be followed over a long period of time. After an echo had been detected on radar, it grew quite rapidly, but after reaching maximum intensity, its shape usually changed more markedly than its size. Figure 53 is a composite of the radar pictures taken by the Illinois State Water Survey's CPS-9 between 1624 and 1714 CST on long range and between 1716 and 1820 CST on short range. The film sequence of echo family J (fig. 53a) begins at 1624 CST (1 hr 24 min after the first echo had been detected on radar), when the echo was near its maximum size and was beginning to form a hook. The hook is clearly outlined by 1638 CST but maintained this shape for only a short time. The first funnel touchdown from this echo was reported at 1645 CST.

The rapid growth of echo family K from the time of detection at 1636 to hook formation at 1712 CST can also be followed in figure 53a. Here again, the hook was observed about 10 min before the first funnel was reported.

The CPS-9 was then shifted to short range (fig. 53b), and the echoes of families L and M were observed until 1820 CST. Both appeared to pass through the same metamorphosis from first detection on radar to maximum development. One interesting feature is the splitting of
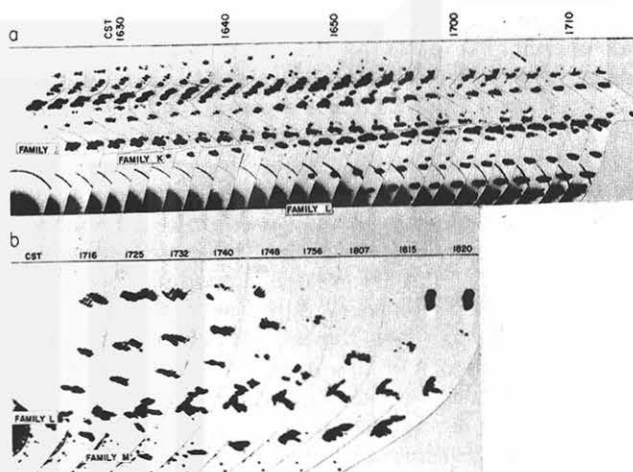

FIGURE 53.—Composite of radar pictures from the Illinois State Water Survey's CPS-9; (a) on long range at 2-min intervals between 1624 and 1714 CST, (b) on short range between 1716 and 1820 CST. Significant features are the almost identical paths followed by family J and K echoes and the hook echoes forming 40–50 min apart in almost the same location.

family L around 1730 when the original echo continued to move in the same direction while the separated part moved to the left and dissipated by 1820 CST.

Of the radar pictures from the various stations chosen for this report, several had nearly constant range, gain setting, and elevation angle over a relatively long period of time. One example is the film from Akron, Ohio (CAK), of which figure 54 shows a composite on long range between 2027 and 2150 CST and on short range between 2155 and 2225 CST. Figure 54a illustrates the growth and change in features of four echo families during a period of approximately 1½ hr. One interesting feature is the space interval of about 50 mi between the strong
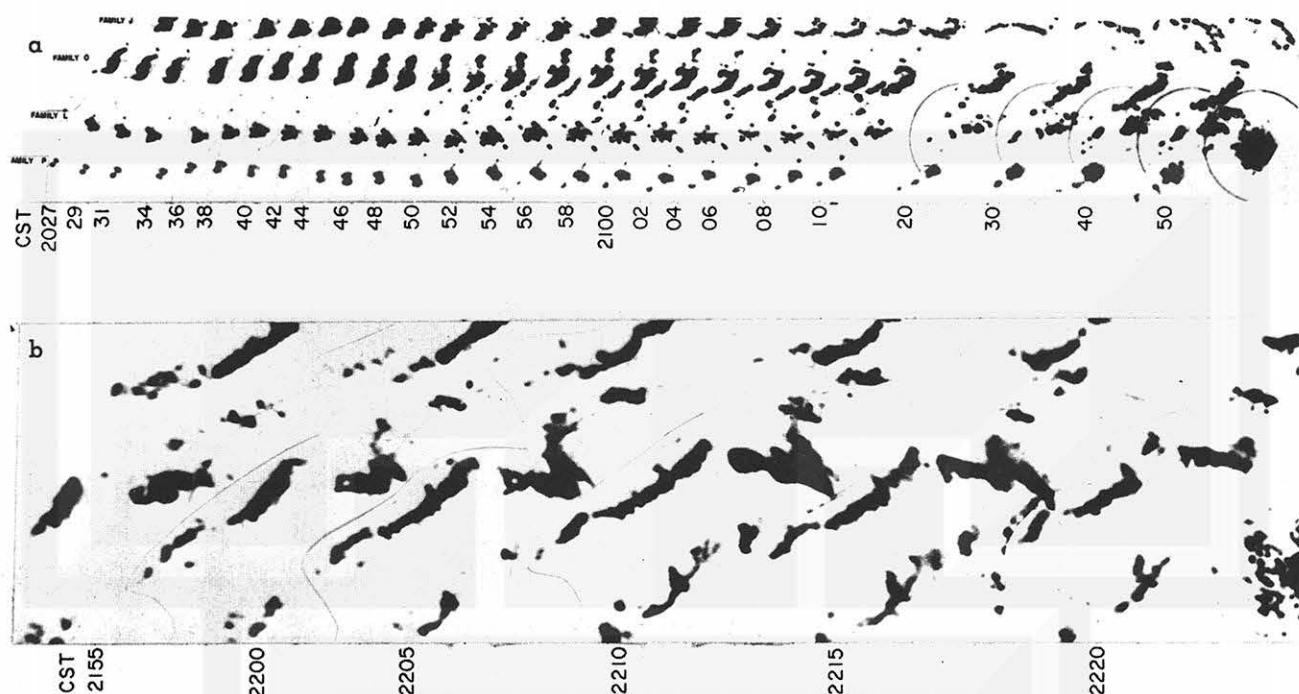
FIGURE 54.—Composite of radar pictures from Akron's Decca 41 (CAK) on Apr. 11, 1965; (a) change in the features of the echoes of four tornado families on long range between 2027 and 2150 CST, one outstanding feature being the almost simultaneous and almost identical change in the echoes of families J and O between 2050 and 2110 CST; (b) the tornado eye, which appears as the clear spot in the echo near the 40-mi range marker, on short range between 2155 and 2220 CST.

echoes, which suggests that the severe storms suppressed the growth of any other convective activity within a range of 20 to 25 mi. Another is the simultaneous and almost identical change in the echo families J and O between 2050 and 2110 CST. At 2155, station CAK changed to short range and figure 54b shows some features of the echo family L as it neared the station. Most significant here is the clear spot or eye that can be seen between 2200 and 2205. The echo exhibited a hook at 2155 but changed to a clear eye by 2200 CST. This tornado's damage path extended from a point south-southwest of Oberlin to Strongsville, Ohio (fig. 41).

Time-space series of cloud echoes such as the above are a valuable aid in the study of the development of severe storms. As the number of radar stations increases, it is hoped that similar sequences will be obtained on days with numerous tornadoes for comparison of succession of events leading to development of severe storms.

6. EARLY STAGE OF TORNADO DEVELOPMENT AS REVEALED BY SATELLITE PHOTOGRAPHS

About 20 min after the first tornado had been reported in northeastern Iowa, TIROS IX, in northbound semi-polar Pass Number 960, took pictures of the Midwestern United States. Although the area of tornado formation was too far from the exposure subpoint to be examined in detail, a vast region of southwesterly flow behind the cold front extending from Iowa to Arkansas was photographed

with relatively small nadir angles. Frames 9 and 10, exposed at 1242.3 and 1241.3 CST, respectively, showed the best coverage of the areas of interest. These were gridded as precisely as possible with the use of the graphical method developed by Fujita (1963) and are shown in figures 55 and 56 with State boundaries superimposed. The nephanalysis chart in figure 57 was made by transposing the cloud patterns from the two frames, gridded with 1° geographic grids. Echoes obtained from the WSR–57 radar photographs taken at the Minneapolis, Chicago, and Detroit Weather Bureau stations were added to this chart.

SIGNIFICANT CLOUD FEATURES ON SATELLITE PHOTOGRAPHS

One significant feature in figures 55, 56, and 57 is the large tongue of clear area extending from New Mexico to Missouri and the faint streaks stretching from the Oklahoma Panhandle to southern Kansas. This area and the very dry air mass B, as shown in the isodrosotherm chart (fig. 58) cover the same geographical area.

Before these and other cloud features in the satellite pictures were interpreted, the visibility, cloud type, and cover charts were analyzed. In figure 59, contours are drawn for every 2 mi to show those areas where visibility was obstructed due to smoke (K), fog (F), haze (H), dust (D), and precipitation near the ground. Either fog or fog mixed with drizzle (LF) is seen practically everywhere inside the moist cold air mass C. In some spots, fog restricted visibility to 1 mi. Inversion-trapped haze and
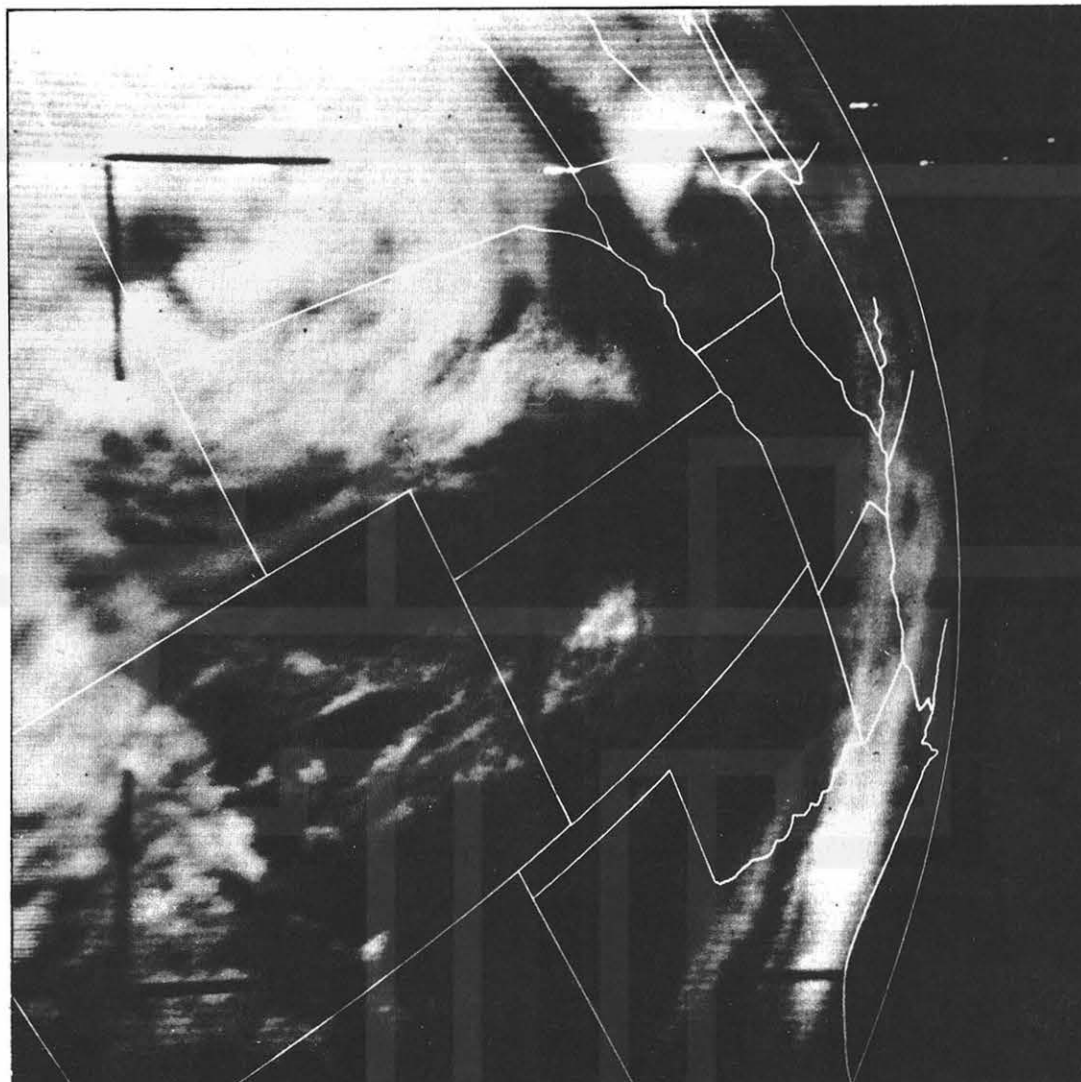
FIGURE 55.—TIROS IX picture (Pass 960, Frame 9), exposed at 1242.3 CST on April 11, showing clear areas behind the dry cold front Photogrammetric data: $H = 801$ km, $\phi^{TSP} = 42.4°$ N., $\theta^{TSP} = 112.7°$ W., $\alpha^{PP} = 116°$, and $\tau = 35.6°$. (ϕ^{TSP} is subsatellite latitude; θ^{TSP}, subsatellite longitude; α^{PP}, azimuth of principal line; τ, tilt of picture.)

smoke were reported from six stations on the downwind side of the Detroit area. The relatively low visibility inside the mesohigh E is mostly due to fog caused by early morning shower activity.

The warm sector A is free from fog and the visibility is more than 7 mi in almost the entire area. With the exception of the northernmost area, visibility inside the warm sector increases near the dry cold front. To the west of the front it increases from 10 to 15 mi, and might have been even greater if more distant ground objects had been available to the observers. Behind the dry cold front, a zone with over 15-mi visibility extends about 150 mi. West of this zone is an area that has low visibility, down to 2 mi, mainly because of dust (D) and blowing dust (BD). This area is extremely large and is seen in the satellite pictures as the faint streaks stretching from the Oklahoma Panhandle to Kansas.

Because these are the first satellite pictures (figs. 55 and 56) of large dust storms over the Midwestern United States, some questions might be raised regarding the reflectance of dust clouds. Satellite pictures often show dust clouds extending from desert regions to nearby ocean surfaces. In such cases, they are easily distinguished against the dark ocean background. Over the Midwestern United States, however, relatively large ground reflectance makes it very difficult to detect dust clouds unless they are very dense and extend to high altitudes. Based upon the isentropic analysis presented in the section that follows, the top of the dust clouds under discussion was estimated to be about 9,000 ft above ground.

The cloud chart (fig. 60) was made by plotting surface reports at 1200 CST. Cloud covers N_h and $(N - N_h)$ were entered inside each station circle as painted and hatched areas, respectively. Conventional cloud symbols are
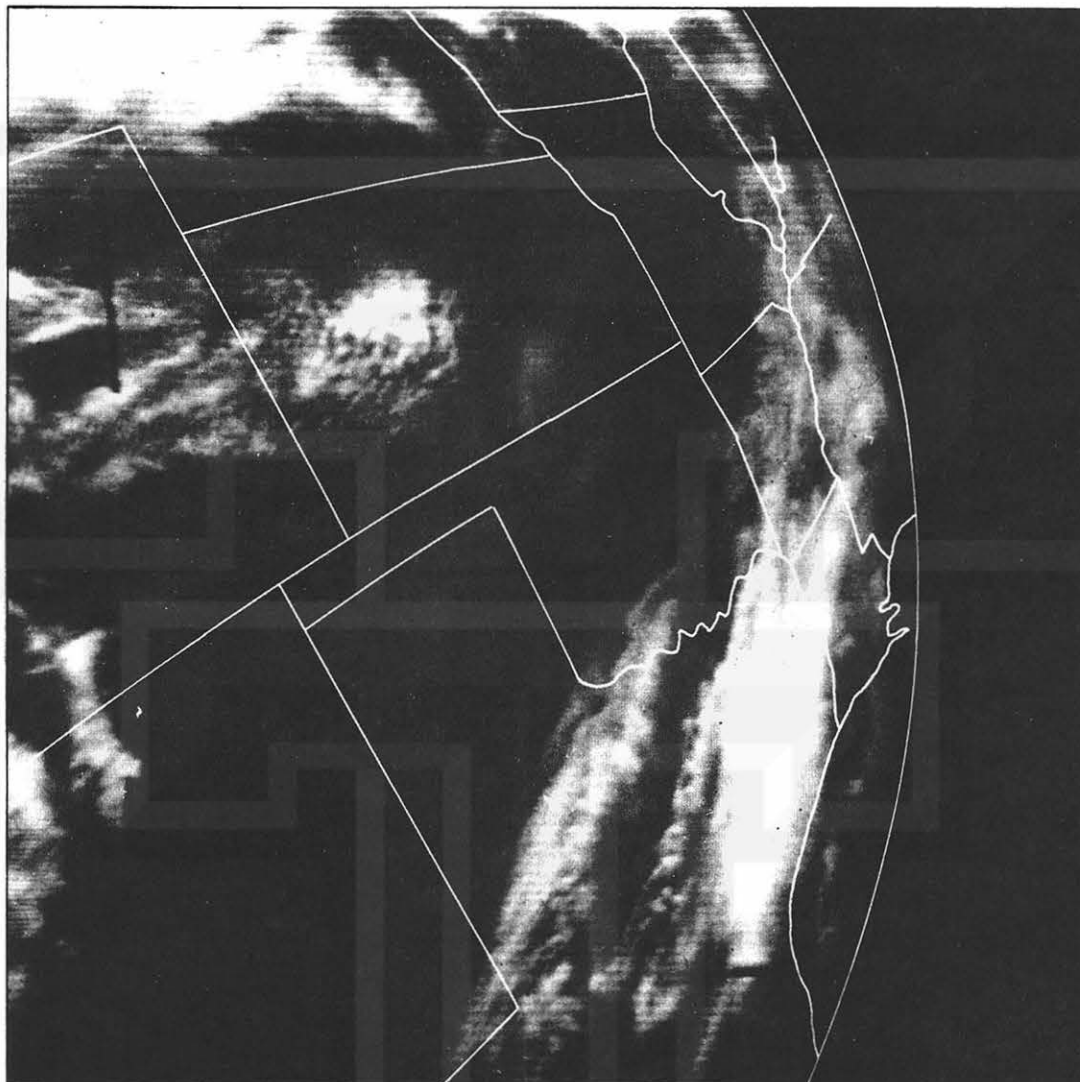
FIGURE 56.—TIROS IX picture (Pass 960, Frame 10), exposed at 1241.3 CST on April 11, showing dust storm inside the clear area. Photogrammetric data: $H = 778$ km, $\phi^{TSP} = 38.4°$ N., $\theta^{TSP} = 113.7°$ W., $\alpha^{PP} = 116°$, and $\tau = 38.0°$. (See fig. 55 for details.)

used, except for T, which refers to towering, and the double subscripts C_{ti}, C_{ss}, which represent thick cirrus and cirrostratus clouds, respectively. A polar jet stream extends from southwest to northeast, and a large area of jet-stream cirrus is seen in Texas south of the jet stream. Another area of cirrus extending from Louisiana eastward seems to be associated with shower activity along the southern end of the dry cold front.

The stippled area in the northern part of the neph-analysis chart represents low stratus overcast mixed with fog. A band of stratocumulus cover extending from Louisiana to Ohio corresponds to the tongue of moist air transported from the Gulf of Mexico by a strong low-level jet with up to 50-kt winds. From the early morning of April 11, several mesoscale convective activities took place, leaving areas of low stratus and stratocumulus

over northwestern Louisiana, southwestern Tennessee, and southern Ohio.

The stations within the area of faint cirruslike clouds seen in the satellite pictures (figs. 55 and 56) reported dust. None reported cirrus or cirrostratus, which eliminates the possibility that the faint clouds consisted partly of high clouds. Note that the northwestern tip of the dust area is bent along the moist cold front as shown in figure 60.

A southwest-northeast cloud line in central Missouri was reported to consist of towering altocumuli extending from Springfield, Mo. Their bases were between 8,000 and close to 9,000 ft above ground, suggesting that they formed near the top of the unstable dry air behind the dry cold front. Due to the extremely low mixing ratio in this air mass, most of the stations reported clear. If we assume an increase in the surface dew-point temperature
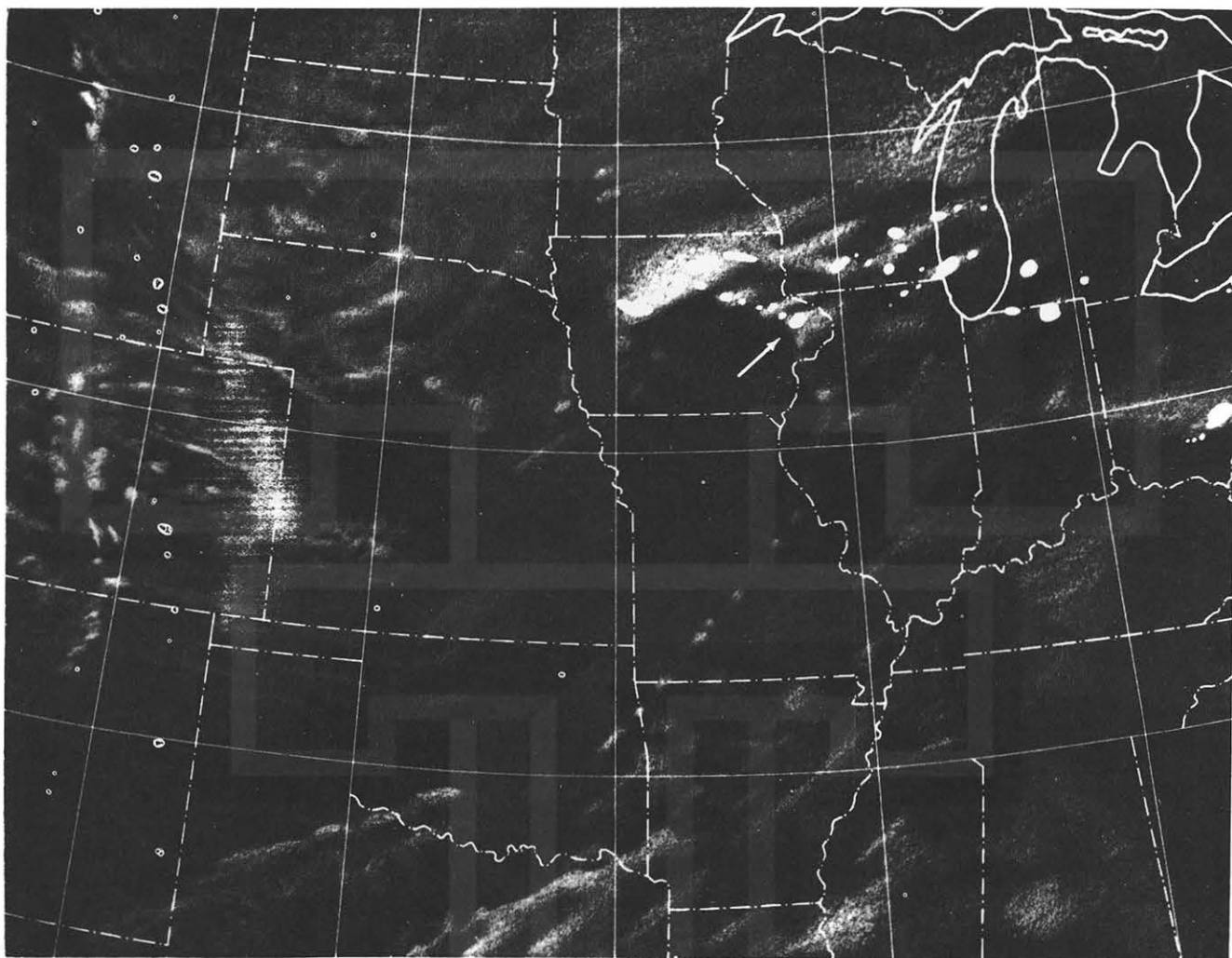
FIGURE 57.—Nephanalysis covering Midwestern United States at 1240–1248 CST on April 11. The echo that produced the first tornado, about 20 min earlier in Iowa, is indicated by an arrow. White spots are radar echoes obtained at the time the satellite pictures were taken.

by 10°C, it is quite feasible that high-base cumuli or altocumulus castellanas were created near the top of the stable layer that characterizes this air mass. Since the orientation of the cloud line is identical to the direction of the mean winds below 9,000 ft, we may indeed assume that a number of artificial lakes and large areas of forest in the Ozark Mountains gave rise to the increment of low-level moisture required to form high-level convective clouds.

East of the dry cold front, the isentropic surfaces intersecting the ground along these isentropes slope up toward the north and northeast. Inside the dome behind the dry cold front, however, the isentropic surfaces are the vertical walls above the isentropes. Because these walls are no longer vertical beyond the dome top, the isentropic flow inside the dome should be limited within them, and air may freely move up and down the walls, bringing about

large-scale vertical mixing as it travels eastward. A vertical cross-section of potential temperatures and winds along the 297°K isentrope inside the dome and its extension outside the dome illustrates this motion (fig. 63). Since this vertical cross-section, extending from Tucson to Buffalo across the Rocky Mountains, includes a vertical wall of 297°K isentropic surface inside the dome of dry cold air mass, we may assume that the air mass was unstable and almost vertically mixed as it traveled from the Southwest arid region to the Midwest. As expected, the dome top was highest over the Rockies, sloping down toward the east. The dust cloud seen in the satellite pictures may have extended to the top of the dome, some 9,000 ft above ground, which probably partly accounts for its presence in these pictures.

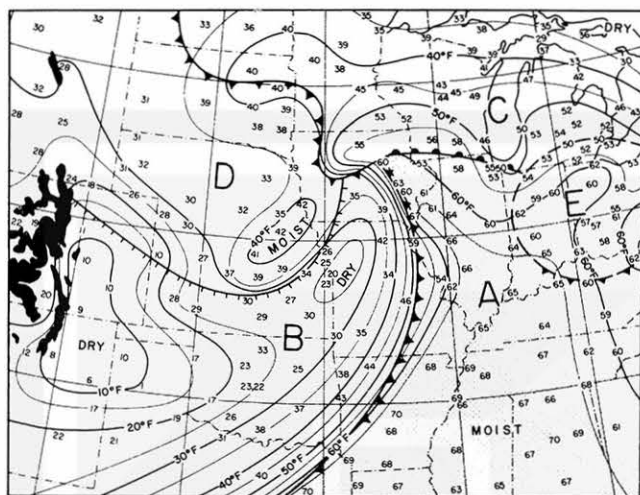The dome of isentropic air was topped by a stable layer about 3,000 ft thick. Within this layer, wind speed in-

FIGURE 58.—Isodrosotherms at 1200 CST on April 11, contoured for every 2°F. Areas of air temperature above 60°F are stippled.
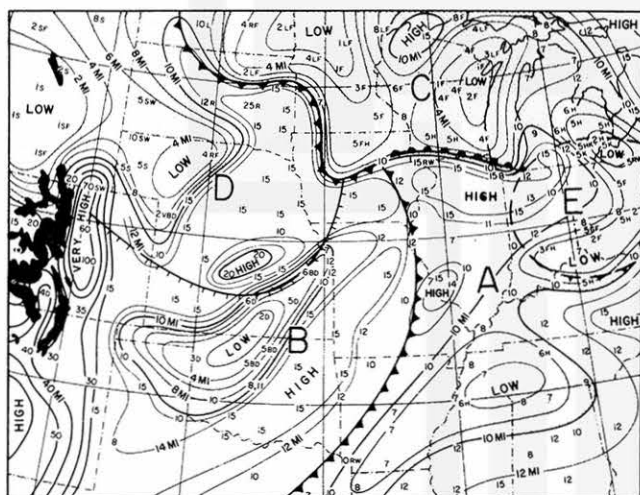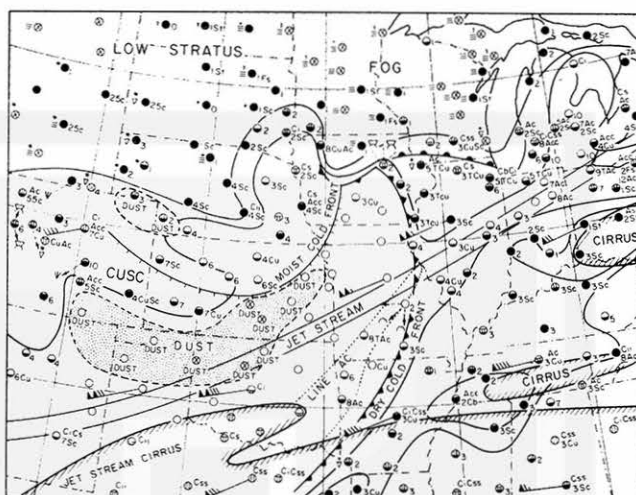

FIGURE 60.—Cloud chart for 1200 CST constructed on the basis of surface reports. The covers of low and other clouds are shown in each station circle by black and hatched areas, respectively. Numbers preceding cloud types indicate the cloud base in 1,000 ft. Entered with conventional symbols are 300-mb winds for 1200 CST.
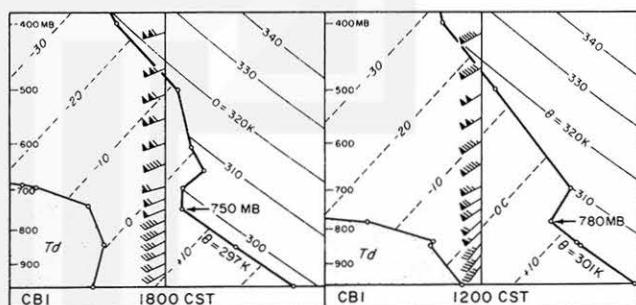

FIGURE 59.—Visibility chart for 1200 CST on April 11, contoured for every 2 mi with thin contours and for every 10 mi with heavy contour lines. Areas of visibility lower than 10 mi are stippled.

FIGURE 61.—Soundings from Columbia, Mo., made at 1200 and 1800 CST on April 11. Note increase in height of the deep isentropic layer above the ground. Soundings were made inside the dry cold air mass in which the isentropic surfaces are curved vertical walls.

creased to about 100 kt, while the leading edge of the dome or the dry cold front was moving eastward at about 50 kt, resulting in a significant downslope motion of midtropospheric westerlies above the dome.

STRUCTURE OF A DRY COLD AIR MASS

Studies of satellite photographs including nephsystems that produce severe storms are relatively few in number, but Whitney and Fritz (1961), Fujita et al. (1963), and Whitney (1963) have shown that nephsystems in their stages of severe-storm formation are characterized by a massive appearance, mostly elliptic but sometimes square-shaped. The reason is that anvil clouds produced by each of the cumulonimbus clouds spread over considerable areas, forming a large oval-shaped boundary when viewed from satellite altitudes. Satellite photographs taken approximately at the onset time of the Palm Sunday tornadoes (figs. 55 and 56) revealed a large tongue of clear area behind a line of expected tornado formations. The nephsystems were not as extensive as reported in the studies referred to above, with the exception of a large cloud area from which no tornadoes were reported, mainly because the pictures were taken around local noon when nephsystems are still in their early stages of development. The tongue of clear area should be investigated in detail as a cause of the intense convective activity that gave rise to the development of an unusual number of tornadoes.

Soundings from Columbia (CBI), Mo., at 1200 and 1800 CST, 3 and 9 hr after the dry cold front had passed, are shown in figure 61. A common but important characteristic in these soundings is the deep layer of dry-adiabatic
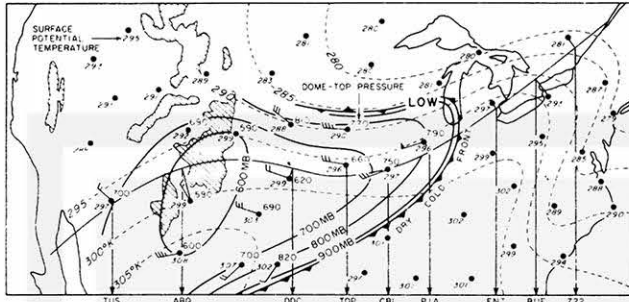
FIGURE 62.—Topography of the top of the dry cold air mass at 1800 CST on April 11. The highest portion of the dome is seen over the Rocky Mountains in Colorado. Winds represent the vector mean of wind velocities inside the dry cold air. The potential temperatures at the ground are entered by each station in °K. A vertical cross-section in figure 63 was drawn along a curved line extending from Tucson to the vicinity of Buffalo.
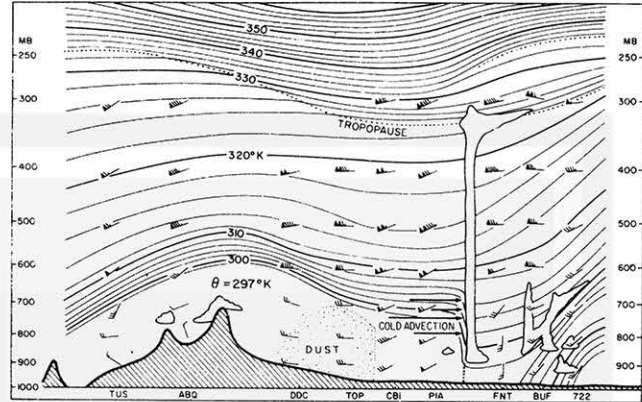

FIGURE 63.—Vertical cross-section along the 297°K isentrope and its extension outside the dry cold air at 1800 CST on April 11. There was little temperature difference on either side of the dry cold front between Peoria and Flint. Due to a steep lapse rate to the west of the front, significant cold advection is seen near the 700-mb surface below a stable layer topping the isentropic flow from the west.

lapse rate topped by a rather stable layer in which a 10°C rise in the potential temperature was observed. In other words, the entropy below 780 mb at 1200 CST was practically constant and expressed by 301°K. Six hours later, the top of the 297°K isentropic layer was at 750 mb, indicating a slight lifting.

When the pressures at the top of the isentropic layer behind the dry cold front were plotted in figure 62, a dome of isentropic air mass reaching 580 mb over New Mexico was found. The contour lines of this dome and the mean wind velocities inside it reveal that the air originated over the southwest desert region and was drawn into the southwestern sector of a well-developed continental cyclone centered in southern Wisconsin. It is important to realize that the entropy is constant along the vertical anywhere within the dome. In horizontal directions, however, the entropy varies between a high of 308°K at El Paso and a low of 288°K at North Platte. The dashed lines in figure 62 are the isentropes of the surface potential temperatures drawn for every 5°K.

Because of the dry-adiabatic lapse rate inside the dome west of the dry cold front and the rather stable lapse rate inside the warm sector ahead of the front, the temperature difference between the warm moist and the cold dry air increased more or less in proportion to the height above the ground. At the dome top at about 700 mb, the temperature was about 5°C lower than the warm moist air east of the dry cold front. In terms of virtual temperature, the dome was about 6°C lower.

When the cold air near the top of the dome was advected eastward at the rate of about 50 kt, it ran over the warm moist air, creating a superadiabatic lapse rate within the warm air just ahead of the leading edge of the dome. The warm moist air then overturned quickly along the leading edge of the top, initiating vigorous convection along the line. The surface dry cold front was not necessarily located directly beneath the leading edge of the dome, which was usually seen 10 to 50 mi east of the former.

The concept of cold advection as well as warm advection in relation to severe-storm development has been discussed

by Fulks (1951), Winston (1953), Sugg and Foster (1954), and Whitney and Miller (1956), among others. The situations they studied involved rather moderate horizontal transport of cold air aloft and/or warm air below and a resulting significant change in stability. In the Palm Sunday storms, however, cold advection took place near the top of the dome of dry cold air as it plowed rapidly eastward, with a dramatic overturning occurring along the leading edge of this air.

7. STABILITY AND DIFFERENTIAL ADVECTION ASSOCIATED WITH TORNADO DEVELOPMENT

The thermodynamical and dynamical structure of the atmosphere that gives rise to vigorous thunderstorms is not yet fully understood. The thunderstorms forming over the Midwestern United States, especially under certain meteorological conditions, are so severe that they overshadow cellular convective clouds scattered above the heated ground. When an isolated thunderstorm or a group of thunderstorms reaches its mature stage, its mesoscale environment is modified, so that small cellular convective clouds around the major storms are considerably suppressed.

In view of the fact that the circulation of a mature thunderstorm is far different from that of a small air parcel rising inside the atmosphere at rest, the use of the so-called "parcel method" should be restricted to small or young clouds that might grow into thunderstorms.

Since the computation of buoyant energy on an adiabatic chart is rather time-consuming, Showalter (1953) proposed a stability index that can be computed from temperature and humidity values on an 850-mb chart and from 500-mb temperatures. The index is based upon the parcel method and is computed by lifting a parcel at the 850-mb surface dry adiabatically to saturation and then moist adiabatically to the 500-mb surface. The

algebraic difference between the temperatures of the lifted parcel and its environment is called the Showalter stability index (SI), the negative value of which indicates instability. Because the index is based on the parcel method, interpretation on a synoptic map is meaningful only over the region away from thunderstorms. Nevertheless, the areas of the SI above +6°C may be regarded as convectively stable, and unusually severe thunderstorm activity may be expected over the region of the SI that is −4°C or lower.

The SI is very easy and quick to compute, since it requires only the 850- and 500-mb charts. However, it occasionally misrepresents the stability of the atmosphere when the source of the moisture to be drawn into a convective cloud is located below the 850-mb surface. When the top of the moist layer is very close to the 850-mb surface, the SI is so sensitive to the height of the moisture top that its interpretation requires a knowledge of the vertical distribution of the moisture below this surface.

For a more realistic stability index based upon the parcel method, Galway (1955) and Winston (1956) proposed the use of a low-level moist layer for lifting. The Severe Local Storm Center unit in Kansas City now uses the mean mixing ratio and the mean potential temperature of the lowest 3,000-ft layer as those of the parcel, which is lifted to the 500-mb surface, first dry adiabatically to saturation and then moist adiabatically. The algebraic difference between the temperatures of the lifted parcel and its environment is called the lifted index (LI). It can be computed whenever radiosonde data are available below 3,000 ft and at 500 mb. Because of the diurnal variation of the air temperature and the mixing ratio within the atmosphere near the surface, the vertical distribution of the air temperature and the mixing ratio have to be forecast for the time of day when the development of severe local storms is predicted. The atmosphere to be lifted for the LI computation would then represent the thermodynamical characteristics at the time of storm formation several hours later.

In practice, however, it is rather difficult to predict three parameters: 1) the mean potential temperature of the lowest 3,000-ft layer, 2) the mean mixing ratio of the same layer, and 3) the 500-mb temperatures required for the LI computation. The computation is therefore usually performed on an adiabatic diagram on the basis of the forecast surface temperature or the forecast surface potential temperature, with both 2) and 3) kept constant.

THE BEST LIFTED INDEX (BLI) AND PRESSURE OF BEST LIFTING (PBL)

As stated above, the LI for each station at the time of predicted severe-storm formation can be computed from the three predicted parameters referred to above. Parameter 3) is closely related to the 500-mb advection, while 1) and 2) vary because of low-level advection and diabatic heating and cooling. The Showalter index, as we have seen, is computed without any predicted values, but the computation of the LI requires at least the predicted surface temperature.

Because it is difficult to obtain a realistic value for the stability of the atmosphere at the time of severe-storm development, an attempt was made to define a LI that could be computed from the measured upper air data without short-range forecasting of selected parameters. The field of the indices thus obtained would represent the instability at the time of the upper air observation, which does not always coincide with the time of storm development. The prediction of the SI field should be made after the field for the sounding time has been established on the chart. Because the 850-mb surface could be higher than the top of a low-level moist layer and because the mean potential temperature of the lowest 3,000 ft is strongly affected by diabatic heating, both the SI and the LI computed from the measured upper air data either misrepresent the true instability or include significant diurnal variation.

The earth's surface is unique in the sense that the vertical velocity is always zero, allowing vertical motion to increase upward under the influence of a convergent field. This does not mean that a vertical current or updraft always starts from the earth's surface. The inflow air of a nocturnal thunderstorm could be coming from some layer slightly above the cold surface air.

To compute the LI as a function of the base of an updraft, we assume a layer of 50-mb thickness above an arbitrary pressure surface to represent the inflow layer (fig. 64). Two open circles in each 50-mb layer represent the mean mixing ratio and the mean potential temperature plotted on each $(P-25)$-mb surface. By lifting the parcel from the $(P-25)$-mb surface dry adiabatically to the condensation level and then moist adiabatically to 500 mb, a LI can be obtained. This index varies naturally as a function of the pressure (or height) at the base of the updraft. In other words, it varies with the pressure when the base of the updraft is moved upward from the ground. Figure 64 illustrates the lifting from three surfaces with pressures P_0, P_1, and P_2, of which the lifting from the surface of pressure P_1 gives the lowest LI, that is, the largest instability.

The lowest LI obtained by moving a layer upward from a $(P-25)$-mb pressure surface is called the best lifted index (BLI), and the pressure and the height of the surface used to obtain the BLI are designated as the pressure of the best lifting (PBL) and the height of the best lifting (HBL), respectively.

To test the use and validity of the BLI and the PBL, the meteorological conditions of the Palm Sunday tornadoes were analyzed. As discussed in sections 3 and 4, the tornadoes occurred in the warm sector east of a dry cold front advancing rapidly across the Midwest. The 850-mb charts in figures 65, 67, and 69 represent the advance of the dry cold front extending from the center of a continental cyclone to Texas. The cyclone moved east-northeast at the rate of about 35 kt. The areas (stippled) with dew-point temperatures above +5°C also moved rapidly eastward as the dry cold front wiped out their western boundaries.

Analyzed in figure 66 are the isolines of the BLI and the PBL computed from the 0600 CST soundings on Apr. 11, 1965, about 5 hr before the Palm Sunday tornadoes
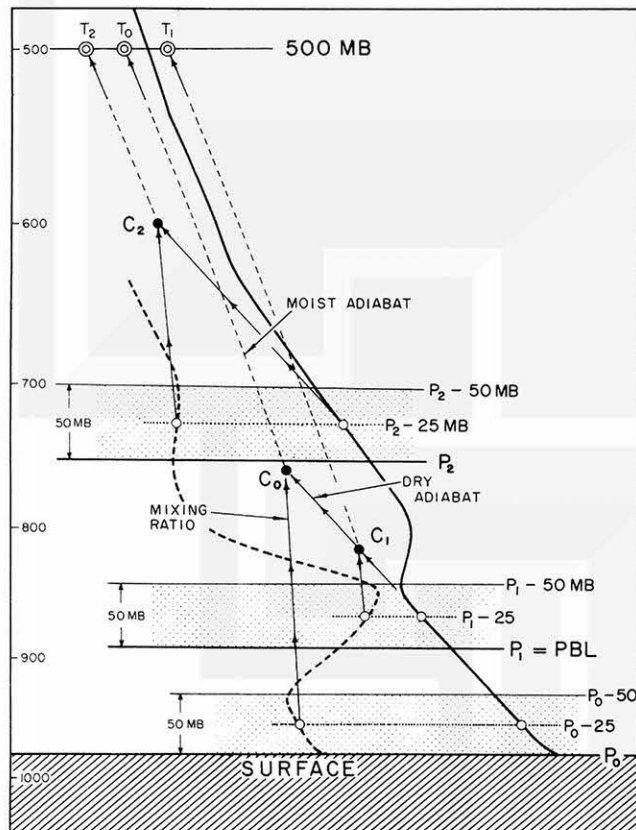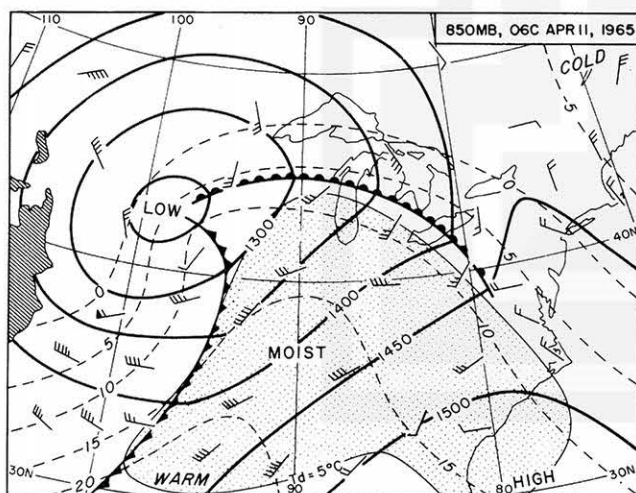
formed in Iowa. A tongue of instability characterized by a BLI below −5°C is seen along the advancing edge of the dry cold front. In some areas west of the front, the BLI exceeds +10°C. Note that the area of the low BLI is entirely within the region where the PBL represents the surface pressure, indicating the BLI can be obtained when the lowest 50-mb air is lifted to the 500-mb surface. Figure 66 also includes the winds aloft corresponding to the PBL. These winds are helpful in determining the motion of the air lifted from the initial surface.

The BLI and PBL patterns at 1800 CST on Apr. 11, 1965 (fig. 68), reveal little change in the BLI values during the 12-hr period. The tongue of instability widened, and a significant gradient of the BLI is seen along the dry cold front. Tornadoes in progress appear as black circles near the northern tip of the tongue of the low BLI in which south-southwest winds prevailed. The decrease in the PBL, or the increase in the HBL, is evident north of the −5°C line where the BLI=0°C line reaches above the 850-mb surface, while the wind directions at the HBL are south or south-southwest. An active warm frontal surface can be expected in such an area, since the combination of the PBL and BLI suggests a favorable condition for lifting from a warm frontal surface. An area of high BLI values west of the dry cold front is characterized by an extremely dry air mass topped by dry westerly winds above 700 mb. Advection of high-level moisture in the area near the lower left corner of the chart resulted in a dome of the HBL, and the BLI associated with this moisture advection was so high that no convective activity could be expected. Most of the area behind the dry cold front is characterized by an almost isentropic temperature

FIGURE 64.—Example of the computation of pressure of the best lifting (PBL) and best lifted index (BLI) on an adiabatic chart.

FIGURE 65.—Fronts, contours (solid lines), and isotherms (dashed lines) on the 850-mb surface for 06 CST on April 11. Stippled area represents dew-point temperatures above 5°C.
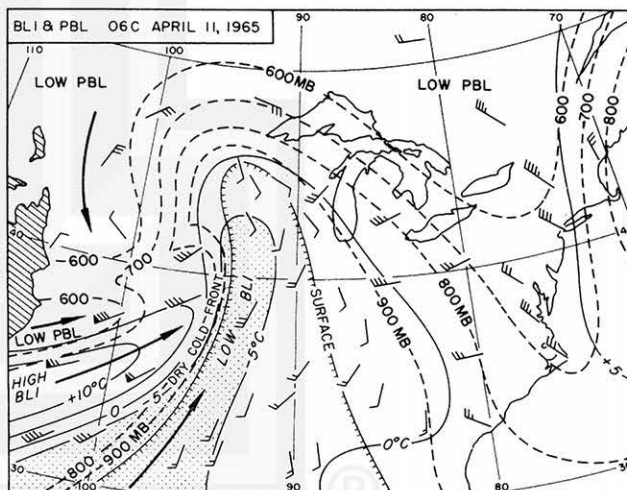
FIGURE 66.—Isobars of PBL are represented by dashed lines and isolines of BLI by light solid lines. Area enclosed by "surface" label indicates that the PBL is identical to pressure at the ground and the stippled area indicates that the BLI is less than −5°C. Plotted winds are those reported at or near the PBL surface. Heavy arrows represent the streamlines of the plotted winds.
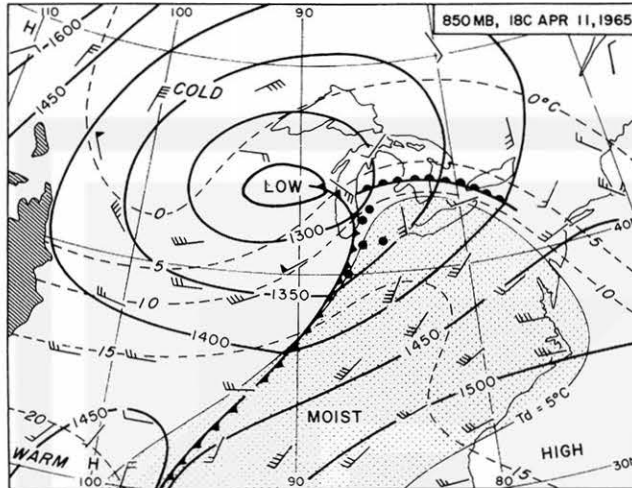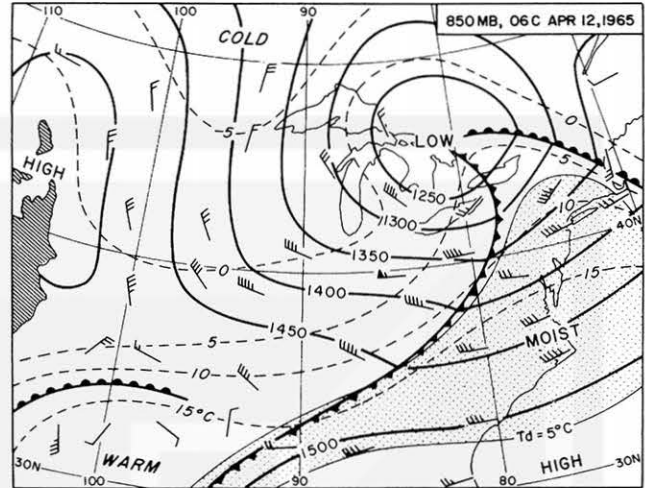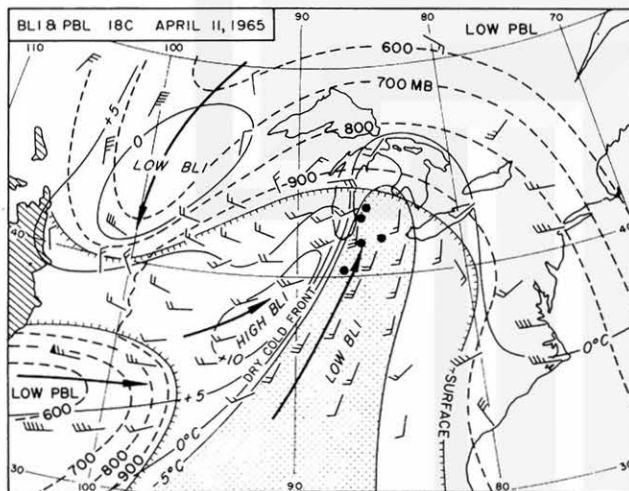
FIGURE 67.—Fronts, contours (solid lines), and isotherms (dashed lines) on the 850-mb surface for 18 CST on April 11. Stippled area represents dew-point temperatures above 5°C.

FIGURE 69.—Fronts, contours (solid lines), and isotherms (dashed lines) on the 850-mb surface for 06 CST on April 12. Stippled area represents dew-point temperatures above 5°C.

FIGURE 68.—Isobars of PBL are represented by dashed lines and isolines of BLI by light solid lines. Area enclosed by "surface" label indicates that the PBL is identical to pressure at the ground and the stippled area indicates that the BLI is less than −5°C. Plotted winds are those reported at or near the PBL surface. Heavy arrows represent the streamlines of the plotted winds. Black circles show position of tornadoes at 18 CST.
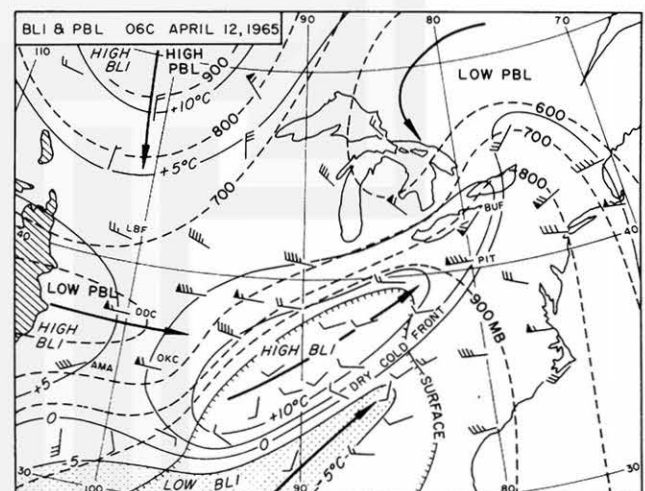
FIGURE 70.—Isobars of PBL are represented by dashed lines and isolines of BLI by light solid lines. Area enclosed by the "surface" label indicates that the PBL is identical to pressure at the ground and the stippled area indicates that the BLI is less than −5°C. Plotted winds are those reported at or near the PBL surface. Heavy arrows represent the streamlines of the plotted winds.

lapse rate from the ground to near 750 mb and low mixing ratio values.

Early Monday morning on Apr. 12, 1965, all tornado activity ended, leaving behind some of the worst damage in decades. The BLI and PBL patterns at 0600 CST on Apr. 12, 1965 (fig. 70), clarify the conditions some 5 hr after the end of the storms.

These patterns, analyzed at 12-hr intervals on April 11 and 12, show a remarkable continuity from one chart to the next, suggesting that the instability regions in the afternoon can be predicted by means of the BLI. When an area is affected by a rapidly moving system, such as a dry cold front, the LI in the afternoon at a specific location computed from a moving sounding does not always include all advective changes that might take place during the next several hours.

LOCAL AND MATERIAL DIFFERENTIAL ADVECTIONS

The term "differential advection" is used to describe a process by which the vertical variation in the horizontal transport of temperature in the atmosphere results in

either an increase or a decrease in the instability of the layer.

Processes of differential advection have been used in earlier studies to explain the destabilization of the atmosphere that produces severe storms and tornadoes (Whitney and Miller 1956) and heavy precipitation (Miller 1955). Crumrine (1965), reporting on differential advection between 850 and 500 mb computed from 15 cases of severe storm activity, found that an average differential advection of about 1°C/hr, when it destabilizes the air mass ahead of an instability line, is favorable for the development of severe storms.

The differential advection investigated by the authors cited above deals with the change in the lapse rate between two levels above a given point on the earth. The temperature T_1 at a height h_1 can then be written

$$\frac{dT_1}{dt} = \frac{\partial T_1}{\partial t} + \mathbf{V}_1 \cdot \boldsymbol{\nabla} T_1. \tag{1}$$

The net change in the temperature should be zero, since we assume that the processes are those of horizontal advection only. Thus we have

$$\frac{\partial T_1}{\partial t} = -\mathbf{V}_1 \cdot \boldsymbol{\nabla} T_1. \tag{2}$$

Combining this with an advective change in temperature at h_2, which is higher than h_1, we obtain the differential advection

$$\frac{\partial (T_2 - T_1)}{\partial t} = \mathbf{V}_1 \cdot \boldsymbol{\nabla} T_1 - \mathbf{V}_2 \cdot \boldsymbol{\nabla} T_2. \tag{3}$$

This differential advection observed above a fixed point on the earth is termed "local differential advection."

If an observer moves with either upper or lower level wind to measure the vertical change in lapse rate, a slightly different differential advection with respect to a moving coordinate system can be obtained. Such a change in the coordinates, which may move with either upper or lower level winds, is meaningful indeed, since an atmosphere travels horizontally until a favorable lapse rate for convection is reached. This differential advection is called the "material differential advection."

The change in temperature thus observed from a moving coordinate can be written

$$\frac{\delta T_1}{\delta t} = \frac{\partial T_1}{\partial t} + \mathbf{C} \cdot \boldsymbol{\nabla} T_1 \tag{4}$$

and

$$\frac{\delta T_2}{\delta t} = \frac{\partial T_2}{\partial t} + \mathbf{C} \cdot \boldsymbol{\nabla} T_2, \tag{5}$$

where δ designates a variation observed from the coordinates moving with velocity $\mathbf{C}$.

First, if we assume that the coordinate system moves with the low-level winds, then $\mathbf{C} = \mathbf{V}_1$ and $\delta T_1/\delta t = 0$. At the higher level, h_2, $\delta T_2/\delta t = -\mathbf{V}_2 \cdot \boldsymbol{\nabla} T_2$, since the local

temperature change is due only to horizontal advection. Substituting in equations (4) and (5) and subtracting we have

$$\frac{\delta T_2}{\delta t} - \frac{\delta T_1}{\delta t} = \frac{\delta (T_2 - T_1)}{\delta t} = -\mathbf{V}_2 \cdot \boldsymbol{\nabla} T_2 + \mathbf{C} \cdot \boldsymbol{\nabla} T_2,$$

$$= -\mathbf{V}_2 \cdot \boldsymbol{\nabla} T_2 + \mathbf{V}_1 \cdot \boldsymbol{\nabla} T_2,$$

$$= (\mathbf{V}_1 - \mathbf{V}_2) \cdot \boldsymbol{\nabla} T_2, \text{ and}$$

$$= -\mathbf{S} \cdot \boldsymbol{\nabla} T_2, \tag{6}$$

where $\mathbf{S} = \mathbf{V}_2 - \mathbf{V}_1$ denotes the vertical shear. This result indicates that the material differential advection when moving with the low-level wind is the inner product of the negative value of the vertical wind shear and the temperature gradient at the upper level.

When the coordinate system moves with the upper wind, $\mathbf{C} = \mathbf{V}_2$, $\delta T_2/\delta t = 0$, and $\delta T_1/\delta t = -\mathbf{V}_1 \cdot \boldsymbol{\nabla} T_1$. Again substituting in equations (4) and (5) and subtracting, we have

$$\frac{\delta T_2}{\delta t} - \frac{\delta T_1}{\delta t} = \frac{\delta (T_2 - T_1)}{\delta t} = \mathbf{V}_1 \cdot \boldsymbol{\nabla} T_1 - \mathbf{C} \cdot \boldsymbol{\nabla} T_1,$$

$$= \mathbf{V}_1 \cdot \boldsymbol{\nabla} T_1 - \mathbf{V}_2 \cdot \boldsymbol{\nabla} T_1,$$

$$= (\mathbf{V}_1 - \mathbf{V}_2) \cdot \boldsymbol{\nabla} T_1, \text{ and}$$

$$= -\mathbf{S} \cdot \boldsymbol{\nabla} T_1. \tag{7}$$

From these results, the differential advection of temperature can be summarized as follows:

LDA = local differential advection = $\mathbf{V}_1 \cdot \boldsymbol{\nabla} T_1 - \mathbf{V}_2 \cdot \boldsymbol{\nabla} T_2$;

MDA–H = material differential advection for high-level wind = $-(\mathbf{V}_2 - \mathbf{V}_1) \cdot \boldsymbol{\nabla} T_1$;

MDA–L = material differential advection for low-level wind = $-(\mathbf{V}_2 - \mathbf{V}_1) \cdot \boldsymbol{\nabla} T_2$.

Of these three differential advections, LDA indicates destabilization of the atmosphere above any fixed point on the earth, MDA–H gives destabilization of the atmosphere below an air parcel moving with the high-level wind, and MDA–L is for a parcel moving with the low-level wind, which will move upward when the lapse rate inside the overlying air column increases.

To find out the change in the stability of the atmosphere before the Palm Sunday tornadoes of Apr. 11, 1965, we analyzed the differential advection field by computing these three different differential advections.

Under the assumption that the tornado-producing convection started when the warm moist air from the Gulf of Mexico was advected northward until the lapse rate of the air column above it became so large that violent overturning took place, we moved the coordinates with the 850-mb winds in computing the differential advection. The 700-mb surface was chosen as the upper level for the advection computation, based upon the finding that cold advection was most significant near the top of the dry cold air mass (fig. 63). That is,

$$\text{MDA–L} = -(\mathbf{V}_{700} - \mathbf{V}_{850}) \cdot \boldsymbol{\nabla} T_{700}. \tag{8}$$
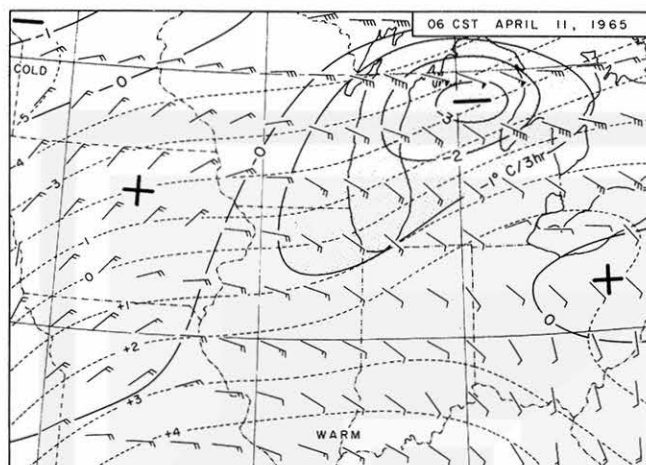
FIGURE 71.—Chart showing isotherms (°C) at 700 mb (dashed lines) and isolines of MDA for low-level winds (MDA–L, solid lines) for 06 CST on April 11. Plotted winds at grid points are $V^{850} - V^{700}$.
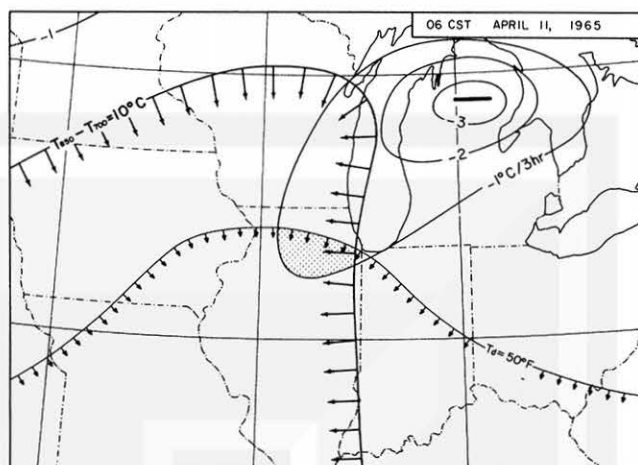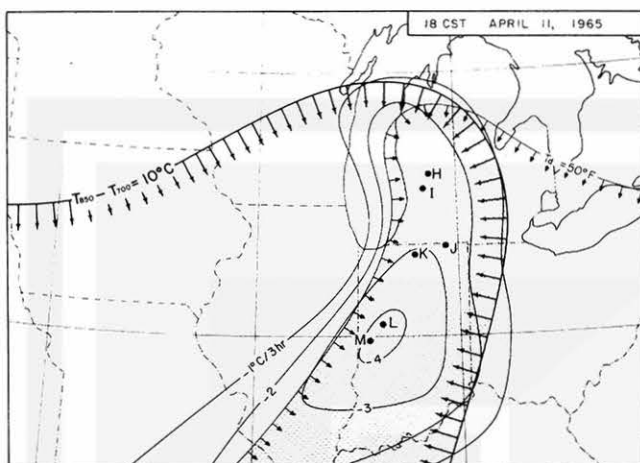

FIGURE 72.—Chart showing MDA–L, in °C/3 hr at 06 CST on April 11, combined with the area in which temperature lapse between 850 and 700 mb is greater than 10°C and the area where the surface dew point is greater than 50°F. The stippled area satisfies simultaneously the conditions of negative differential advection greater than 1°C/3 hr, a surface dew point greater than 50°F, and a temperature lapse between 850 and 700 mb greater than 10°C.

Figure 71 shows the fields of T_{700} and $(V_{850} - V_{700})$ and the isolines of MDA–L computed from these fields. The 700-mb isotherms were obtained by smoothing the temperature field analyzed over a much larger area. The winds $V_{850} - V_{700} = -S_{850}^{700}$ entered at grid points on the chart were computed from the streamline and isotach field of the vertical wind shear obtained from observed upper winds. The MDA–L contoured for every 1°C/3 hr indicated an area of negative MDA–L, or increasing lapse rate, over lower Michigan at 0600 CST on April 11.

No severe storms were reported in this area, but when the areas of T_d higher than 50°F and of $T_{850} - T_{700}$ were higher than 10°C were combined with it, a small area was found to satisfy the conditions of large initial lapse rate, high moisture content, and large negative differential advection (stippled area, fig. 72). Similar computations were made for 1200 CST, but data for the charts were obtained from only a few observed winds and the interpolated isotherm patterns, making the computation of MDA–L very difficult. A small area satisfying the same three conditions was located in north-central Iowa, however, and it was in this region that the first of the Palm Sunday tornadoes was reported around 1230 CST.

At 1800 CST the rate of differential advection had increased to a maximum negative value of over −4°C/hr. As figure 73 reveals, a large negative MDA–L existed along the advancing side of the dry cold front, which then extended from Lake Michigan to Missouri. The MDA–L behind this front was slightly positive, suggesting that the entire air mass between the 850- and 700-mb surfaces was pushing eastward without noticeable differential advection.
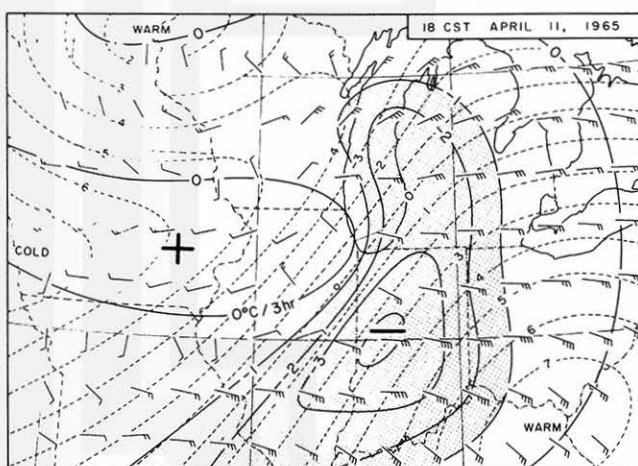
FIGURE 73.—Chart showing isotherms (°C) at 700 mb (dashed lines) and isolines of MDA–L (solid lines) for 18 CST on April 11. Plotted winds at grid points are $V^{850} - V^{700}$.

The three parameters were combined in figure 74 and it is of interest that, as figure 74 shows, all the tornadoes in progress at 1800 CST were inside the stippled area that satisfies all of the three conditions discussed above.

Figure 74.—Chart showing MDA–L in °C/3 hr at 18 cst on April 11, combined with the area in which temperature lapse between 850 and 700 mb is greater than 10 and the area where the surface dew point is greater than 50°F. The stippled area satisfies simultaneously the conditions of negative differential advection greater than 1°C/3 hr, surface dew point greater than 50°F, and a temperature lapse between 850 and 700 mb greater than 10°C. Black circles represent locations of tornadoes at chart time.
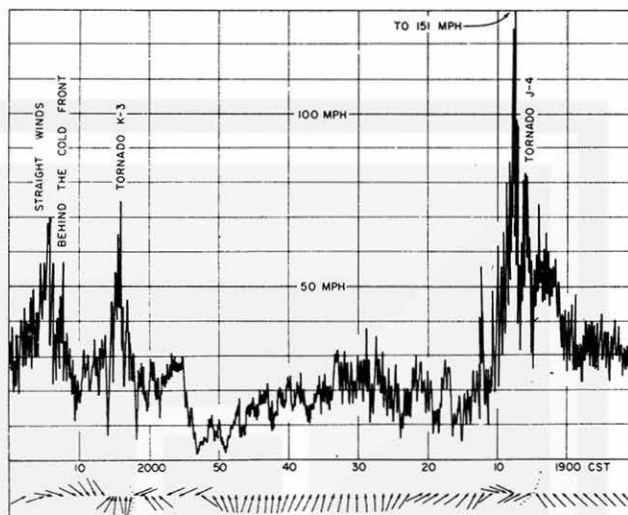
Figure 75.—Wind recorder trace from Tecumseh, Mich., on April 11 when two tornadoes passed north of the station. The recorder pen went off the chart at 151 mi hr⁻¹. A combination of wind direction and wind speed indicates that the peak gusts at 1908 and 2004 cst were caused by two tornadoes, and that the one at 2014 cst was the result of straight winds associated with the passage of the cold front. (Courtesy of the Tecumseh Community Health Study, the University of Michigan.)

8. WIND SPEEDS ASSOCIATED WITH THE TORNADOES

RECORDED TRACES OF TORNADO AND TORNADO CYCLONE WINDS

The Palm Sunday tornadoes left more than 30 damage paths over a six-State area, but only one anemometer was near enough to a path to record tornado-related winds. It was located at Mayers Airport, north of Tecumseh, Mich., and was operated by the Tecumseh Community Health Study, the University of Michigan. As indicated in figure 30 in section 4, the wind tower was located along the southern boundary of a very wide damage path resulting mainly from tornado J–4. The anemometer recorded a peak gust of 151 mi hr⁻¹ at 1907 cst. About 1 hr later, another tornado, K–3, passed north of the same anemometer, recording a 75-mi hr⁻¹ peak gust at 2004 cst. The recorder trace converted into rectangular coordinates with wind direction added is shown in figure 75, where we see that the wind speed increased from about 30 to 151 mi hr⁻¹ in about 15 min, then dropped back to 30 mi hr⁻¹ in 3 to 4 min. After the first tornado, J–4, had passed, the wind direction returned to southerly and remained so until about 10 min before the arrival of the second storm, K–3. The latter was located just ahead of the cold front, referred to previously as a dry cold front. Note that a straight westerly wind with a gust up to 70 mi hr⁻¹ came shortly after this storm.

The analysis in section 5 of the radar echoes showed that these two tornadoes were born from two separate thunderstorms that traveled along almost identical paths. A reduced gain picture of these thunderstorms taken by
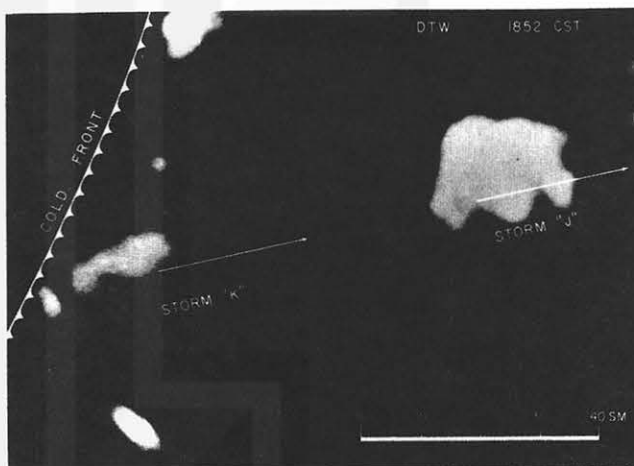
Figure 76.—WSR–57 picture from Detroit taken at 1852 cst with the cold front superimposed. Comparison of this picture with figure 75 shows the relationship between the peak gusts and the weather systems that produced them.

the Detroit (DTW) WSR–57 radar at 1852 cst is given in figure 76. Both echoes show a distinct hook with a cyclonic finger located in the southwest quadrant.

To study the 151-mi hr⁻¹ gust recorded at Tecumseh, Mich., in relation to tornado J–4, a 40-min section of the wind trace in figure 75 was enlarged. Figure 77 shows the enlargement, with wind velocities plotted at the
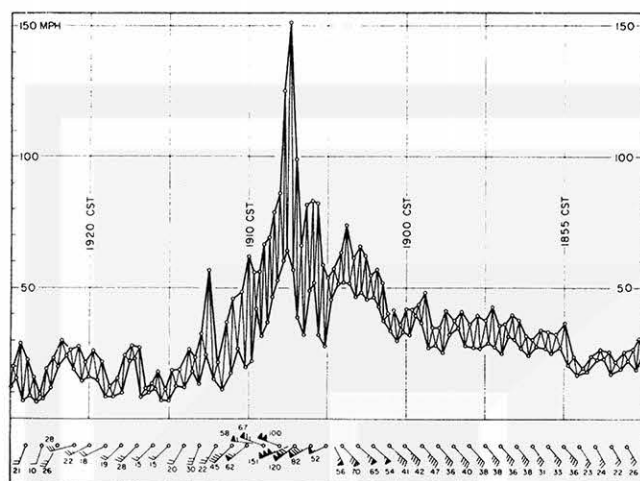
FIGURE 77.—Enlargement of the wind recorder trace appearing in figure 75. For the wind speed chart, both time and speed of all visible maximum and minimum values were read from the recorded trace and then connected with straight lines. At the same time, successive maximum and minimum values were separately joined to show the range in the variation of gusty winds. Wind velocities plotted at the bottom represent 1-min means of maximum values in miles per hour.

FIGURE 78.—Damage area in relation to the hook echo at the time of the highest recorded wind (upper chart) and to the space section of the mean maximum winds (lower chart).

FIGURE 79.—Space section of relative winds obtained by subtracting 60 mi hr^{-1}, the translational velocity of the storm, from the 1-min means of maximum winds. Due to the rapid motion of the tornado cyclone, the relative winds computed tend to blow through the tornado cyclone near the ground. Inside the tornado area, as indicated by the dashed circle, the relative winds are circulating around the tornado center.

bottom. The successive maxima and minima are connected by heavy lines to show the range of the wind fluctuation. The numbers next to the plotted winds represent the gust speed in knots. The highest gust of 151 mi hr^{-1} occurred between 1907 and 1908 CST when the direction was shifting rapidly from west-southwest to west-northwest, suggesting that it was recorded when the tornado center was passing just north of the station.

Figure 78 illustrates the wind field in relation to the damage area and to the radar hook echo J, which produced four tornadoes of the combined mode. Tornado J–4 was of the series mode. The upper chart in the figure indicates that the wind tower was located near the southern boundary of the damage path and that the diameter of the eye in the PPI echo was approximately the width of the path. This does not mean that the diameter of the tornado eye was over 2 mi; it could have been considerably smaller. The lower chart shows the space cross-section of winds converted from the time cross-section of the Tecumseh winds. The wind pattern seems to be affected by the cyclonic circulation of the tornado cyclone, as well as by the tornado near the cyclone center.

Since tornado J–4 was one of the series of tornadoes belonging to a combined-mode family, we may assume that it moved east-northeast with the center of the tornado cyclone at 60 mi hr^{-1}. Because of the very low pressure around the tornado center, the surface wind field around the tornado axis represents a circular wind field superimposed upon a straight flow that represents

the translational motion of the storm. Figure 79, obtained by subtracting the 60-mi hr^{-1} straight flow from the winds recorded in figure 78, shows the streamlines of relative flow. There are two important features in this figure. First, the tornado circulation appears only inside the dashed circle in the figure. Second, outside this area the relative winds beneath the echo are more or less straight with increasing wind speed toward the tornado-
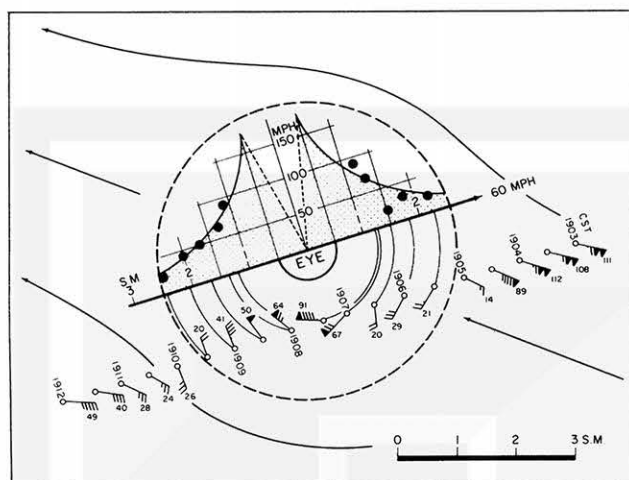
FIGURE 80.—Enlargement of the field of relative winds shown inside the dashed circle in figure 79. The area within the circle, 5 mi in diameter, is characterized by a tangential wind speed inversely proportional to the radius. From the widespread damage path, the radius of the circle of maximum wind is estimated to be about half a mile. The wind around this radius would be over 175 mi hr^{-1}.

cyclone center, which in this case represents the tornado center. It is, therefore, difficult to use the relative winds as shown in figure 79 to depict the flow accompanying the tornado cyclone. The whirling wind around tornado J–4 is presented in figure 80 in an enlargement of a portion of figure 79. The dashed circle represents the boundary of the wind field of tornado J–4. Shown in the upper half of this circle is the profile of the tangential wind speed plotted against the radii in the front and rear sectors of the storm. As we see, the tangential wind speed increases toward the center in inverse proportion to the radius, implying that the eye or the core circulation of this tornado was surrounded by an irrotational vr vortex. The circulation of the vortex is estimated to be

$$\Gamma = 2\pi r v \simeq 180\pi \text{ mi}^2 \text{ hr}^{-1}.$$

If we assume that this circulation remains constant everywhere outside the core, the maximum wind at the core boundary would be

$$V_{max} = \frac{\Gamma}{2\pi r_{core}} \simeq \frac{90}{r_{core}},$$

which is inversely proportional to the core radius. Tornado J–4 produced widely scattered medium damage north of the wind tower. If we assume that the 3-mi-wide damage path was caused by a tornado with a core 1 mi in diameter, V_{max} would be about 180 mi hr^{-1}. The maximum wind speed, therefore, including the translational motion of the storm would be about 240 mi hr^{-1}.

Tornado K–3 also contributed to the overall damage path north of Tecumseh, although eyewitness accounts indicate that the first one, J–4, caused most of the damage. Figure 75 shows that the maximum wind speed at Tecumseh associated with the second one, K–3, was only 75 mi hr^{-1}, or slightly more than the translational velocity of the tornado. It is likely, therefore, that Tecumseh was located near the fringe of the second tornado.

RELATIVE SURFACE WINDS AND PERTURBED WINDS ACCOMPANIED BY FAST-MOVING TORNADOES AND TORNADO CYCLONES

The wind velocity representing a vortex motion around a tornado axis near the surface can be obtained by subtracting the translational velocity of the tornado center from the total wind. Figures 79 and 80, thus obtained, show that the surface winds around a fast-moving tornado are very similar to those inside a rotating air column.

A question arises immediately concerning the diameter of such an air column inside which the tangential speed decreases outward. According to figure 80, the diameter seems to be about 5 mi. A relative wind of about 20-mi hr^{-1} tangential speed is seen along the outermost boundary, indicated by a dashed circle. This rotating air column, 5 mi in diameter, seems to act as an obstacle to the relative winds from the east-southeast. At the ground, where theoretically the air does not move even inside a tornado, the relative wind velocity should be opposite to that of the translational velocity of the tornado. A rotating air column such as the one shown in figure 80 must, therefore, be undercut by an extremely shallow layer. As the height above the ground increases from the order of inches to feet, the relative winds change quickly into those representing a column circulation around the center of a traveling tornado. This implies that the tornado inflow takes place inside a very shallow layer just above the ground, although what is taking place aloft is not known.

Because a tornado cyclone is accompanied by a much weaker wind system than a tornado, relative surface winds inside a tornado cyclone do not always represent a relative flow. Figure 79 shows that relative surface winds of a fast-moving tornado cyclone appear to blow through the region of the cyclone. Since the tornado cyclone is located over a region where the southerly surface winds are about 30 mi hr^{-1}, a moving tornado cyclone with a few millibars pressure drop at the center is not strong enough to modify the 30-mi hr^{-1} southerly wind or 55-mi hr^{-1} relative wind from the east-southeast into a cyclonic flow within its area.

Assuming, however, that a tornado cyclone induces perturbed winds no matter how fast it travels, we can obtain the field of perturbed winds by subtracting estimated undisturbed winds from the total winds recorded by the Tecumseh wind recorder. With time changes in the undisturbed wind taken into consideration, changing linearly from SSE 31 mi hr^{-1} at 1850 CST to S 31 mi hr^{-1} at 1925 CST, figure 81 shows the field of perturbed wind
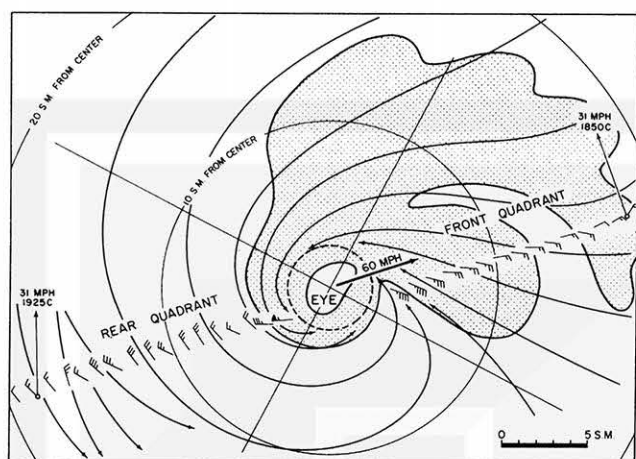
FIGURE 81.—Perturbed wind field accompanied by the tornado cyclone in figure 75. Note that the wind field shows a definite sign of circulation and convergence, since this part of it represents the vector difference between the actual wind and the undisturbed wind computed under the assumption that there was no tornado cyclone.
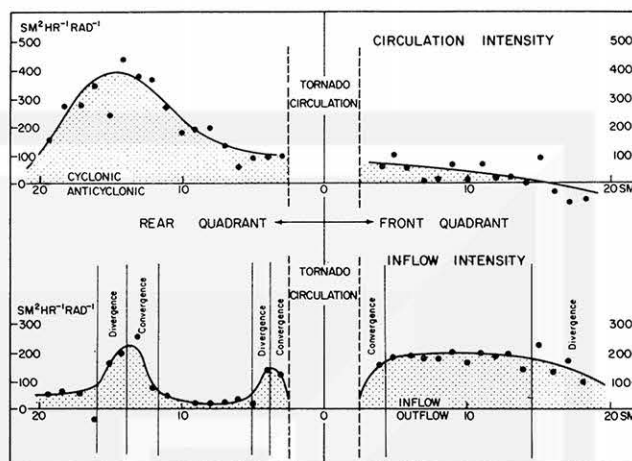

FIGURE 82.—Radial distribution of circulation intensities inside the front and rear quadrant of the tornado cyclone. The intensities were computed from the perturbed winds as a function of the distance from the storm center.

resulting from tornado cyclone J as it was moving north of Tecumseh. A dashed circle in the figure represents the region of the whirlwind around the tornado center. Winds outside the circle form a spiral flow extending about 20 mi from the tornado cyclone center. One notes that the streamlines of the perturbed winds are quite asymmetric, suggesting that most of the inflow occurs in the front quadrant (fig. 81) of the tornado cyclone. The quantitative aspects of such asymmetry can be understood from figure 82, where the intensities of the circulation and the radial outflow are plotted as functions of the radius. These intensities are defined by $V_t r$ and $V_r r$, which can be integrated, respectively, as

$$\Gamma = \int_0^{2\pi} V_t r d\theta, \quad \text{circulation,}$$

and

$$F = \int_0^{2\pi} V_r r d\theta, \quad \text{influx,}$$

where V_t is the tangential velocity, V_r is the radial velocity, and θ is the horizontal angle around the cyclone axis. The product of V and r represents the circulation or outflow per unit angle around the cyclone axis. Its intensity is a function of r and θ within the tornado cyclone.

Figure 82 indicates that the circulation intensity is negative or very small in the front quadrant some 20 mi away from the center. As the distance from the center decreases, the intensity gradually increases to about 100 (stat mi)^2 hr^{-1} rad^{-1}. This increase continues after the center has passed, reaching a maximum in the rear quadrant about 15 mi from the center. We may postulate, therefore, that a certain time is required for the surface winds to acquire a cyclonic circulation when a tornado

cyclone aloft moves over an area. In the case of tornado cyclone J, about 40 min was required for the air parcel to travel from the front to the rear quadrant of the tornado cyclone.

The field of inflow intensity within the tornado cyclone was also quite asymmetric. In the front quadrant the inflow increased to a maximum about 15 mi from the center, but the inflow intensity was more or less constant outside a circle about 8 mi in diameter. The inflow intensity around this circle was about 150 (stat mi)^2 hr^{-1} rad^{-1}. If constant convergence inside the circle is assumed, the mean convergence would be about 20 hr^{-1}, or about 500×10^{-5} sec^{-1}.

NATURE OF CHARACTERISTIC CYCLOIDAL MARKS ON THE GROUND

Since Van Tassel (1955) first reported on the elliptic marks left by the North Platte Valley tornado of June 27, 1955, several other such phenomena have been reported. Prosser (1964) found a large number of cycloidal marks in a series of vertical aerial photographs along the path of a Nebraska tornado of May 5, 1964. The aerial survey of the Palm Sunday tornadoes (as reported in section 4) revealed a large number of well-defined cycloidal marks in Indiana and Ohio.

Such marks have not yet been interpreted fully, but both Van Tassel and Prosser concluded that they are closely related to the rotational and translational motions of a tornado. To determine the estimated tangential wind speed, Van Tassel assumed that the marks were produced by something being carried with the speed of the revolving wind within the tornado funnel. Using C as the circumference of the ellipse, N as the number of scratch rings per mile, and S as the translational speed of the
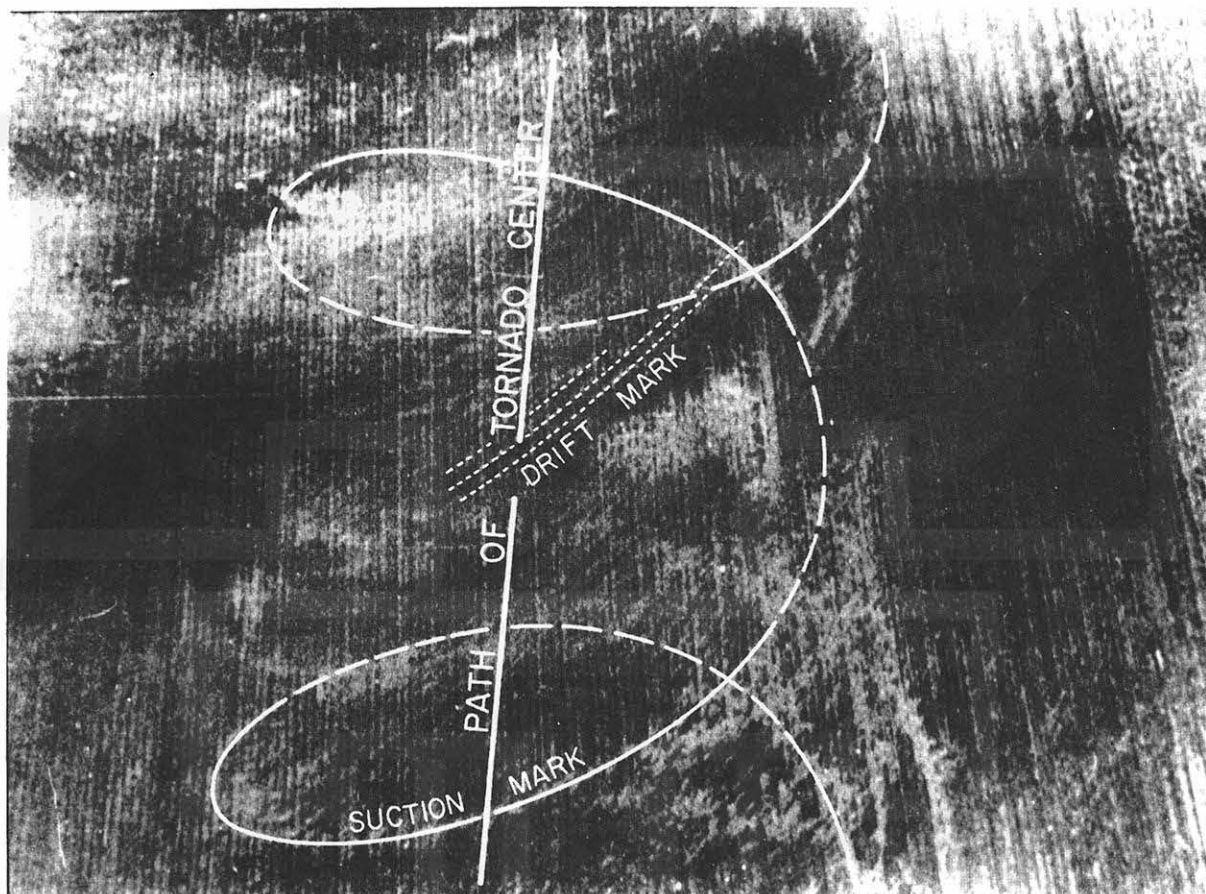
FIGURE 83.—Aerial photograph of typical suction and drift marks left by a tornado on an unplowed field. The picture was taken with a 135-mm telephoto lens over the area shown in figure 32.

tornado as input data, he estimated a tangential wind speed of 484 mi hr^{-1}. Prosser, on the other hand, considered these marks to be the probable result of light reflected differently from the disturbed and the disturbed areas. This was based upon his close inspection of high-resolution aerial photographs and also upon a damage survey by R. E. Meyers, State Climatologist for Nebraska, who stated that "the path gave the impression than an enormous vacuum cleaner had swept the ground clean of vegetation, loose soil, all other movable objects." Careful examination of these photographs by Prosser led him to make the important suggestion that the vortex diameter was oscillating about the mean since the radius of curvature of closed loops varied along the tornado path.

In an attempt to find out the nature of these marks from the Palm Sunday case, a number of 35-mm telephoto pictures of the marks left by the Palm Sunday tornadoes were taken from a low-flying Cessna–310. Figure 83 reveals their detailed structure and an overall view is given in figure 35. A cycloidal line superimposed upon the telephoto picture was drawn by following smoothly one of the most

pronounced lines in the picture. As we see, there are a few more cycloidal marks within the one cycle of the cycloid, suggesting strongly that several "spots" rotating around the tornado center were responsible for producing the marks. If we, like Prosser, assume that these spots represent areas of very strong suction capable of vacuum-cleaning the soil on a plowed field, it is feasible to determine their size and position relative to the tornado center.

Closer inspection of a number of telephoto pictures and repeated visual observation from an altitude of 500 ft led us to believe that the cycloidal lines in Indiana and Ohio caused by the Palm Sunday tornadoes were not loosened or blown-off soil from plowed fields. The early date of the tornadoes makes it unlikely that the fields had been recently plowed. The Nebraska tornado studied by Prosser, on the other hand, occurred on May 5 when some fields could have been plowed before the tornado occurred.

Prosser believed that the marks were the result of differential soil characteristics, while we think that they represent narrow bands of debris accumulation. It is

agreed, however, that they represent loci spots that act like nature's vacuum cleaners. In the Nebraska tornado, the vacuum cleaner was so strong that it loosened up and cleaned off the soil and vegetation. The debris accumulation seen during the Palm Sunday events can be hypothesized as being the result of vacuum cleaners strong enough to converge debris but not capable of sucking up the accumulation a few inches above the ground.

A household vacuum cleaner head with 15 ft sec^{-1} suction speed may be calculated to produce a convergence of

$$\text{conv} = \frac{\text{suction speed}}{\text{height of head above the floor}} = 100 \text{ sec}^{-1}$$

when the head is placed about 2 in. above the floor. If we assume a convergence of 10 sec^{-1} near the ground, only $\frac{1}{10}$ that of a household vacuum cleaner, it would result in vertical motions of 5 ft sec^{-1} at 6 in. above the ground, 10 ft sec^{-1} at 1 ft, 100 ft sec^{-1} at 10 ft, etc.

Although we do not know the exact magnitude of the convergence giving rise to the formation of the cycloidal ground marks, it is obvious that they can be produced only if the convergence near a tornado center is concentrated at several spots that rotate around the center. If the convergence takes place uniformly around a circular area, a uniform damage belt such as that produced by a rotating grinder would be expected.

The size of these spots with strong convergence, as determined from the width of cycloidal lines, was only several to 20 ft, implying that the convergence inside a tornado is concentrated at several spots which rotate around the traveling tornado center. Such spots of concentrated convergence may be called "suction spots," and the ground marks appearing along their loci "suction marks." Suction marks, if preserved, would represent a group of cycloidal curves; however, due to strong winds at the rear of a traveling tornado, the marks produced by suction spots moving in the front are either partially or totally destroyed by the spots at the rear. This is why in aerial pictures we frequently see the rear half of the cycloidal marks more distinctly. Before a tornado wind ends, the rear half will be swept by the remainder of the whirlwind, and "drift marks" seen in figure 83 are the common features produced by debris blown off in the direction of these final strong winds.

SHAPE OF CYCLOIDAL MARKS, THEIR LOOP WIDTH, AND LOOP SHIFT

If a suction spot is assumed to rotate around the tornado center at a constant radius, the locus of the spot can easily be computed as a function of the translational speed, U, the tangential speed, V, and the radius, R, between the spot and the tornado center. The parametric equations of a cycloid with the x-axis taken along the path of a tornado center are

$$y = R \sin \omega t \text{ and } x = Ut + R \cos \omega t \qquad (9)$$

where ω denotes the angular velocity of a suction spot and t is the time measured from the initial x-axis crossing of the spot. If $c = \omega t/2\pi$, the total rotation number of a suction spot around the tornado center, is substituted in (9) and if the resulting equation is differentiated in order to obtain the slope, then

$$\frac{dy}{dx} = \frac{dy}{dt} \bigg/ \frac{dx}{dt} = \frac{V \cos 2\pi c}{U - V \sin 2\pi c} = \frac{n \cos 2\pi c}{1 - n \sin 2\pi c} \qquad (10)$$

where $n = V/U$, the ratio of the tangential and the translational speeds. Equation (10) indicates that the slope of the cyloidal curve is a function of both n and c and does not depend on R. This means that the overall shape of a cycloidal mark depends only on n.

Figure 84 was drawn by changing n from 1.0 to 10. The height and width of the loop increase with n becoming very close to $2R$ when n exceeds 10. The loop width is measured as the difference of x when the slope changes from plus infinity to minus infinity, which occurs when

$$1 - n \sin 2\pi c = 0 \text{ or } 2\pi c = \sin^{-1} (1/n). \qquad (11)$$

The time corresponding to this rotation angle is

$$t = 2\pi c/\omega = 2\pi c R/V,$$

which is now put into (9) to obtain

$$x_1 = \frac{2cR}{n} + \frac{R\sqrt{n^2 - 1}}{n} \text{ and } x_2 = \frac{(\pi - 2\pi c)R}{n} - \frac{R\sqrt{n^2 - 1}}{n}.$$

Thus we have

$$w = x_1 - x_2 = \frac{R}{n} \left\{ 2\sqrt{n^2 - 1} - \pi + 2 \sin^{-1} \frac{1}{n} \right\} \qquad (12)$$

where w denotes the width of the loop that naturally increases with n.

To define a nondimensional quantity related to the loop width, we introduce the ratio of w and $2R$:

$$W = w/2R = n^{-1} \left(\sqrt{n^2 - 1} - \frac{\pi}{2} + \sin^{-1} n^{-1} \right), \qquad (13)$$

which may be called the "relative loop width." Since this quantity clearly varies as the function only of n, we can determine n from measured values of W. Figure 85, showing the variation of n as a function of W, permits us to determine V from a suction mark on an aerial photograph and the known value of U.

When a large number of suction marks (fig. 85) appear, it is very difficult to identify the loops produced by a single suction spot that has rotated more than once around the tornado center. Then the distance of the loop shift, s, can be estimated from W and R. We shall now define the nondimensional quantity S as

$$S = s/2R = \frac{2\pi R}{n} \bigg/ 2R = \frac{\pi}{n} \qquad (14)$$
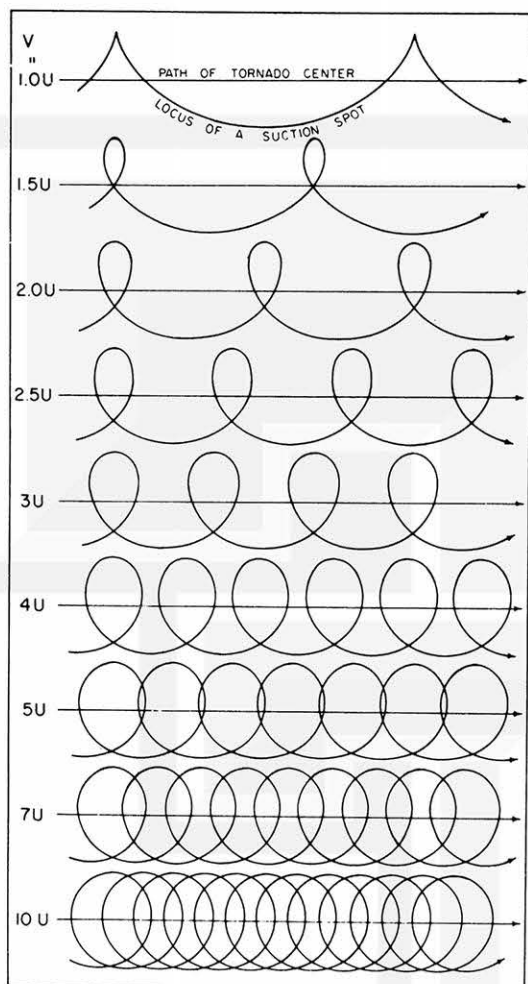
FIGURE 84.—Theoretical cycloidal suction marks obtained by increasing the ratio of tangential velocity, V, to translation velocity U, from 1.0 to 10.0. Note that the size of the loops increases as the tangential speed increases.
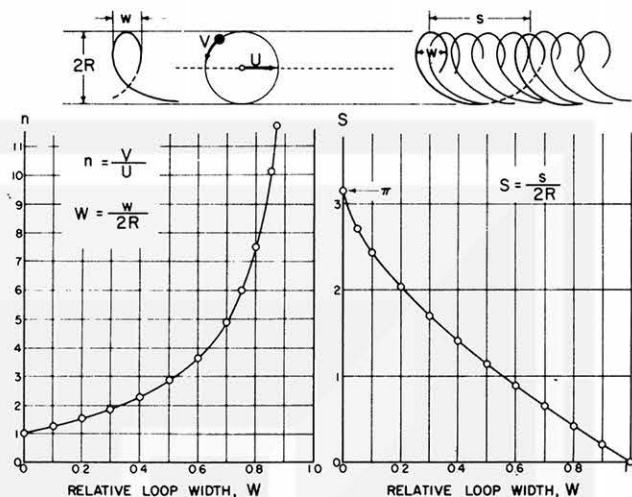

FIGURE 85.—Variation of n, the ratio between tangential and translational speeds, and S, the relative shift, as functions of relative loop width, W, which can be measured on a rectified aerial photograph showing suction marks. This figure is used in determining both n and S from aerial photographs.

TABLE 1.—*Relative loop width, W, in increments of 0.01, versus n, the ratio of tangential to translational speeds*

	0.00	0.01	0.02	0.03	0.04	0.05	0.06	0.07	0.08	0.09
0.0	1.00	1.05	1.08	1.11	1.14	1.16	1.19	1.21	1.24	1.26
0.1	1.29	1.31	1.33	1.36	1.38	1.41	1.44	1.46	1.49	1.51
0.2	1.54	1.57	1.60	1.63	1.66	1.69	1.72	1.75	1.78	1.81
0.3	1.85	1.88	1.92	1.95	1.99	2.03	2.07	2.11	2.15	2.19
0.4	2.24	2.29	2.33	2.38	2.43	2.48	2.54	2.60	2.65	2.71
0.5	2.78	2.84	2.91	2.98	3.06	3.13	3.21	3.30	3.39	3.48
0.6	3.58	3.68	3.78	3.90	4.02	4.14	4.27	4.42	4.57	4.72
0.7	4.89	5.08	5.27	5.48	5.70	5.95	6.21	6.49	6.81	7.15
0.8	7.52	7.94	8.40	8.91	9.49	10.14	10.89	11.76	12.76	13.95
0.9	15.38	17.13	19.31	22.12	25.86	31.09	38.95	*	*	*

*No values computed because of too large n.

TABLE 2.—*Relative loop width, W, in increments of 0.01, versus S, the relative loop shift*

	0.00	0.01	0.02	0.03	0.04	0.05	0.06	0.07	0.08	0.09
0.0	3.14	2.97	2.90	2.83	2.76	2.70	2.64	2.59	2.54	2.49
0.1	2.44	2.40	2.36	2.31	2.27	2.23	2.18	2.15	2.12	2.08
0.2	2.04	2.00	1.97	1.94	1.90	1.87	1.84	1.80	1.76	1.73
0.3	1.70	1.76	1.64	1.60	1.57	1.54	1.52	1.49	1.46	1.43
0.4	1.40	1.37	1.35	1.32	1.29	1.26	1.24	1.21	1.18	1.16
0.5	1.13	1.10	1.08	1.05	1.02	1.00	0.98	0.95	0.93	0.90
0.6	0.88	0.85	0.83	0.81	0.78	0.76	0.73	0.71	0.69	0.66
0.7	0.64	0.62	0.60	0.58	0.55	0.52	0.50	0.48	0.46	0.44
0.8	0.42	0.40	0.38	0.35	0.33	0.31	0.29	0.27	0.25	0.22
0.9	0.20	0.18	0.16	0.14	0.12	1.10	0.08	0.06	0.04	0.02

which may be called the "relative loop shift." Since n and W are functions of each other, we are able to express S as a function of W only. The right-hand diagram in figure 85 shows the relative loop shift as a function of W. It is evident that S decreases from a maximum value of π to zero as the relative loop width increases to 1.0.

More accurate values of n and S are given in tables 1 and 2, in which both quantities are computed by increasing W at 0.01 intervals. The tables permit us to obtain n between 1.00 (when $W=0.00$) and 38.95 (when $W=0.96$), a range sufficient for analytical purposes, since there will be no tornado when n is less than 1.0 and since cycloidal marks are too close to each other if W exceeds about 0.9.

ESTIMATED WIND SPEEDS FROM COMPUTATION OF THE ROTATIONAL RATE OF SUCTION SPOTS

We have shown in the preceding section that n, the ratio of tangential and translational speeds of a suction spot, can be obtained by measuring W, the relative loop width on an aerial photograph. Under the fair assumption that a suction spot rotates around the tornado center, we obtain the tangential speed of a suction spot as a product of n and U_{TOR}, the translational speed of the tornado.

The speed of a fast-moving tornado seems to be rather constant, probably because tornadoes generally tend to move with the speed of the parent thunderstorm. Figure 86 is a time-space diagram of the L family of six Palm Sunday tornadoes in series mode that traveled from Indiana to Ohio (fig. 35), leaving an almost straight damage path 274 mi long in 4 hr 23 min. From the slope of a diagonal line through the black dots in the figure, U_{TOR} was estimated at 62.5 mi hr^{-1}.

To apply the technique of cycloidal curve analysis presented in the preceding section, a photograph of a group of suction marks taken along the path of tornado family L was investigated in detail. The horizontal scale and the estimated path of the tornado center are superimposed on the photograph, shown in figure 87.
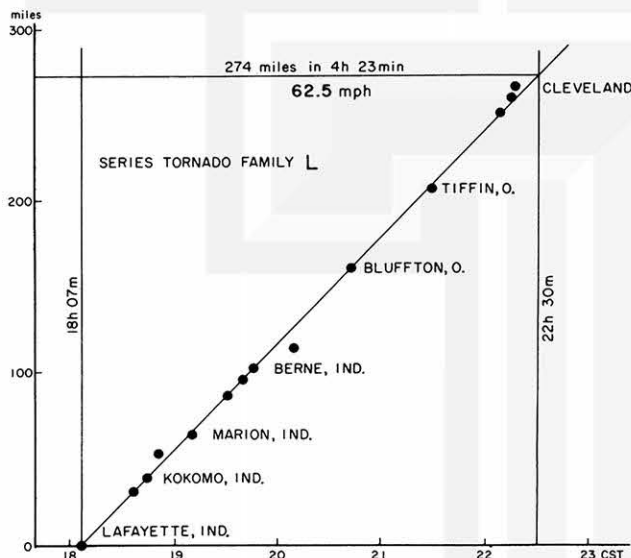
FIGURE 86.—An x–t diagram showing the time and locations of family L tornadoes in Indiana and Ohio. Refer to figure 48 for a more detailed picture.

The traced suction marks in figure 88 permitted us to compute the relative loop width, W, which can be converted into both n and S by using the two curves in figure 85. We computed S to represent the distance of the loop shift. We followed one persistent suction spot, a, during one rotation period and another, e, during four rotation periods to determine locations of their periodic appearances. The open circles with numbers 1 through 7 are the estimated positions of the tornado center after the suction marks had completed each revolution around the center. By assuming $U_{TOR}=62.5$ mi hr^{-1}, we can convert the distance of travel during each revolution into the rotational period. The rotational periods thus obtained are given in seconds in figure 88.

This figure also shows the positions of the suction spots when the tornado center was at locations 1 through 7. In determining these positions, we obtained the radius vectors by measuring the distance between the loop tops and the path of the tornado center. The phase angles were computed from the positions of the bases of perpendiculars dropped from each loop top to the path of the tornado center.

Of interest is the change in the stippled area obtained by connecting the suction spots smoothly. Their number varied between 4 and 5 and their radius vectors changed considerably from time to time. The rotational period decreased as the mean diameter of the stippled area shrunk with the eastward movement of the storm. This would imply that 1) the shrinkage of the area increased the rotational rate, probably keeping the angular momentum constant and 2) the stippled area represents the central core of the tornado, which deformed rather rapidly.

The mean tangential speeds of the suction spots when the tornado center was at locations 1 through 7 were 110, 114, 111, 118, 118, 111, and 104 mi hr^{-1}, respectively. By adding 62.5 mi hr^{-1} to these values, we obtain the maximum ground speeds of 172, 176, 173, 180, 180, 173, and 166 mi hr^{-1}, respectively. The tangential speeds are very similar to those of seven pendants appearing at the base of a sheared-off funnel obtained by Fujita (1960) from motion pictures of the Fargo tornadoes of June 20, 1957, which were 112 (90), 112 (60), 93 (30), 100 (60), 111 (110),
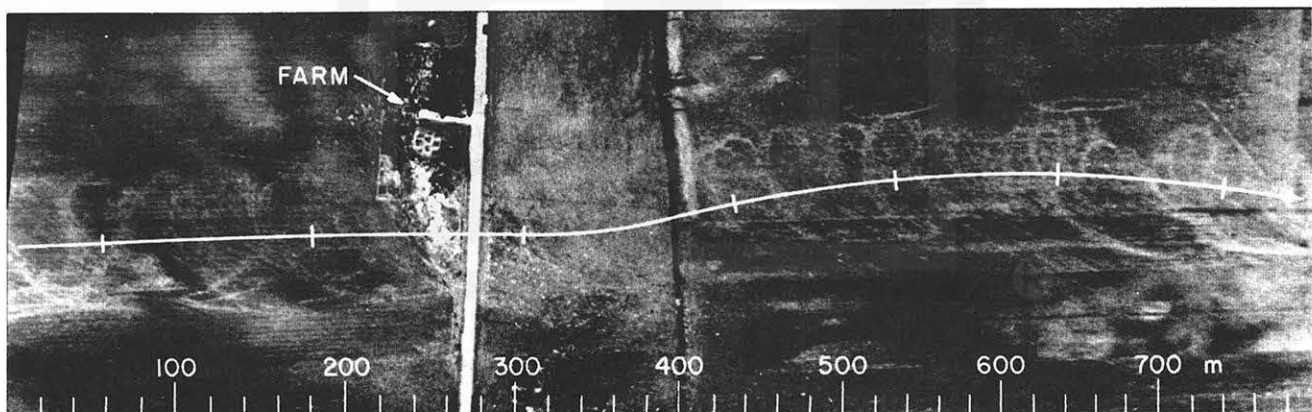
FIGURE 87.—Rectified aerial photograph showing a large number of cycloidal suction marks. Refer to figure 35 for the original photograph.
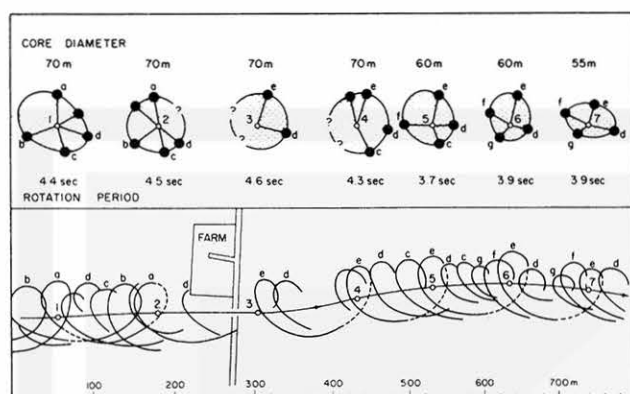
FIGURE 88.—Change in the shape of the tornado core as determined from the analysis of the cycloidal suction marks shown in the lower part of figure 87. Core diameter in meters, rotation periods, and funnel positions 1 through 7 are given in the upper part. Note that the rotational rate increased as the core diameter decreased, suggesting a conservation of angular momentum.

100 (100), and 102 mi hr^{-1} (90), respectively. (The numbers in parentheses are the distances in meters of the pendants from the funnel center.)

These results provide a reasonable basis for assuming that the suction spots rotate around the tornado center with approximately the rotational rate of the funnel.

9. SUMMARY AND CONCLUSIONS

Outbreaks of families of tornadoes over large areas and periods of time, such as during the Palm Sunday events, are very rare. Since they provide a vast amount of valuable data that can be used to reconstruct the atmospheric conditions leading to their formation, as well as a better understanding of their dynamical structure, translational and rotational speeds, and direction of motion, it is essential that all types of data relevant to a tornado outbreak be gathered. Particularly important are eyewitness reports and still and moving pictures of the tornado cloud and funnel. Understandably, under storm conditions few think about recording data, and during the Palm Sunday tornadoes, the exact time of occurrence, which is a very important fact for researchers, was generally neglected in the eyewitness report.

Aerial photographic surveys of damage paths of a large number of tornadoes are valuable because particular patterns left by the tornadoes can be used to determine quantitatively their dynamical characteristics. Patterns found to be significant in the photographic survey were: 1) scratch marks, 2) suction marks, 3) drift marks, 4) debris marks, and 5) patterns of uprooted trees.

Typical damage such as exploded houses, torn trees, etc. is, of course, important for determining the relative intensity and extent of the damage, but its potential value in determining the dynamical structure is limited, and such damage can be photographed from the ground for computation purposes. Ground surveys and photographs of certain significant parts of suction marks, drift marks, and scratch marks found in aerial surveys are also of great help in accurate measurement and identification of specific features.

A great advantage in making an aerial survey of tornado damage paths is the exact determination of the positions of tornadoes in relation to radar echoes and other observations. With the excellent radar coverage over the Midwest during the Palm Sunday tornadoes it was possible to match a specific echo with the tornado or tornadoes that produced a certain damage path. The radar echo times could then be used to determine the time of tornado occurrence.

Combining the radar pictures from all stations within range of the tornado outbreak made it possible to draw a composite picture of the echo pattern in relation to the advancing dry cold front and to study the direction and rate of motion of the echoes with respect to the midtropospheric winds.

An overall cloud picture of the Midwest was obtained from TIROS IX as it passed over the area about 20 min after the first tornado touchdown in Iowa. It showed a tongue of clear area with several extensive dust storms to be closely related to the development of the violent convection that gave rise to the formation of the unusually large number of tornadoes. The visual boundary of the tongue determined the leading edge of the dry cold air, and the opacity of the dust clouds suggested the extreme thickness of the dust or the height of the isentropic cold dome.

The two new parameters proposed here, namely the best lifted index and the pressure of best lifting, were tested and it was shown that their patterns could be predicted by simply taking advective factors into consideration. Also tested was the material differential advection, which represents the differential advection observed from the coordinate system moving with either the high- or low-level winds.

From the direct wind measurements and indirectly computed measurements of the tornado winds, five important characteristics of tornado circulation were found: 1) a tornado circulation is characterized by a nearly circular core surrounded by an irrotational vortex, 2) there are several spots of strong suction along the edge of the core, 3) the core changes its shape and diameter, 4) the rotational rate of the core increases as the mean core diameter decreases, and 5) a tornado cyclone surrounding a tornado is almost axially symmetric as far as the pressure field is concerned, but the front and the rear sides are dominated by convergence and circulation, respectively.

ACKNOWLEDGMENTS

REFERENCES

Browning, K. A., and Fujita, T., "A Family Outbreak of Severe Local Storms: A Comprehensive Study of the Storms in Oklahoma on May 26, 1963, Part 1," *Special Reports*, No. 32, Contract No. AFCRL-65-695(1), U.S. Air Force Cambridge Research Laboratories, Bedford, Mass., Sept. **1965**, 346 pp.

Crumrine, H. A., "The Use of Horizontal Temperature Advection, the 850-500 Mb. Thickness, and the 850-500 Mb. Shear Wind in Severe Local Storms Forecasting," paper presented at the 244th National Meeting of the American Meteorological Society on Cloud Physics and Severe Local Storms, Reno, Nev., Oct. 18–22, **1965**.

Feris, C., Vermoch, J., and Yario, H., "Tornadoes in Northern Illinois, Palm Sunday, April 11, 1965," Chicago Forecast Center, U.S. Weather Bureau, Chicago, **1965**, 64 pp., (unpublished manuscript).

Fujita, T., "Mesoanalysis of the Illinois Tornadoes of 9 April 1953," *Journal of Meteorology*, Vol. 15, No. 3, June **1958**, pp. 288–296.

Fujita, T., "A Detailed Analysis of the Fargo Tornadoes of June 20, 1957," *Research Paper* No. 42, U.S. Weather Bureau, Chicago, Dec. **1960**, 67 pp.

Fujita, T., "A Technique for Precise Analysis for Satellite Data: Volume I. Photogrammetry," *Meteorological Satellite Laboratory Report* No. 14, U.S. Weather Bureau, Washington, D.C., Jan. **1963**, 106 pp.

Fujita, T., Ushimima, T., Hass, W. A., and Dellert, G. T., Jr., "Meteorological Interpretation of Convective Nephsystems Appearing in Tiros Cloud Photographs," *Proceedings of the First International Symposium on Rocket and Satellite Meteorology, Washington, D.C., April 23–25, 1962*, John Wiley & Sons, Inc., New York, **1963**, pp. 357–387.

Fulks, J. R., "The Instability Line," *Compendium of Meteorology*, American Meteorological Society, Boston, **1951**, pp. 647–652.

Galway, J. G., "The Lifted Index Predictor of the Showalter Stability Index," U.S. Weather Bureau, Kansas City, Mo., **1955**, 7 pp., (unpublished manuscript).

Hoecker, W. H., Jr., "The Dimensional and Rotational Characteristics of the Tornadoes and Their Cloud System," *Research Paper* No. 41, U.S. Weather Bureau, Washington, D.C., **1960**, pp. 53–113.

Miller, J. E., "Intensification of Precipitation by Differential Advection," *Journal of Meteorology*, Vol. 12, No. 5, Oct. **1955**, pp. 472–477.

Newton, C. W., and Fankhauser, J. C., "On the Movements of Convective Storms, With Emphasis on Size Discrimination in Relation to Water-Budget Requirements," *Journal of Applied Meteorology*, Vol. 3, No. 6, Dec. **1964**, pp. 651–668.

Newton, C. W., and Katz, S., "Movement of Large Convective Rainstorms in Relation to Winds Aloft," *Bulletin of the American Meteorological Society*, Vol. 39, No. 3, Mar. **1958**, pp. 129–136.

Penn, S., Pierce, C., and McGuire, J. K., "The Squall Line and Massachusetts Tornadoes of June 9, 1953," *Bulletin of the American Meteorological Society*, Vol. 36, No. 3, Mar. **1955**, pp. 109–122.

Prosser, N. E., "Weather Note—Aerial Photographs of a Tornado Path in Nebraska, May 5, 1964," *Monthly Weather Review*, Vol. 92, No. 12, Dec. **1964**, pp. 593–598.

Showalter, A. K., "A Stability Index for Thunderstorm Forecasting," *Bulletin of the American Meteorological Society*, Vol. 34, No. 6, June **1953**, pp. 250–252.

Staats, W. F., and Turrentine, C. M., "Some Observations and Radar Pictures of the Blackwell and Udall Tornadoes of May 25, 1955," *Bulletin of the American Meteorological Society*, Vol. 37, No. 10, Dec. **1956**, pp. 495–505.

Sugg, A. L., and Foster, D. S., "Oklahoma Tornadoes, May 1, 1954," *Monthly Weather Review*, Vol. 82, No. 5, May **1954**, pp. 131–140.

Van Tassel, E. L., "The North Platte Valley Tornado Outbreak of June 27, 1955," *Monthly Weather Review*, Vol. 83, No. 11, Nov. **1955**, pp. 255–264.

Weather Bureau Survey Team, *Report of Palm Sunday Tornadoes of 1965*, U.S. Weather Bureau, Washington, D.C., May **1965**, 64 pp.

Whitney, L. F., Jr., "Severe Storm Clouds as Seen From Tiros," *Journal of Applied Meteorology*, Vol. 2, No. 4, Aug. **1963**, pp. 501–507.

Whitney, L. F., Jr., and Fritz, S., "A Tornado-Producing Cloud Pattern Seen From Tiros I," *Bulletin of the American Meteorological Society*, Vol. 42, No. 9, Sept. **1961**, pp. 603–614.

Whitney, L. F., Jr., and Miller, J. E., "Destabilization by Differential Advection in the Tornado Situation of 8 June 1953," *Bulletin of the American Meteorological Society*, Vol. 37, No. 5, May **1956**, pp. 224–229.

Winston, J. S., "The Weather and Circulation of May 1953—One of the Worst Tornado Months on Record," *Monthly Weather Review*, Vol. 81, No. 5, May **1953**, pp. 135–140.

Winston, J. S., "Forecasting Tornadoes and Severe Thunderstorms," *U.S. Weather Bureau Forecasting Guide* No. 1, U.S. Weather Bureau, Kansas City, Mo., Sept. **1956**, 34 pp.

MESOMETEOROLOGY PROJECT - - - RESEARCH PAPERS

(Continued from front cover)

* out of print

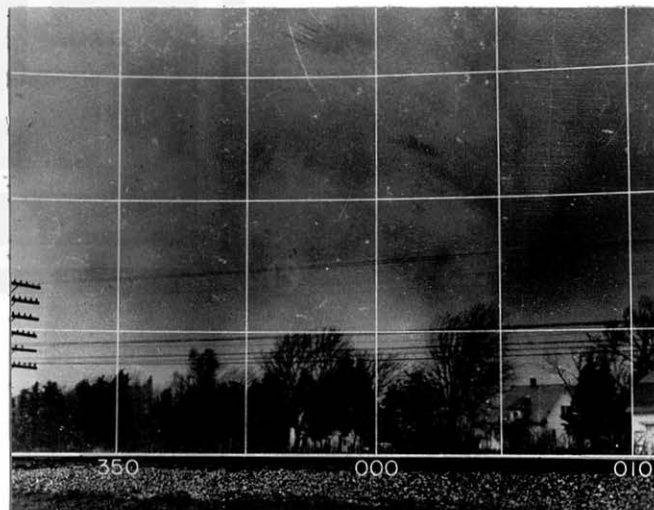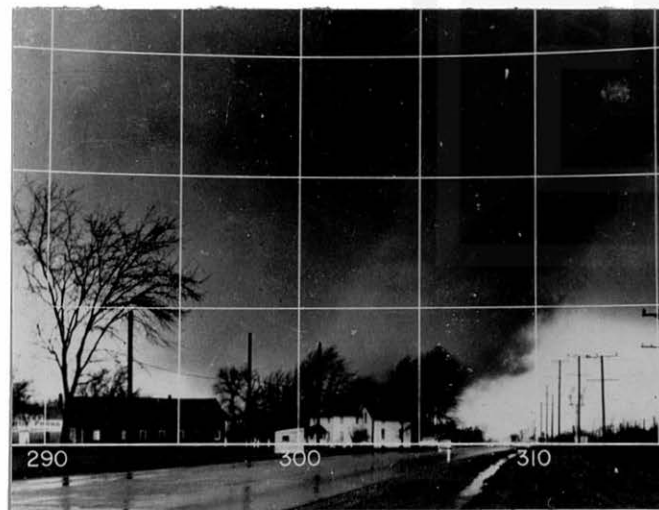# SATELLITE AND MESOMETEOROLOGY RESEARCH PROJECT - - - PAPERS

(Continued from inside back cover)

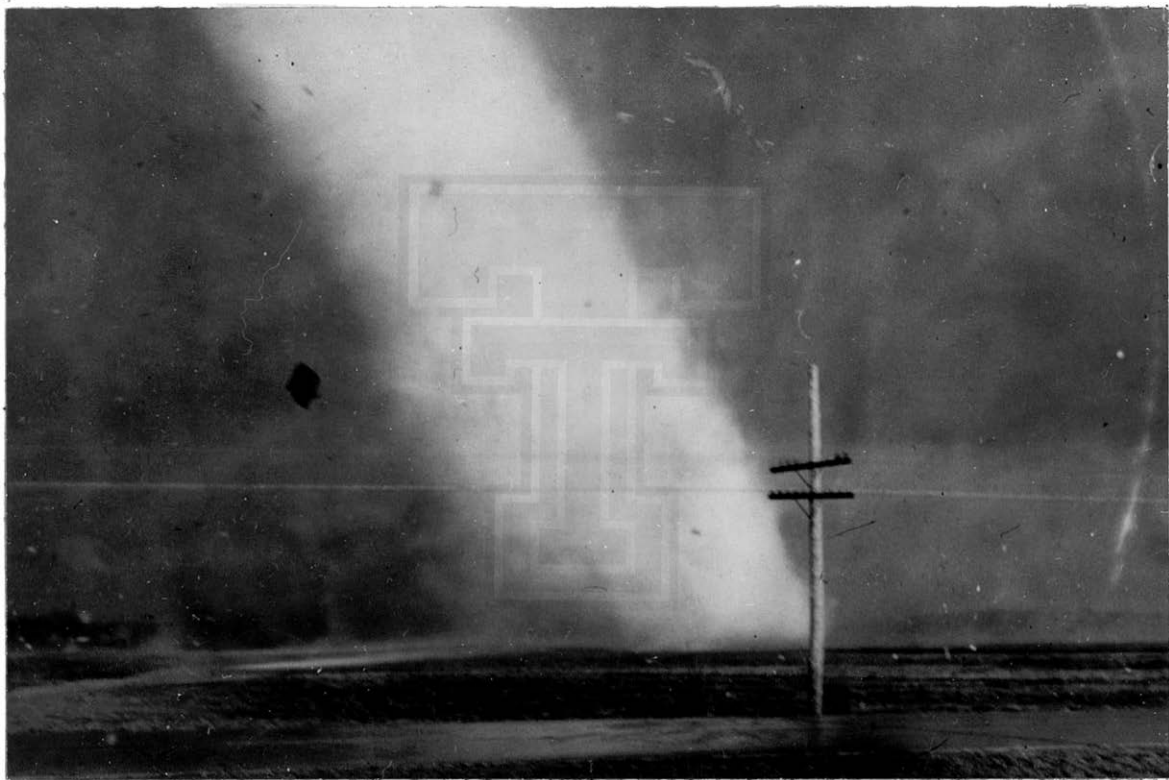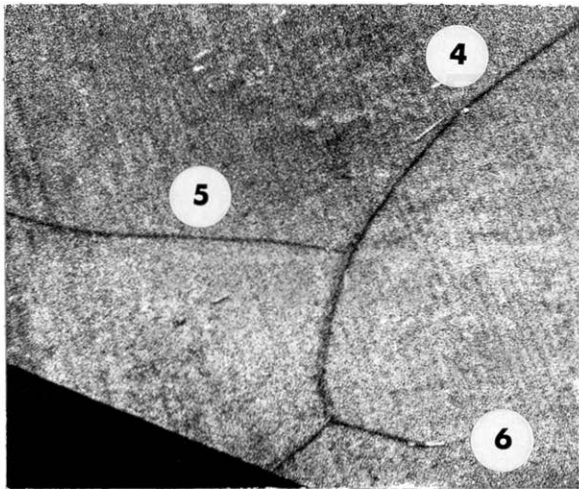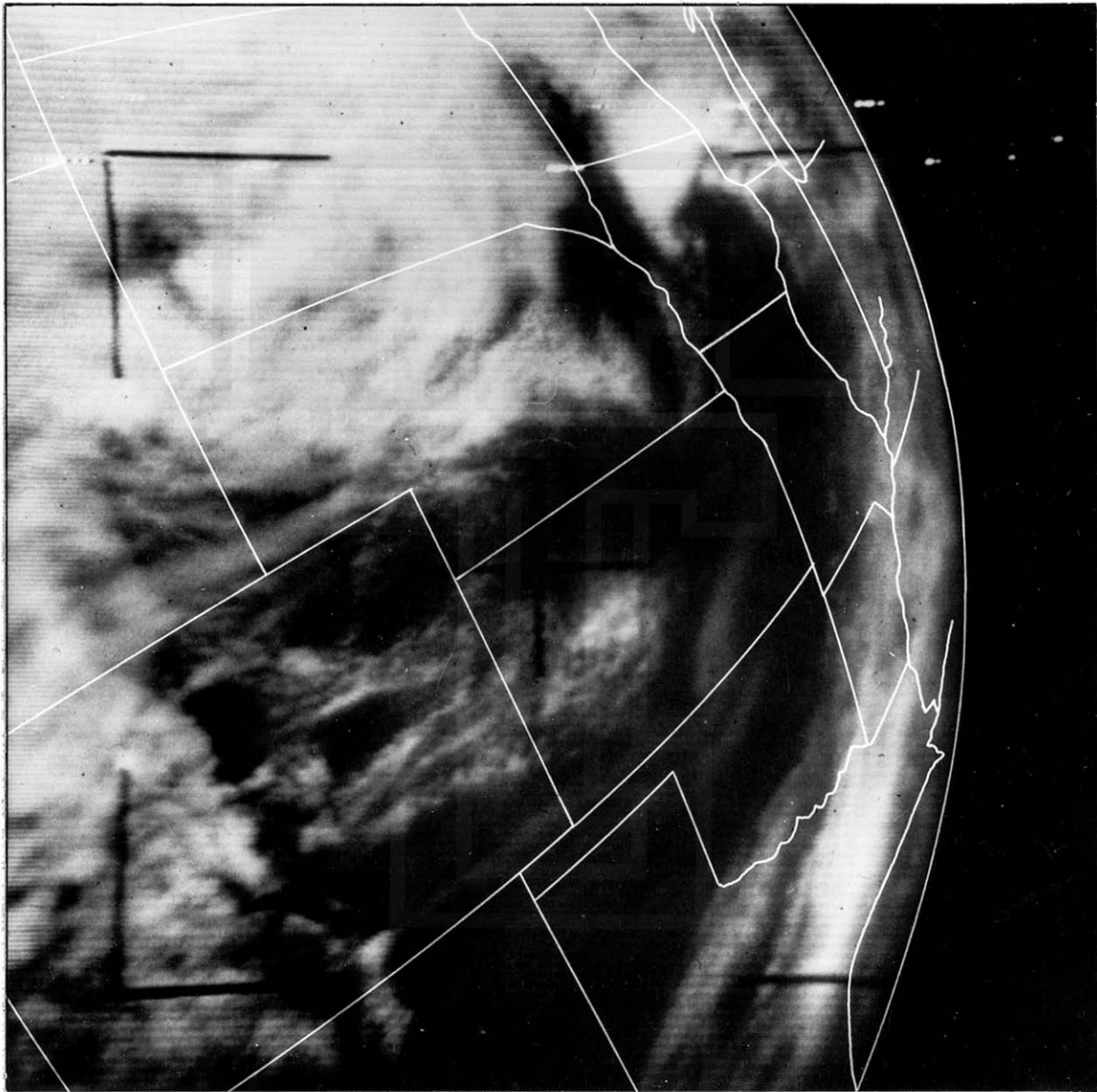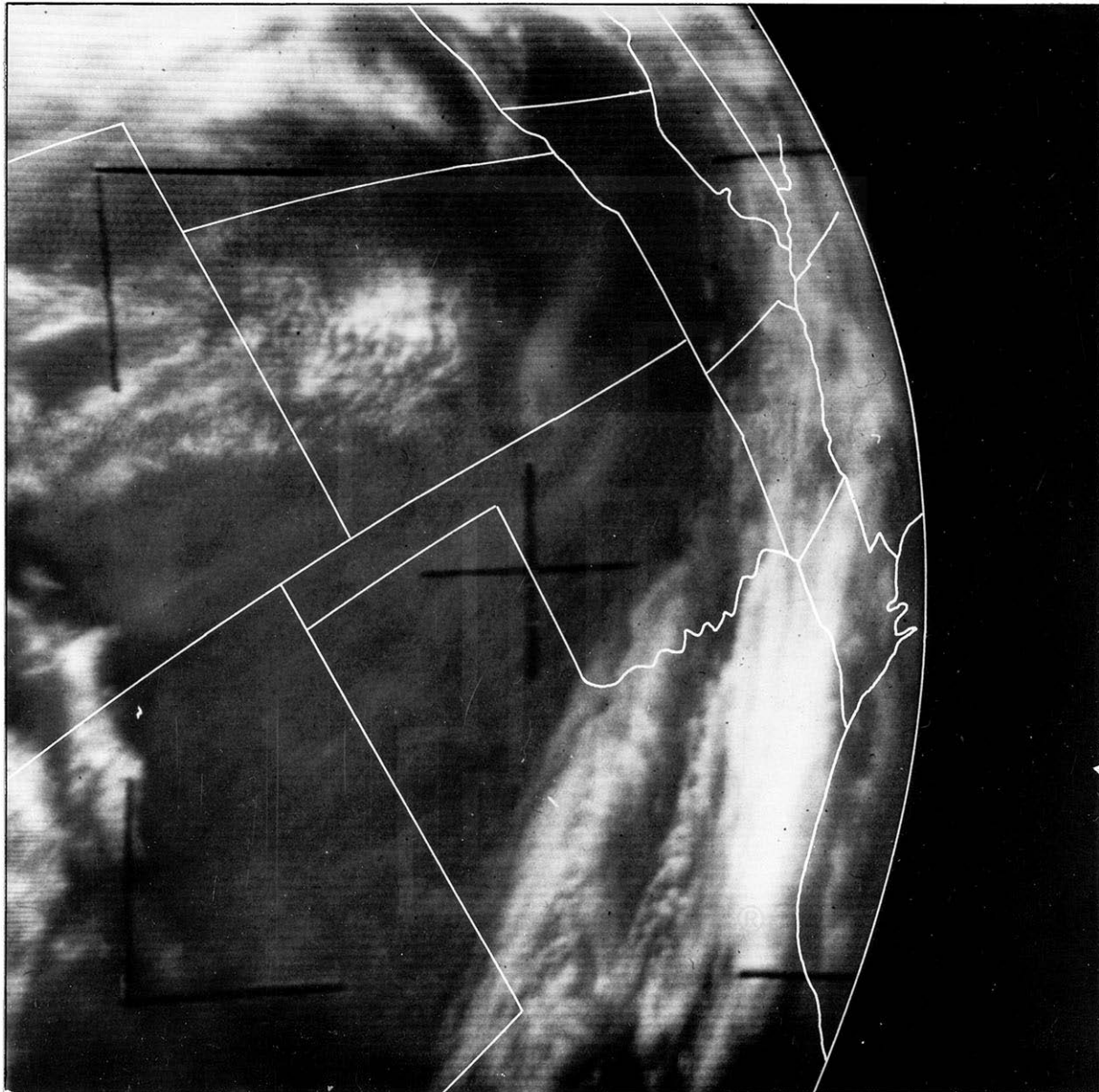See a Bug... Call Arab
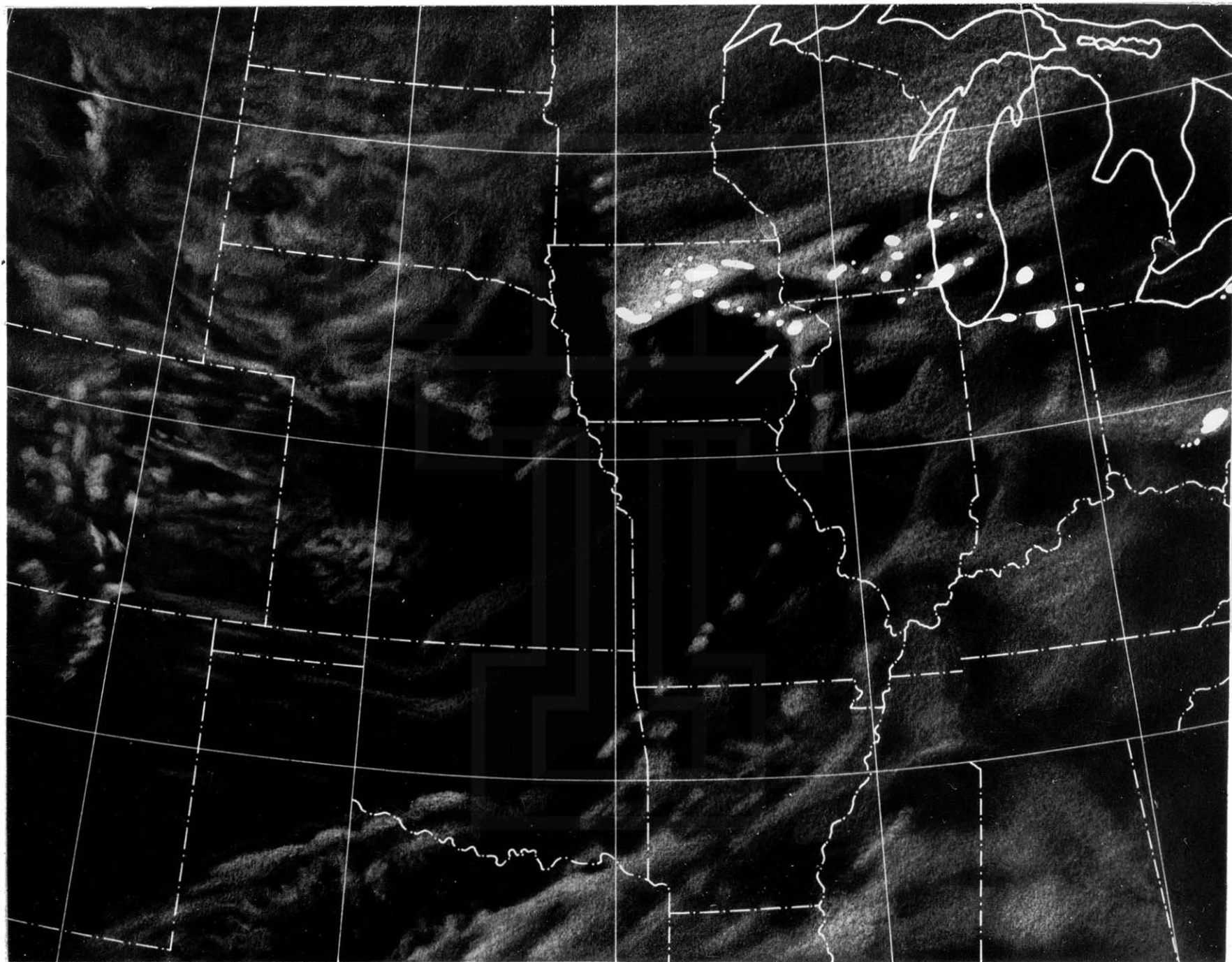
TERMITE & PEST CONTROL

DTW   1852 CST

COLD FRONT

STORM "J"

STORM "K"

0   10   20   30   40 SM